# Final Report on the Evaluation of Packed-Bed and Fluidized-Bed Cell Technology for the Destruction and Removal of Contaminants in Alkaline Waste Solutions.

by

D. T. Hobbs

Westinghouse Savannah River Company
Savannah River Site
Aiken, South Carolina 29808

J. O' Bockris
Texas A&M University
TX USA

J. Kim
Texas A&M University
TX USA

DOE Contract No. DE-AC09-89SR18035

# DISCLAIMER

Distribution:

T. B. Fryberger, DOE-HQ
W. L. Kuhn, PNL
A. M. Blackmon, DOE-SR, 703-A
M. Schwenker, DOE-SR, 703-H
L. M. Papouchado, 773-A
W. L. Tamosaitis, 773-A
J. E. Surma, PNL
R. E. White, USC
S. D. Fink, 773-A
D. T. Hobbs, 773-A
M. C. Thompson, 773-A
TIM, 773-52A

WSRC-TR-95-0310

Keywords: Electrolysis, Nitrate, Nitrite, Salt, Metals, Waste Management

Retention time: permanent

June 30, 1995

TO: S. D. Fink, 773-A

FROM: D. T. Hobbs, 773-A DT. Hobbs

# Final Report on the Evaluation of Packed-Bed and Fluidized-Bed Cell Technology for the Destruction and Removal of Contaminants in Alkaline Waste Solutions

Attached is the final report authored by J. O'M. Bockris and J. Kim of the Texas A&M University under the SCUREF contract #AA00900T, Task Order #112, to the University of South Carolina. This report completes milestone # E.1. of Technical Task Plan SR1-3-20-04, "Electrochemical Destruction of Nitrates and Organics", October 17, 1994, funded by the Efficient Separations and Processing Cross-Cutting Program of the Office of Technology Development.

Samuel D. Fink 8-13-95
Authorized Derivative Classifier

Samuel D. Fink, Group Manager
Authorized Reviewing Official

Savannah River Technology Center
Westinghouse Savannah River Company
Aiken, SC 29808

Prepared for the Department of Energy Office of Technology Development, Office of Environmental Management under Contract DE-AC09-89SR18035

# PACKED-BED AND FLUIDIZED-BED ELECTRODES

prepared for
the Department of Energy Office of Technology Development,
Office of Environmental Management
under Contract
DE-AC09-89SR18035

John O'M. Bockris and Jinseong Kim
Surface Electrochemistry Laboratory
Department of Chemistry
Texas A&M University
College Station, TX 77843

CONTENTS

## INTRODUCTION

Disposing of the large quantity of nuclear waste that has been produced within the DOE complex is an area of active research and development. Electrochemical processes have been reported for the treatment of alkaline wastes including the destruction of nitrate and nitrite [1] and the removal of metals such as Tc and Ru [2].

Electrolytic recovery of metals from dilute solution has been reported using conventional porous electrodes such as felt electrode and reticulated electrode [3], but use of such electrodes is limited. The pores of such electrodes become blocked as a consequence of metal deposition. If an attempt is made to regenerate these electrodes by dissolution of the deposited metals, oxygen evolution on the matrix competes with dissolution of metals deposited within the pores. On the other hand, the use of three dimensional packed-bed and fluidized-bed electrodes having large surface area per unit volume would offer an improvement on felt or reticulated system because of the greater ease of regeneration.

Two major electrochemical reactions concerned in this research are the reduction of nitrate and nitrite ions and the deposition of metals such as chromium, mercury, and ruthenium. In strong alkaline solutions, nitrates and nitrites are reduced to nitrogen, ammonia and other products [1,4]. Thermodynamic data for the reduction of nitrate and nitrite ions in alkaline solutions are as follows[5].

$NO_3^- + H_2O + 2e^- \rightarrow NO_2^- + 2OH^-$ E = 0.01 V

$NO_3^- + 3H_2O + 5e^- \rightarrow \frac{1}{2}N_2 + 6OH^-$ E = 0.25 V

$NO_2^- + 2H_2O + 3e^- \rightarrow \frac{1}{2}N_2 + 4OH^-$ E = 0.406 V

$NO_2^- + 5H_2O + 6e^- \rightarrow NH_3 + 7OH^-$ E = -0.165 V

$2NO_3^- + 5H_2O + 8e^- \rightarrow N_2O + 10OH^-$ E = 0.08 V

$2NO_2^- + 2H_2O + 4e^- \rightarrow N_2O_2^{2-} + 4OH^-$ E = -0.14 V

$NO_3^- + 2H_2O + 3e^- \rightarrow NO + 4OH^-$ E = -0.144 V

$N_2 + 4H_2O + 4e^- \rightarrow N_2H_4 + 4OH^-$ E = -1.16 V

Among those reactions, production of nitrogen, nitrous oxide, and ammonia have been

studied. To rationalize the rates of the reductions of nitrate and nitrite to nitrogen or ammonia, one has to know the exchange current densities as well as the equilibrium potentials for those reductions. Thus, these reactions were studied in synthetic waste solution whose composition is shown in Table 1 at planar and three-dimensional electrodes.

Three-dimensional electrodes provide large areas for electrochemcal reactions and increase the probability of reaction because the electrolytic solutions are forced to flow through the electrodes. However, the potential distribution in the electrodes is nonuniform (i.e., the potential difference at the particle-solution interface varies with the position of the conductive particles in the beds). Consequently possibility of selecting certain elements for reaction is diminished. Therefore, it is important to predict potential and current distribution in three-dimensional electrodes. Two cases have been examined with three-dimensional electrodes; activation controlled condition and diffusion controlled condition, as given below [6-8].

Mathematical treatment for the activation-controlled condition was initiated by Newman and Tobias with the assumption that Ohm's law applies to the potential difference in the solution [6]. Their treatment for a flooded electrode can be applied to a packed-bed electrode basically. The value of the resistivity of metallic phase needed to be corrected by the contact resistance between particles. On the other hand, an expanded mathematical model for a fluidized-bed electrode was published by Fleischmann and Oldfield [7] who considered the charge sharing during a collision is the key for charge transport. For an activation-controlled reaction, the current through a three-dimensional electrode is dependent on the resistivity of the solution phase, the resistivity of the electrode phase, and the overpotential. One of the basic expressions for the current - potential relations in three-dimensional electrode is;

$$\exp\left(-\frac{\alpha_c F \eta_{x=L}}{RT}\right) - \exp\left(-\frac{\alpha_c F \eta_{x=0}}{RT}\right) = \frac{\alpha_c F}{2 i_o A R T (\sigma_m - \sigma_s)}\left(\frac{\sigma_m}{\sigma_s} - \frac{\sigma_s}{\sigma_m}\right) j^2 \qquad (1)$$

where $\alpha_c$ is the transfer coefficient, F is the Faraday constant, $\eta_{x=L}$ and $\eta_{x=0}$ are the overpotentials at the positions x = 0 (bottom of the bed) and x = L (top of the bed), respectively, R is the gas constant (8.314J/mole·K), T is the temperature, $i_o$ is the exchange current density, $\sigma_e$ and $\sigma_m$ are the specific conductivity of the solution phase and the metallic phase in a bed electrode, respectively, and j is the superficial current density, which is obtained by the total current devided by the cross-sectional area of the bed, and A is the specific area per unit volume of electrode which is usually represented as

$$A = \frac{area}{volume} = \frac{4\pi r^2}{\frac{4}{3}\pi r^3}(1-\epsilon) = \frac{3(1-\epsilon)}{r} \qquad (2)$$

where r is the radius of a particle, and $\epsilon$ is the voidage of the bed electrode.

For a diffusion-controlled reaction [8], the superficial current density can be described by means of the following equation;

$$j = nFuC(1-\exp(-\frac{L}{\lambda})) \qquad (3)$$

where n is the number of electrons transferred, u is the velocity of the electrolytic solution through the electrode, C is the concentration of the electroactive species, L is the lenght of the bed, and $\lambda$ is the characteristic length given by

$$\lambda = \frac{\delta u}{DA\epsilon} \qquad (4)$$

where $\delta$ is the diffusion layer thickness, u is the velocity of the solution, D is the diffusion coefficient of the electroactive species, A is the specific area per unit volume of the electrode, and $\epsilon$ is the voidage of the bed electrode. The diffusion layer thickness is the parameter involving the complexity of the mass transfer in the bed

electrodes. The order of magnitude of the average value of the diffusion layer thickness is about 0.001cm with a solution velocity of 1cm/sec.

The experimental parameters to be examined in this report are the average radius of the particles which the bed electrode is made up of, the velocity of the solution through the bed electrode, and the length of the bed. The size of the particles is the key parameter to decide the specific area A as shown in equation (2), and thus, the superficial current density as shown in equations (1), (3) and (4). The velocity or flow rate of the solution (the flow rate is the velocity times the cross-sectional area of the bed) is one of the key parameters in equations (3) and (4). Further more, the velocity of the solution through a fluidized bed electrode is important in determining the specific conductivity of the discontinuous metallic phase in which charge sharing takes place during collisions of particles [9]. The length of the bed is involved in the determination of the superficial current density in a mass transfer controlled system as shown in equation (3) and is involved intrinsically in the overpotential term in equation (1).

The fundamental approach is to find current-potential relations for the electrochemical reactions taking place in the treatment of the wastes. With these i-V curves measured, the potential to be applied at the bed electrodes is determined, that achieves high current efficiency especially for the mass transfer controlled system.

Aside from the parametric investigations, electrocatalytic effects on the electrochemical reductions of nitrate and nitrite was investigated. Suitable electrode materials were determined. The effect of the concentrations of metals in the wastes was also investigated because the metals are deposited on the surface of the particles behaving as electrodes and eventually change the electrocatalytic properties of the bed electrodes.

With the optimized parameters determined in this research, conceptual design was initiated for the practical application of three-dimensional electrode systems to the treatment of the waste.

## EXPERIMENTAL

Experiments were carried out at planar electrodes and at three-dimensional electrodes. The electrochemistry at planar electrodes was carried out for obtaining current-potential relations of the electrochemical species concerned. Other parametric studies were carried out at three dimensional electrodes - a packed bed electrode and a fluidized bed electrode. Quantitative and qualitative analyses were carried out with UV/VIS Spectroscopy, Gas Chromatography (GC), Titrimetry, and X-ray Photoelectron Spectroscopy (XPS).

### 1. Electrochemistry at planar electrodes

#### 1.1. Electrochemical Cell

The electrochemical cell used is shown in Figure 1. The main body, made of Pyrex glass, involves a connector into which a working electrode compartment is inserted, and a Luggin capillary tip, into which a reference electrode is introduced. The end of the Luggin capillary is 0.2 cm diameter. The upper compartment also made of Pyrex glass contains a joint for gas purging, a bubbler, and a glass tube whose end is fritted glass and is used for the counter electrode.

The reference electrode was the Saturated Calomel Electrode (Fisher Scientific Co.) which has a standard potential of +0.24 V versus the Normal Hydrogen Electrode. The potentials indicated in this report are on the Normal Hydrogen Scale. The counter electrode was Pt gauze.

#### 1.2. Preparation of Working Electrode

A cylindrical metal specimen (Ni, Pt, Fe, Ti, Pb, Graphite, or Ebonex$^{TM}$($Ti_nO_{2n-1}$)) was inserted into a polyethylene or glass tube. One end of the metal specimen was connected to a copper wire inside the tube with a silver paste (E-solder from Acme Co.). The other end, which was in contact with the solution was polished with Emery paper (#600) and alumina suspensions (1 $\mu$m, 0.3 $\mu$m, and 0.05 $\mu$m) to give a mirror like surface. Before every use, the electrode was polished with alumina suspensions,

rinsed thoroughly with a deionized water. A Milli Q water system was used to prepare deionized water having 14 MΩ·cm.

1.3. Gas Purification

The electrolytic solution in the electrochemical cell was purged with nitrogen (99.9%) gas or argon (99.998%) gas before every run of electrochemical experiment to remove the oxygen from the solution. Nitrogen gas used for the deoxygenation of the electrolyte was purified with a 13X molecular sieve column and a column of heated copper chips (ca. 300 °C). The molecular sieves were frequently activated by baking in an oven at 150 °C and the copper chips were discarded after when they were covered with copper oxides. Argon gas was used without any further purification since the purity was already acceptable.

1.4. Electrolyte Preparation

The chemicals for preparing the electrolytic solutions were NaOH (EM Inc., GR grade), $NaNO_3$ (EM Inc., GR grade), $NaNO_2$ (Spectrum Chemical Co., A.C.S. reagent) $Hg(NO_3)_2 \cdot H_2O$ (Fisher Inc.), and $K_2CrO_4$ (Fisher Inc.). No further purification was carried out for these chemicals. Deionized water was used to make the electrolytic solutions.

Among the nitrosyl ruthenium compounds, $[Ru(NO)(NO_2)_x(OH)_y(H_2O)_z]^{q+}$, where $x+y+z = 5$ and $q = 3-x-y$, known to be present in the nuclear waste solution, sodium tetranitronitrosyl ruthenate(II), $Na_2[RuNO(NO_2)_4OH] \cdot 2H_2O$, was prepared by the procedure suggested by Fletcher et al. [10].

1.5. Instruments

An AMEL potentiostat model 550 controlled the potential of the working electrodes and current was obtained via an AMEL interface model 560. The currents were recorded by means of a Hewlett Packard 7044B X-Y recorder or a Philips 8271 XYt recorder.

## 2. Electrochemistry at 3-dimensional Electrodes

### 2.1. Electrochemical Cell

A schematic of the electrochemical cell for the packed-bed electrode or the fluidized-bed electrode is shown in Figure 2. The main body of the cathodic compartment made of Pyrex glass (4cm diameter) involves a glass connector which a current collector is connected through, a fritted glass which the electrode particles are rested on, and a Luggin tip for the introduction of reference electrode or for removal of air trapped under the fritted glass. The upper compartment was made of Pyrex glass having three internally threaded glass connectors for introduction of the Luggin tip for the reference electrode, gas purging tube, and a bubbler or a gas collector.

The cathode compartment is connected through a Nafion® 117 film to the anodic compartment which has a counter electrode (Pt gauze). The electrolyte in the anodic compartment was stagnant while the electrolyte in the cathodic compartment was flowing through the bed electrodes.

### 2.2. Flow System

The electrolyte in the cathodic compartment was circulated through a pump (March Mfg. Inc., Model TE-MDX-MT-3 ) The flow rate was controlled by adjusting the inlet of a pump and was measured with a flowmeter (Cole-Parmer Co., Catalog # L-03268-86).

For packed bed electrode studies, the electrolyte flows downward in the bed whereas for fluidized bed electrode studies, the electrolyte flows upward. The direction of flow was easily switched by interchanging the inlet and the outlet connnections in the cathodic compartment. (see Figure 3)

### 2.3. Particles

The bed materials for the parametric studies were Ni(99.9%) particles (Johnson-Matthey Co.) and were grouped into five ranges (16-20 mesh, 24-35 mesh, 35-60 mesh, 50-100 mesh, and 100-150 mesh) with appropriate sieves (Gilson

Company Inc.). Before each experiment, the Ni particles were washed with 30% $HNO_3$ and rinsed with distilled water throughly, then packed in the cell.

For electrocatalytic studies, Pb shots (99%, 1.3mm from Alfa Chemical Co.) and Fe powder (99%, -40+70 mesh from Alfa Chemical Co.) were used. These particles were immersed in 30% $HNO_3$ for 10 seconds, washed with distilled water thoroughly, and then packed in the cell.

### 2.4. Dimensions of the Bed Electrode

The apparent cross-sectional area of the bed electrode was determined by the inner diameter of the main body of the cathodic compartment to be 12.6 $cm^2$. The length of the bed in the cell (usually about 2 cm) was varied from 1 cm to 6 cm to study the effect of the length of the bed on the rate of the reduction of nitrate and nitrite. At the bottom of the bed is the current collector, which was cut from a Ni gauze (60x60 mesh per square inches 0.007 inch wire diameter, Electrosynthesis Co. Inc.).

### 2.5. Temperature

The temperature of the electrolyzing system was controlled from 15 °C to 76 °C with an ice-water bath or a heating band wrapping a glass tubing through which the electrolytic solution was passed. The temperature was measured with a thermometer or a Chromel-Alumel thermocouple.

## 3. Analysis

### 3.1. UV/VIS Spectroscopy

Quantitative analysis by UV/VIS spectroscopy was carried out to determine the concentrations of nitrate, nitrite, and chromate. The characteristic wavelengths for nitrate, nitrite, and chromate are 300 nm, 353 nm, and 372 nm, respectively. The molar absorptivities for nitrate, nitrite, and chromate in 1.33M NaOH at 300 nm, 353 nm, and 372 nm are shown in Table 2.

Since the initial concentrations of the nitrate and nitrite were 1.95 M and 0.66

M, the absorbance of the solution was higher than 1. Thus, the samples were diluted by a factor of 20 for the absorbance to be in the range of 0 to 1. The dilution consisted of taking 0.2 mL of the sample and adding 3.8 mL of 1.33 M NaOH. The diluted solution was transferred to a quartz cuvette (pathlength = 1 cm, Uvonic Instruments Inc.)and the absorbance measured at desired wavelengths with a Perkin-Elmer Lambda 3B UV/VIS spectrophotometer.

3.2. Gas Chromatography (GC)

GC analysis was used to determine the gas products of the electrolysis of nitrate and nitrite. For the analysis of ammonia, 10 $\mu$L of the solution was injected into a Porapak N column (80/100, 6 feet long, 1/8 inches stainless steel tubing from Alltech Co.) that was installed in a Varian 3400 Gas Chromatograph. The temperatures of the injector, column, and detector were 250 °C, 120 °C, and 250 °C, respectively. Flow rate of the carrier gas (Ar, 99.998%) was about 25 cc/min. The detector was a Thermal Conductivity Detector (TCD). The salts not evaporized in the injector were frequently removed to prevent blocking the gas flow through the column.

For the analysis of nitrogen gas, 400 $\mu$L of gaseous sample was injected into a 13X Molecular Sieve column (80/100, 6 feet long, 1/8 inches stainless tubing from Alltech Co.). The temperatures of the injector, column, and detector were 120 °C, 40 °C, and 120 °C, respectively.

The gas concentrations were obtained from the areas of the peaks measured by a Hewlett Packard 3390A Integrator. The GC was calibrated once a week.

Since there were traces of gaseous products (e.g., nitric oxide and nitrous oxide) that could not be detected with a GC, a Matheson-Kitagawa Gas Detector System was employed to analyze these gases. The amounts of the gases were determined by the chemical reactions of chromophoric groups with the gases inside a tube through which 100 mL of the gas sample passed. The nitrogen oxides length-of-stain detector tubes were supplied from Matheson Co.

### 3.3. Titrimetry

Titration with 0.1M potassium hydrogen phthalate (KHP) was carried out to measure the content of ammonia. Firstly, 1 mL of the electrolyzed solution was titrated with the KHP solution. Another 1 mL of the electrolyzed solution was heated up in a boiling water-bath for 10 min and titrated with the KHP solution. The difference in the number of the moles of KHP required for the neutralization of the two solutions was considered the content of ammonia in the electrolyzed solution.

### 3.4. X-ray Photoelectron Spectroscopy (XPS)

The XPS technique was employed to identify the deposits from the solutions. In this case, the sample was removed from the electrolyzing cell, washed with distilled water, dried in a desiccator for one day, and transfered to the introduction chamber of the XPS. After the sample was introduced into the main vacuum chamber, and the vacuum chamber evacuated to $10^{-8}$ torr. The sample was irradiated by Mg $K_{\alpha}$ X-ray (1,253.6 eV). The energies of the electrons were detected and compared with the reference values given in a handbook for the identification of particular atoms in the sample.

## RESULTS AND DISCUSSION

### A. Parametric Studies

1. Polarization at a Planar Ni Electrode

a. Reduction of Nitrate and Nitrite

Figure 4 shows the I-V relation for the electrochemical reduction of a synthetic waste solution containing 1.95 M $NaNO_3$, 0.66 M $NaNO_2$, and 1.33 M NaOH at a planar Ni electrode. Each current value was obtained from the current-time response when the potential of the electrode was applied for 10 minutes. Compared with the currents in 1.33 M NaOH (open circles in Figure 4), there is a dramatic increase of the current in the solution containing 1.95 M $NaNO_3$, 0.66 M $NaNO_2$, and 1.33 M NaOH (closed circles in Figure 4) at a planar Ni electrode at the potential very near to -0.75 V vs NHE. There are three Tafel slopes in three different regions-ca. 300 mV/decade in region I, 30 mV/decade in region II, and 180 mV/decade in region III.

b. Deposition of Hg

The average concentration of mercury in the liquid phase of the high-level nuclear waste at the Savannah River Site is $2.2 \times 10^{-6}$ M. Since the solubility product of HgO is $10^{-25.4}$ [11], the mercury exists as HgO in the waste solution. The solubility of HgO in a molecular form is $10^{-3.6}$ [11]. From the equilibrium constant ($10^{-4.5}$) for $HgO + OH^- \rightleftarrows HgO(OH)^-$, 16.7% of mercury exists as $HgO(OH)^-$ in 1.33 M NaOH. Thus, the major mercury species in the nuclear waste is HgO or $Hg(OH)_2$. The equilibrium potential for the reduction of $Hg(OH)_2$ to Hg metal is +0.098 V(NHE) [12]. An expected limiting current density is calculated from

$$i_L = \frac{nFDC}{\delta} \qquad (5)$$

where n is the number of electron transfered, F is the Faraday constant (96500 Coulombs/mole), D and C are the diffusion coefficient and the concentration of the electroactive species in mole/cm$^3$, respectively, and $\delta$ is the diffusion layer thickness in cm. Experimentally, the deposition of mercury occurs at +0.1V (See Figure 5) and a limiting current (20 $\mu$A/cm$^2$) was observed when the applied potential was more cathodic than -0.1 V and when the concentration of Hg(II) was 0.5 mM. From equation (5), the theoretical value for the limiting current density is 20 $\mu$A/cm$^2$ with $\delta$ = 0.05 cm and D = 1x10$^{-5}$ cm$^2$/sec. These fair agreements confirm that mercury as $Hg(OH)_2$ is reduced to Hg metal and deposited on the surface of the electrode.

The XPS study shows that the product of the electrochemical reduction of the solution containing 0.5 mM $Hg(NO_3)_2$, 1.95 M $NaNO_3$, 0.66 M $NaNO_2$, and 1.33 M NaOH at -0.1 V for 10 minutes made two peaks at 100.2 eV and 104.4 eV (see Figure 6) and these are in good agreement with the reference values of 99.7 eV ($4f_{7/2}$) and 103.8 eV ($4f_{5/2}$) for mercury.

c. Deposition of Ru

Figure 7 shows the I-V relation for the electrochemical reduction of the Ru compound, $Na_2[RuNO(NO_2)_4OH]\cdot 2H_2O$, in the synthetic waste solution at a planar Ni electrode. The half-wave potential was -0.4 V. In the diffusion limiting current region, the current was proportional to the concentration of the Ru compound in the solution. From equation (5), the diffusion coefficient of the Ru compound was calculated to be 0.5x10$^{-5}$ cm$^2$/sec with assumption that $\delta$ be 0.05 cm and n as 2. The use of n = 2 implies the product of the electrochemical reduction is Ru metal because the oxidation state of Ru in the form of $[RuNO(NO_2)_4OH]^{2-}$ is +2. The deposition of Ru as the product of the electrochemical reduction of $[RuNO(NO_2)_4OH]^{2-}$ was confirmed by means of X-ray Photoelectron Spectroscopy. The peaks in the XPS for the Ni electrode which had been in the solution containing 0.04 mM $Na_2[RuNO(NO_2)_4OH]\cdot 2H_2O$, 1.95 M $NaNO_3$, 0.66 M $NaNO_2$, and 1.33 M NaOH at -0.5 V for 1 hour includes 280.5 eV and 284.5 eV (see Figure 8) which are in good

agreement with the reference values of 280.0 eV ($3d_{5/2}$) and 284.1 eV ($3d_{3/2}$) for ruthenium.

d. Reduction of Chromate

Figure 9 is the i-V curve for the reduction of chromate in 1.33 M NaOH solution at a Ni electrode. When the overpotential is small, it follows the Tafel relation. However, as the overpotential shifts to a value more cathodic than -0.5 V, the current is diminished. This reaction is represented as

$$CrO_4^{2-} + 4H_2O + 3e^- \rightleftarrows Cr(OH)_3 + 5OH^- \qquad E = -0.23\ V$$

Unlike Hg or Ru, the product of the reduction of chromate is not chromium but chromic hydroxide. The existence of chromic hydroxide not elemental chromium was confirmed with the XPS data. The peaks in the XPS for the Ni electrode that had been in the solution containing 30 mM $K_2CrO_4$ and 1.33 M NaOH at -1.5 V for 10 minutes include 576.9 eV and 586.6 eV (see Figure 10). These values are in good agreement with the reference values of 576.6 eV ($2p_{3/2}$) and 586.3 eV ($2p_{1/2}$) for chromic hydroxide rather than 574.1 eV ($2p_{3/2}$) and 583.4 eV ($2p_{1/2}$) for elemental chromium.

2. Polarization at Three-Dimensional Electrodes

a. Reduction of Nitrate and Nitrite

Figure 11 shows the Tafel lines for the synthetic waste solution containing 1.95 M $NaNO_3$, 0.66 M $NaNO_2$, and 1.33 M NaOH at a packed-bed and a fluidized-bed electrode that consist of spherical Ni particles (100-150 mesh) with a cross-sectional area of 12.6 $cm^2$ and length of 2 cm. The Tafel slopes were 340 mV/decade at -0.9 V which is about twice as much as the Tafel slopes at a planar electrode (See Figure 4).

A potentiostatic electrolysis of 0.1M $NaNO_3$ in 1.33M NaOH at -0.7 V was performed at a Ni-particle (50-100 mesh) packed-bed electrode (Figure 12). The total current increased to 1.12 A after 1.5 hours and then decreased (Figure 12a). The concentration of nitrate decreased exponentially and the concentration of nitrite in the

solution increased aymptotically and then decreased. Since there was no nitrite initially, the reduction of nitrate was considered to produce nitrite as an intermediate. The concentration of ammonia as an end product increased as the electrolysis time passed. Since the total amount of nitrate, nitrite, and ammonia after the electrolysis was not the same as the initial concentration of nitrate, other unidentified products may exist.

b. Deposition of Hg

Figure 13 shows the i-V curves for the reductions of $Hg(OH)_2$ and Ru(III) at a packed-bed and a fluidized bed electrode. The bed was composed of Ni particles (50-100 mesh, average particle radius = 0.011 cm) and the length of the bed was 2 cm. The limiting current region coincides with the region at a planar electrode (Figure 5)

The limiting current at the packed bed electrode (Figure 13a) for the reduction of the solution containing 0.5 mM $Hg(NO_3)_2$, 1 mM $RuCl_3$, 1.95 M $NaNO_3$, 0.66 M $NaNO_2$, and 1.33 M NaOH was 50 mA at -0.1 V. The limiting current at the fluidized bed (Figure 13b) for the reduction of the solution containing 0.5 mM $Hg(NO_3)_2$, 1 mM $RuCl_3$, 1.95 M $NaNO_3$, 0.66 M $NaNO_2$, and 1.33 M NaOH was 2 mA at -0.1 V. Since the limiting current at a fluidized bed electrode was less than at a packed bed electrode, the effective conductivity of discontinuous metallic phase has to be taken into account.

c. Deposition of Ru

Since the deposition of the Ru complex at a planar electrode was a diffusion-controlled process (see Figure 7), the decrease in the concentration of the Ru complex by electrolysis at a packed-bed electrode follows the relation described as [8b]

$$C = C_o \exp[-\frac{aut}{V}(1-\exp(-\frac{L}{\lambda}))] \qquad (6)$$

where a is the cross-sectional area of the packed bed electrode, u is the flow rate in cm/sec, t is the time, V is the volume of the electrolytic solution, L is the length of the

bed, and $\lambda$ is the characteristic length of the bed given in the equation (4). Figure 14a shows the decrease of the concentration of the Ru complex in the electrolysis of 500 mL of the solution containing 0.4 mM Ru complex, 0.1 M $NaNO_3$, and 1.33 M NaOH at a packed bed electrode at -0.7 V. The bed was composed of Ni particles (50-100 mesh, average particle radius = 0.011 cm) and the length of the bed was 2 cm. Figure 14b is the $\ln(C/C_o)$ - time plot. From this plot, the slope for initial electrolysis was obtained to be 3/(15 min) = 1/300 $sec^{-1}$. From equation (6) with the constants given as a = 12.6 $cm^2$, u = 0.26 cm/sec, and V = 500 $cm^3$, exp(-L/$\lambda$) was obtained to be 0.49 thus $\lambda$ = 2.8 cm. With a value for the diffusion coefficient of the Ru complex = $0.5 \times 10^{-5}$ $cm^2$/sec (section A.1.c), $\epsilon$ = 0.4, and A = 160, the diffusion layer thickness was obtained to be $3.4 \times 10^{-3}$ cm.

d. Reduction of Cr

Figure 15a shows the decrease of the concentration of chromate in the solution containing 0.3 mM $K_2CrO_4$, 0.1 M $NaNO_3$ and 1.33 M NaOH (0.5 L) when the solution was electrolyzed at -0.7 V at a Ni partcle (50-100 mesh, average particle radius = 0.011cm) packed bed electrode. The cross-sectional area was 12.6 $cm^2$ area and its height was 2 cm. From the slope of log C - time plot (Figure 15b), the diffusion layer thickness was calculated to be $2.6 \times 10^{-3}$ cm initially and it becomes 0.02cm as the electrode surface was covered with the product of the reduction of chromate.

As seen in Figure 15a, the concentration of chromate in the solution was decreased exponentially by the electrolysis at -0.7 V when the initial concentration of chromate was 0.3mM. However, when the initial concentration was 3 mM, it was difficult to find the decrease of the concentration of chromate or the reduction of nitrate in the solution by electrolysis at -0.7 V. This suggests that the electrode surface is covered with the product of the reduction of chromate and the electrode is passivated. The apparent surface area of the packed bed electrode used in this experiment was about 4000 $cm^2$ when the average particle radius was 0.011 cm and the voidage was assumed to be 0.4 for randomly packed spherical particles.

Considering the number of sites at an electrode surface $10^{-8}$ mole/cm$^2$, the number of moles to make a monolayer at this packed bed electrode is $4x10^{-5}$ moles. Suppose the roughness of the surface of each particle be 10 (i.e., the real surface area of the electrode be 40000 cm$^2$), the number of moles required to have a monolayer becomes $4x10^{-4}$ moles. Since the volume of the solution used in the electrolysis was 0.5 L, the critical concentartion is 0.8 mM (i.e., the concentration of chromate that is sufficient to passivate the cathode).

Figure 16 shows the change of the concentration of chromate in the solution containing 3 mM $K_2CrO_4$, 2 $\mu$M $Hg(NO_3)_2$, 40 $\mu$M Ru complex, 1.95 M $NaNO_3$, 0.66 M $NaNO_2$, and 1.33 M NaOH when the solution was electrolyzed at -0.7 V at a Ni packed bed electrode and at a Pb bed electrode. The average particle radii were 0.034 cm for Ni and 0.065 cm for Pb. The bed size were identical (cross-sectional area = 12.6 cm$^2$, the length = 2 cm). The concentration of chromate decreased to 0.6 mM at the Pb packed bed electrode but to 2.6 mM at the Ni packed bed electrode. The diffusion layer thickness at the Pb packed bed electrode was obtained to be $2.33x10^{-3}$ cm.

The removal of chromate from the solution at the Pb packed bed electrode is possible because the reduction product of chromate at Pb electrode is not chromic hydroxide, but the chromic dioxide anion, $CrO_2^-$, Thus, the inhibition problem that is significant in case of Ni electrode does not occur. Since the reduction of chromate at a Pb electrode does not form an inhibiting chromic hydroxide on the electrode, Pb particles are a better choice as the packing particles in a packed bed electrode for electrochemical treatment of the solution containing chromate as well as nitrate. Chromic dioxide anion is slowly converted to $Cr(OH)_3$ in a strong alkaline solution [13]. A process for chromate removal from the waste solution is thus divided into two steps - the electrochemical reduction of chromate to chromic dioxide anion at Pb electrode annd filtration of the remaining solution after some period of time to remove $Cr(OH)_3$.

3. Particle Size Effect

a. At a Packed-Bed Electrode

The rates of the reduction of the electrolytic solution containing 1.95 M $NaNO_3$, 0.66 M $NaNO_2$, and 1.33 M NaOH at -0.8 V at a Ni packed-bed electrode were investigated. The current for the solution reduction represents the rate of the reaction. The rate decreased as the size of the particles increased (solid points and lines in Figure 17). This decrease was explained in terms of the 'specific surface area' of the particles, that was defined in the introduction section. As seen in the equation (2), the specific area of the bed electrode decreases as the radius of the particle increases. With a fixed volume of the bed, the effective total area decreases as the radius of the particle increases. Thus, the current proportional to the surface area decreases as the radius of the particle increases at a packed-bed electrode.

b. At a Fluidized-Bed Electrode

The dependence of the reduction rate of the electrolytic solution containing 1.95 M $NaNO_3$, 0.66 M $NaNO_2$, and 1.33 M NaOH at -0.8 V at fluidized-bed electrodes on the particle size was complicated (open points and broken lines in Figure 17). Not only the specific surface area of the particle, but also the effective specific conductivity of the discontiniuous metallic phase have to be taken into account.

Unlike a packed-bed electrode, a fluidized-bed electrode has the particles moving around and colliding with each other. The effective specific conductivity is an average conductivity considering the contact and the separation of particles. This term, derived by Fleischmann and Oldfield and modified by Kreysa [9], is represented as

$$\sigma_m = \frac{2\pi v_p C}{\sqrt[3]{h}(\sqrt[3]{h}-1)} \qquad (7)$$

where $v_p$ is the velocity of the particle in the fluidized bed electrode and C is the double layer capacitance in $F/cm^2$, and h is the length of the fluidized bed normalized

with repect to the length of the bed at static sate. The dimensionless number h can be obtained from the measurement of the bed length at each flow rate. The velocity of the particle inside the fluidized bed electrode as a function of particle radius has been determined empirically. Usually, the particle velocity is considered proportional to the particle radius. Thus, the effective conductivity of the discontinuous metallic phase is proportional to the radius of the particle. Since the current is proportional to the conductivity, it follows that the current is proportional to the size of the particles in a fluidized bed electrode.

Thus, there are two competing factors maximizing current at a fluidized-bed electrode; the effective total area which is inversely proportional to the particle size, and the effective conductivity which is proportional to the size. This competition results in a maximum current at the average radius of the particle of 0.017 cm when the flow rate is 50 cc/min (Figure 17a). As the flow rate increases (from Figure 17a to Figure 17d), the slope of current vs. radius of the particle decreases. This is because the up-thrust force by the flow increases as the flow rate increases. Thus, the resistivity of the discontinuous metallic phase becomes a dominating factor as flow rate increases (i.e., less particle contact).

4. Flow Rate Effect

The effect of the flow rate on the rate of the reduction the electrolytic solution containing 1.95 M $NaNO_3$, 0.66 M $NaNO_2$, and 1.33 M NaOH at -0.8 V at a packed-bed (solid circles) and a fluidized-bed (open triangle) electrode is shown in Figure 18. The effect of the flow rate on the rate of the reduction at a packed-bed electrode is relatively small compared with the effect at a fluidized bed electrode.

In case of a fluidized-bed electrode, when the average radii of the particles are 0.0063 cm and 0.017 cm, the rates reach a lower limit with the flow rate of 70 cc/min and 400 cc/min, respectively (Figure 18a and 18b). When the particles are too heavy ($<r> = 0.036$cm) to be moved by the flow, the rates remain nearly constant and very similar to that obtained for a packed-bed electrode (Figure 18c).

The bed length of a fluidized bed electrode normalized with respect to the bed

length of static state, that is symbolized as a dimensionless parameter, h, depends on the flow rate. With spherical Ni particles, the effect of the flow rate on the normalized bed length is shown in Figure 19. The normalized bed length is linearly dependent on the flow rate when the average particle radius is from 0.0063 cm to 0.017 cm. When the average particle radii were bigger than 0.036 cm, the particles in a Ni fluidized bed did not move even at a flow rate of 500cc/min.

5. Length of the Bed

Figure 20 shows the effect of the length of the bed on the rate of the reduction the electrolytic solution containing 1.95 M $NaNO_3$, 0.66 M $NaNO_2$, and 1.33 M NaOH at -0.8 V at a packed-bed (Figure 20a) and a fluidized-bed (Figure 20b) electrode. The average particle radius was 0.0113 cm.

At a packed-bed electrode, the total current for the reduction of the solution was found to increase with the length of the bed and then reach a limit at about 4 cm. This kind of limitation of bed length is due to the ohmic drop through the solution phase. When the solution resistivity is 1 Ωcm, the ohmic drop through the solution phase is estimated to be 0.6 V. Thus, part of the bed electrode becomes inactive. The depth of the active electorde in a bed electrode is called the effective depth, Thiele parameter, or penetration depth [14]. This is defined as the length of the electrode where 90% of the total current was transferred. In Figure 20a, the penetration depth is estimated to be 4 cm.

At a fluidized-bed electrode, the tendency of an increase in the reduction rate with an increase in the bed length diminished as the electrolyte flow rate increased through the fluidized-bed electrode. The penetration depth is strongly dependent on the flow rate. When the flow rate were 50 cc/min and 100 cc/min, the penetration depths were about 4.5 cm and 5.5 cm, respectively. When the rate was higher than 200 cc/min, it was difficult to determine the penetration depth. The primary variable for the penetration depth in a fluidized bed electrode is the effective conductivity of the discontinuous metallic phase.

6. Concentration Effect

a. Ru complex

Figure 21 shows the variations of the concentrations of nitrate and nitrite by potentiostatic electrolysis of 0.1 M $NaNO_3$ in 1.33 M NaOH at -0.7 V (vs NHE) within a Ni (50-100 mesh) packed-bed electrode in the presence of 0 mM, 0.04 mM, and 0.4 mM of the Ru nitrosyl complex. The decrease of the nitrate concentration with time varied slightly with the addition of the ruthenium complex, whereas the maximum concentration of nitrite decreased with an increase in the initial concentration of the ruthenium complex. Since the applied potential (-0.7 V) was more cathodic than the potential for mass transfer controlled reduction for the Ru complex (-0.5 V) in the section A.1.c., the electrode surface was considered to be partially covered with Ru metal. Also, the reduction of nitrite is considered to be faster at Ru than at Ni.

b. Chromate

As seen in section A.1.d or A.2.d, the product of chromate reduction has an inhibing effect. Addition of chromate to the electrolytic solution containing 0.1 M $NaNO_3$ in 1.33 M NaOH decreased the rate of the reduction of nitrate (Figure 22). From the concentration of nitrate in the electrolyzed solution, the rate constants for the reduction of nitrate in 1.33M NaOH containing 0, 0.03 mM, and 0.3 mM $CrO_4^{2-}$ at -0.7 V (vs NHE) at a Ni particles (50-100 mesh, average particle radius = 0.0113 cm) packed-bed electrode were obtained to be 0.1768 $hr^{-1}$, 0.0915 $hr^{-1}$, and 0.0627 $hr^{-1}$, respectively. Considering the particle size and bed size, one can convert the rate constants at -0.7 V as $1.223 \times 10^{-8}$ $cm^{-2}sec^{-1}$, $0.635 \times 10^{-8}$ $cm^{-2}sec^{-1}$, and $0.435 \times 10^{-8}$ $cm^{-2}sec^{-1}$, respectively. The peak current during the electrolysis also decreased with increasing concentration of chromate (Figure 22b). This clearly shows the inhibition of the reduction of nitrate by the chromate.

## B. Electrocatalysts

### 1. At Planar Electrodes

Figure 23 shows the polarization curves for the reduction of nitrate (1.95 M) in 1.33 M NaOH solution at Ni (Figure 23a) and Ti (Figure 23b), and for the reduction of nitrate (1.95 M) and nitrite (0.66 M) in 1.33 M NaOH at Pb (Figure 23c), Fe (Figure 23d), Graphite (Figure 23e), and Ebonex (Figure 23f) electrodes. At these electrodes, the reduction of nitrate takes place at the potentials less cathodic than the potentials for the hydrogen evolution reaction.

At a Ni electrode, the polarization curve in the solution containing 1.95 M $NaNO_3$ and 1.33 M NaOH looks similar to the i-V curve for the reduction of the solution containing 1.95 M $NaNO_3$, 0.66 M $NaNO_2$, and 1.33 M NaOH shown in Figure 4. The reduction of nitrate was divided into three regions - region I (from -0.4 to -0.65 V, slope = 0.3 V/decade) for the reduction of nitrate to nitrite, region II (from -0.65 to -0.8 V, slope = 0.03 V/decade) for the reduction of nitrite, and region III (more cathodic than -0.8 V, slope = 0.18 V/decade) for the reduction competing with the hydrogen evolution reaction. The equilibrium potential for the reduction of nitrate to nitrite is

$$NO_3^- + H_2O + 2e^- \rightleftarrows NO_2^- + 2OH^- \qquad E^\circ = 0.01V$$

The current density at -0.6 V was 22 $\mu A/cm^2$. The exchange current density for the reduction of nitrate to nitrite at a Ni electrode was thus obtained to be $2 \times 10^{-7}$ $A/cm^2$. The reduction of nitrite produces nitrogen or ammonia. Since the oxidation states of nitrogen atom in nitrogen and in ammonia gas are 0 and -3, respectively, the number of electrons required to reduce nitrite (oxidation state = +3) to nitrogen or ammonia are 3 or 5, respectively. Without the final state of the reduction, the exchange current density for the reduction of nitrite at a Ni electrode can not be determined.

The Tafel slope for the reduction of 1.95 M $NaNO_3$ in 1.33 M NaOH was 0.185

V/decade at a Ti electrode at the potential between -1.0 V and -1.2 V vs NHE (Figure 23b). The dramatic change of the Tafel slope as at a Ni electrode did not occur at the Ti electrode.

The Tafel slope is represented as

$$\frac{dE}{d(\log i)} = \frac{0.06}{\alpha} \qquad (8)$$

where E is the potential, i is the current density, and $\alpha$ is the transfer coefficient. The transfer coefficient is usually near to 0.5 when a rate determining step involves one electron transfer and when there is no electron-transfer quasi-equilibrium step before the rate determining step. In this case, the transfer coefficient is identical to the symmetry factor, $\beta$. At a Pb electrode, the Tafel slope for the reduction of the solution containing 1.95 M $NaNO_3$, 0.66 M $NaNO_2$, and 1.33 M NaOH was 176 mV/decade at potentials between -1.0 V and -1.5 V vs NHE (Figure 23c). The transfer coefficient for the reduction was then 0.33, which is less than the common value, 0.5. It is speculatively possible to see a distortion of a symmetric barrier in the fact that the potential of zero charge for Pb is -0.6 V on the Normal Hydrogen Scale [15]. In the potentials between -1.0 V and -1.5 V vs NHE, the nitrate ion will be approaching a negative surface and be repelled outward toward the solution (see Figure 24a). Thus the direction of distortion of symmetrical barrier would give a symmetry factor, $\beta$, less than 0.5, which is in consistent with the results. The mechanism for the reduction of nitrate at Pb electrode are proposed as follows.

$$(NO_3^-)_{sol} \rightleftarrows (NO_3^-)_{ad} \qquad \{1\}$$

$$(NO_3^-)_{ad} + H_2O + e^- \rightarrow (NO_2)_{ad} + 2OH^- \qquad \{2\}$$

$$(NO_2)_{ad} + e^- \rightleftarrows (NO_2^-)_{ad} \qquad \{3\}$$

$$(NO_2^-)_{ad} \rightleftarrows (NO_2^-)_{sol} \qquad \{4\}$$

or

$$(NO_2^-)_{ad} + H_2O + e^- \rightleftarrows (NO)_{ad} + 2OH^- \qquad \{4'\}$$

where step {2} is the rate determining step. The equilibrium potential for the reduction of nitrate to ammonia is -0.17 V. From the current density, 2.24 mA/cm$^2$, at -1.2 V, the exchange current density is calculated to be $3.16 \times 10^{-9}$ A/cm$^2$ with assuming that ammonia is the final product of the reduction process.

At the Fe electrode (Figure 23d), the Tafel slope was 85 mV/decade, i.e., $\alpha$ = 0.68. In order to rationalize a symmetry factor now larger than 0.5, it is relevant to observe that the potential range for the reduction of nitrate on Fe is around -0.95 V, i.e., 0.35 V less negative than in the situation for the approach of nitrate to the Pb electrode surface. Distortion of the symmetrical barrier forwards the electrode, not away from it, is hence understandable (Figure 24b). The rate determining step at Fe electrode is then still step {2}. From the current density, 2.13 mA/cm$^2$, at -0.9 V, the exchange current density for the reduction of nitrate to ammonia was $5.5 \times 10^{-12}$ A/cm$^2$. Though the exchange current density at the Fe electrode was less than at the Pb electrode, the current at a fixed potential was higher at the Fe electrode than at the Pb electrode because of the higher Tafel slope for Pb (Figure 24c). Thus, Fe electrode is favored for the reduction of nitrate at practical rates. However, the major concern of this research is to find electrocatalysts that produce nitrogen gas as the product rather than ammonia.

Electrochemical reduction of nitrate was also carried out at graphite electrode (Figure 23e). At the graphite electrode, the i-V curve had an interesting shape. The current at -1.3V had a maximum. The sudden decrease of current at a potential more cathodic than -1.35V seems to be coupled to the increase of the current for hydrogen evolution. This kind of phenomenon was found in the reduction of nitrate and nitrite in a strong alkaline solution at a Pt electrode [4]. This phenomenon may be interpreted in the following way. The rate determining step for the reduction of nitrate is step {2}, the rate of which is dependent on the coverage of the nitrate ions and water molecules on the surface. When the water molecules are reduced to hydrogen atoms

and hydroxide ions (i.e., the process of hydrogen evolution in alkaline solution), the coverage of water molecules may be reduced and, in turn, the rate of step {2} is reduced. From Figure 23e, the reduction rate of the nitrate reaction is about 15 $mA/cm^2$. Over this range of potentials, the hydrogen evolution rate is increased by only 2-3 $mA/cm^2$. However, in the Heyrovski mechanism of the hydrogen evolution reaction in alkaline solution involving a rate determining step of

$$H_2O + H_{ad} + e^- \rightarrow H_2 + OH^-,$$

the steady state coverage of $H_{ad}$ would be nearly 1 (i.e., the area of the electrode available to nitrate reduction radically reduced).

Why does not this phenomenon take place at Ni, Pb or Fe? This is related to the mechanism of hydrogen evolution at the electrodes. At Ni or Fe electrodes in alkaline solution [16], the hydrogen evolution reaction follows the Volmer mechanism which involves a low coverage of hydrogen.

$$H_2O + e^- \rightarrow H_{ad} + OH^-$$

At a Pb electrode, the exchange current density for the hydrogen evolution is small enough to have a low coverage of hydrogen. Thus no effect of the kind observed in Figure 23e will be observed.

A higher overpotential is required to reduce nitrate at the Ebonex™ electrode (Figure 23f). The current for the reduction of nitrate was about twice as much as the current for hydrogen evolution. Even though Ebonex™ is known as a stable material in a strong alkaline solution, it is not appropriate for use as an electrode for the reduction of nitrate. With similar reasoning, graphite is also abandoned because its ratio of the nitrate reduction current to the hydrogen evolution current is small compared with those values at Pb or Fe electrode.

2. At Bed Electrodes

Figure 25 shows the variations of the concentrations of nitrate and nitrite by potentiostatic electrolysis of the solution containing 1.95 M $NaNO_3$, 0.66 M $NaNO_2$, and 1.33 M NaOH at -0.9 V (vs NHE) within a Ni (50-100 mesh, average particle

radius = 0.0113cm) packed-bed electrode. With increasing time, the concentration of nitrate decreased while the concentration of nitrite increased.

The reduction of nitrate is considered to be consecutive as follows.

$$NO_3^- \rightarrow NO_2^- \qquad k_1$$

$$NO_2^- \rightarrow \text{product} \qquad k_2$$

Thus,

$$-\frac{d[NO_3^-]}{dt} = k_1[NO_3^-] \tag{9}$$

and

$$\frac{d[NO_2^-]}{dt} = k_1[NO_3^-] - k_2[NO_2^-] \tag{10}$$

From the equation (9),

$$[NO_3^-] = [NO_3^-]_o\, e^{-k_1 t} \tag{11}$$

and from the equations (10) and (11)

$$[NO_2^-] = [NO_2^-]_o\, e^{-k_2 t} + \frac{k_1}{k_2 - k_1}[NO_3^-]_o\,(e^{-k_1 t} - e^{-k_2 t}) \tag{12}$$

Using the initial concentrations of nitrate (1.95 M) and nitrite (0.66 M), the apparent rate constants were obtained from the equations (11) and (12). The initial rates (=rate constant times initial concentration) for the reductions of nitrate and nitrite as a function of applied potential are shown in Figure 26.

The rate of the reduction of nitrate to nitrite reaches a limit at -0.9 V. The rate at -0.9 V was $8.6 \times 10^{-6}$moles/sec. From this value, the current was calculated to be 1.7 A. Since the cross-sectional area of the bed electrode was 12.6 $cm^2$, the limiting superficial current density (total current divided by the cross-sectional area of the bed)

for the reduction of nitrate to nitrite was 140 mA/cm$^2$. If the reduction of nitrate to nitrite is diffusion-controlled, the limiting superficial current density should be 97 A/cm$^2$ from equation (3) with the diffusion layer thickness of 0.001cm, the voidage of 0.4, and the diffusion coefficient of $10^{-5}$ cm/sec$^2$. Thus, the limit in the reduction rate is not from the depletion of the concentration.

The superficial current density is explained as follows. One factor affecting the limiting density is that only a portion of the bed electrode is active for the reduction of nitrate. According to Goodridge and Wright [17], most of the Faradaic current passes through the interface at the top of the bed electrode. If only 1% of the bed electrode is active, the limiting current density for the reduction of nitrate would be 970 mA/cm$^2$. However, such a low percentage of active bed seems unreasonable.

Another factor that limits the reduction rate is satuation of nitrate coverage on the electrode surface. If the reduction of nitrate goes through the adsorption of nitrate and the rate depends on the adsorption coverage, the reduction rate would face a limititation with increasing overpotential. A model for the reduction of nitrate to nitrite is shown in Figure 27.

If the cleavage of N-O bond and the formation of $OH^-$ are rate determining, the limit of the nitrate reduction rate by the saturation of the nitrate coverage becomes a possibility. The other possible factor is that the hydrogen evolution competes for active sites with nitrate reduction. Since the equilibrium potential for the hydrogen evolution at pH 14 is -0.83 V vs NHE, the number of sites for the reduction of nitrate is reduced when the applied potential is more cathodic than this potential. The rate constant with increasing overpotential thus has an asymptote due to loss of active sites for the nitrate reduction.

Figure 28 is the log(rate) vs potential plot for the reduction of nitrite. Since the reaction rate is proportional to the current, the relation of the rate to the potential is

$$\frac{\partial \log(rate)}{\partial E} = -\frac{\alpha}{0.059} \qquad (13)$$

where $\alpha$ is the transfer coefficient of the reduction and is usually near to 0.5 at a planar electrode. Since the slope in the Figure 28 was 1/0.65, the $\alpha$ value was 0.091, far from the usual value of 0.5. According to the theory for the 3-dimensional electrodes [6,7,9], the slope, di/dE, at a three-dimensional electrode is one-half of the slope at a planar electrode. Thus, the $\alpha$ value at a planar Ni electrode was deduced to be 0.18, which is also well below 0.5. Thus, other effects like adsorption must be considered [15]. A model for the reduction of nitrite is shown in Figure 29. The reduction of nitrite at a Ni electrode in a strong alkaline solution is proposed as

$$NO_{2,sol}^- \rightleftarrows NO_{2,ad}^- \qquad \{4\}$$

$$NO_{2,ad}^- + e^- + H_2O \rightarrow NO_{ad} + 2OH^- \qquad \{4'\}$$

When the competitive adsorption of nitrite, nitrate, and water molecule is taken into account, a large $\alpha$ value is not reasonable [15]. Additional studies are needed to determine the detailed mechanism for nitrite reduction.

Figure 30 shows the yield percent for ammonia produced by the potentiostatic electrolysis of the solution containing 1.95 M $NaNO_3$, 0.66 M $NaNO_2$, and 1.33 M NaOH at various potentials. The yield percent for ammonia increased dramatically at -0.9 V. With a cathodic potential less tahn -0.8 V, the yield percent was less than 35%. The yield percent was calculated from the ratio of the number of moles ammonia produced to the number of moles of nitrate and nitrite reduced. From a comparison of Figure 26 and Figure 30, the higher the reduction rate, the higher the yield percent of ammonia.

Figure 31 shows the increase of nitrogen with time as a product of the potentiostatic electrolysis of 300 mL of the solution containing 1.95 M $NaNO_3$, 0.66 M $NaNO_2$, and 1.33 M NaOH at -1.0 V (vs NHE) at a Ni (50-100mesh, average particle radius = 0.0113 cm) packed-bed electrode. Before the electrolysis, the electrolytic solution was throughly purged with Ar for 1 hour. The $O_2$ and $N_2$ peaks at the initial sample was from the ambient air introduced while the syringe was transferred from cell to the injection port of GC. The major component of the initial sample was Ar which was not detected because the carrier gas in the GC was Ar.

The amount of nitrogen gas in 400 $\mu$L of the vapor sample increased as electrolyzing time increased. After 12 hours electrolysis, 75 mL of vapor was collected. Half (38 mL) of the vapor was nitrogen gas (see Figure 31). Since the solubility of nitrogen in water is 2%, total volume of the solution is 0.3 L, and the vapor presure of nitrogen is about 0.5 atm, the amount of nitrogen dissolved in the electrolyte is calculated to be 3 mL. Thus, the electrolysis produced about 41 mL of nitrogen ($N_2$). By the ideal gas law, the number of moles of nitrogen produced was about $3.6 \times 10^{-3}$ moles. For this electrolysis, the number of moles of ammonia produced was 0.168, and those of nitrate and nitrite reduced was 0.3. From the mass balance law, 0.13moles of nitrogen-containing products are still missing. Other products such as nitrogen oxide ($NO_2$), nitrous oxide ($N_2O$) and nitric oxide (NO) are possible products.

Table 3 shows the experimental results from the potentiostatic electrolysis of the waste solution at packed-bed electrodes. Columns (a), (b), and (c) in the Table 3 show the effect of potential on the electrolysis at a Fe packed-bed electrode. As the potentail shifts in a cathodic direction, the rate of nitrogen production increases a little while the yield percent for ammonia remains constant (60%). The concentration of hazardous products, NO and $NO_2$, decreases when the potential was shifted in the cathodic direction.

The rate constants for the reduction of nitrate and nitrite were plotted in Figure 32. It does not seem that the rate constants follow Tafel relation (i.e., $k \propto \exp(-b\eta)$ where $\eta$ is the overpotential and b is $\alpha F/RT$). This is because the reduction is coupled with hydogen evolution. The hydrogen evolution reaction interferes with the reduction of nitrate and nitrite by forming a competing reaction on the electrode surface. Even worse, the reduction of nitrate and nitrite was coupled with extensive corrosion of the Fe electrode. After 24 hour electrolysis, the concentration of Fe in the solution was $3 \times 10^{-4}$ M.

Columns (d) through (h) in Table 3 represent the effect of particle size on the electrolysis. The yield percent for ammonia was about 57% while that for nitrogen

was just 1 or 2%. The effect of particle size on the reduction of nitrate and nitrite is shown in Figure 33. The rate constants shown in the figure are apparent rate constants not geometrical rate constants per unit area. The apparent rate constant is inversely proportional to the radius of the particle.

$$k_{app} = k_{re} A V_e = k_{re} \frac{4\pi r^2}{\frac{4}{3}\pi r^3}(1-\epsilon)V_e = k_{re}\frac{3(1-\epsilon)}{r} \times V_e \qquad (14)$$

where $k_{app}$ is the apparent rate constant, $k_{re}$ is the rate constant per unit area, A is the specific area of the electrode in $cm^2/cm^3$, and $V_e$ is the volume of the bed electrode, r is the radius of particle, and $\epsilon$ is the voidage of the bed electrode. This relation is shown in Figure 33 as a broken line. The experimental values apparently deviated from this line when the radius of the particle was 0.0113 or 0.00625 cm. This deviation is explained in terms of hydrogen evolution. Hydrogen formed within the bed electrode will escape from the bed easily when the particle is big enough for the bed to have a wide channel. When the particle is small, hydrogen gas will be trapped inside of the bed and polarize the electrode.

At the Pb particle packed-bed electrode (columns (i) and (j) of Table 3), the reduction of nitrate and nitrite produced about 20% of ammonia and 8% of nitrogen. The major product of the reduction of nitrate at Pb electrode was nitrite. The ratio of the yield product for nitrogen to the yield product for the ammonia at the Pb electrode was higher than at Ni or Fe electrode. This is because there is less hydrogen to combine with nitrogen to form ammonia at the Pb surface than at Ni or Fe surface. The hydrogen evolution reaction at Pb is much less than at Ni or Fe. Thus, the reduction of nitrite to form ammonia is considered to involve hydrogen atom that is produced from water reduction in a strong alkaline solution.

The final product of the reduction of nitrate was reported dependent on the electrocatalysts [18,19]. Homogeneous catalysts like cobalt-cyclam (1,4,8,11-tetraazacyclotetradecane) [18] produced ammonia or hydroxylamine while

heterogeneous catalysts like bare metals [19] produced nitrogen as well as ammonia. Thus, a dimerization of intermediate of the reduction of nitrate was considered to be a key process to produce nitrogen [20]. If the intermediate has more chance to react with hydrogen atom at the electrode surface than to dimerize, the product will be ammonia.

### C. Temperature

Table 4 shows the effect of temperature on the experimental results of the potentiostatic electrolysis of the solution (0.25 L) containing 1.95 M $NaNO_3$, 0.66 M $NaNO_2$, and 1.33 M NaOH at -1.2 V vs NHE at a packed bed electrode which is composed of Pb particles (average particle radius = 0.065 cm). The cross-sectional area of the bed was 12.6 $cm^2$ and the length of the bed was 1 cm. The flow rate of the solution through the bed electrode was controlled at 200 cc/min.

As the temperature of the electrolytic solution increased, the reduction rates for nitrate ($k_1$) and nitrite ($k_2$) increased. From the equation

$$k=k_o\exp(-\frac{\alpha\eta F}{RT}) \qquad (15)$$

where k is the rate constant, $k_o$ is the pre-exponential factor, $\alpha$ is the transfer coefficient, $\eta$ is the overpotential, F is the Faraday constant, R is the gas constant, and T is temperature, the dependence of the rate constants on the temperature could be obtained on the assumption that the pre-exponential factor is constant (Figure 34). The values of $\alpha\eta$ for the reduction of nitrate and for nitrite were 0.116 V and 0.148 V, respectively. From equation (15), there should be a linear relationship between ln k and 1/T. However, the relation between ln k and 1/T was not linear. The non-linear dependence reflects the variable temperature dependence on the multiple-step, consecutive reactions occuring in the reduction of nitrate and nitrite.

Analysis of the electrolyzed solution showed that the yield for ammonia

increases as temperature increases. The same effect was found for the production of hydrogen. Thus, an increase in the evolution of hydrogen at the electrode surface is believed to be responsible for the increase in the yield of ammonia. Electrodes that have high overpotential for hydrogen evolution (e.g., Pb) should produce less ammonia, Clearly, ammonia production is reduced at lower temperatures. However, at lower temperatures the nitrate and nitrite reduction rates are also lower.

## D. Design

Based on the experimental results, electrochemical treatment of an alkaline nuclear waste solution containing nitrate, nitrite, Hg, Cr, and Ru is proposed as follows: (1) electrochemcial deposition of mercury at Ni electrode at potentials between 0.1 and -0.2 V, (2) electrochemical deposition of ruthenium and reduction of chromate at a Pb electrode, and (3) reduction of nitrate and nitrite to ammonia and nitrogen.

### 1. Electrochemical Deposition of Mercury at a Packed-Bed Electrode

In a packed-bed electrode, the concentration of electroactive species at the outlet of the bed is represented as follows [8b].

$$C_o = C_i \exp(-\frac{\epsilon DAL}{\delta u}) \qquad (16)$$

where $C_i$ and $C_o$, respectively, are the concentrations of the electroactive species at the inlet and at the outlet of a packed-bed electrode (see Figure 37), $\epsilon$ is the voidage of the bed, D is the diffusion coefficient of the electroactive species, L is the length of the bed electrode, $\delta$ is the diffusion layer thickness, u is the flow rate of the electrolyte through the electrode, and A is the specific area of the bed material which is defined in equation (2)

With $\epsilon$ = 0.4, $\delta$ = $10^{-3}$ cm, and D = $1 \times 10^{-5}$ $cm^2/sec$, equation (15) is

rearranged as

$$\frac{C_i}{C_o} = \exp\left(\frac{7.2x10^{-3} L}{ru}\right) \qquad (17)$$

Figure 35 and Figure 36 show the theoretical ratio of $C_i/C_o$ as functions of electrode length (L), particle radius (r) and flow rate (u). Suppose a cell has a packed bed electrode of which the bed length is 5 cm and the particle radius is 0.05cm, the flow rate will be determined to be 0.16 cm/sec for the outlet concentration to be one hundredth of the inlet concentration. Then, the characteristic length of the bed is calculated to be 1.1 cm from equation (4). Since the concentration of mercury(II) in the waste is 2.2$\mu$M, the superficial current density (current divided by the cross-sectional area of the bed) for the deposition of mercury is calculated to be 0.07mA/cm$^2$ from equation (3). The cross-sectional area of the bed electrode is determined by the amount of current to be applied. At a current of 0.5 A, the cross-sectional area of the bed is 7100 cm$^2$. From the result of the section A.2.b., the potential more cathodic than -0.1 V vs NHE is required when the electrode are composed of Ni particles.

2. Electrochemical Deposition of Ruthenium and Reduction of Chromate

At a Pb electrode, ruthenium is deposited on the electrode surface while chromate is reduced to water soluble Cr(III) at a potential of -0.7 V vs NHE, where both reactions are diffusion controlled. Since the concentration of chromate in the waste is 3 mM, the current for the reduction of chromate is very high as calculated in equation (3) - ca. 1000 A - when the same bed electrode size is employed as described in the previous section.

Since the concentration of the Ru complex in the waste is 40 $\mu$M, the potentiostatic electrolysis of the waste at -0.7 V at a Pb packed bed electrode (bed length = 5 cm, the cross-sectional area = 7100 cm$^2$, particle radius = 0.05 cm, flow rate = 0.16 cm/sec) will diminish the concentration of the Ru complex to 4 $\mu$M when

the diffusion coefficient of the complex is $0.5 \times 10^{-5}$ cm/sec$^2$ as obtained in the section A.1.c.

Simultaneously, the concentration of chromate in the outlet of the packed bed will be 0.03 mM assuming a diffusion coefficient of $10^{-5}$ cm/sec$^2$. Since the product of the reduction of chromate at a Pb electrode is soluble in a strong alkaline solution, the product will not inhibit the reduction of the Ru complex even at -0.7 V. Another bed electrode will diminish the concentration of chromate to 0.3 $\mu$M. Upon standing in a post electrochemical cell tank, the chromate reduction product will precipitate as chromic hydroxide. Filtration will remove the precipitate from the waste. The filltered solution will then be treated for the reduction of nitrate and nitrite.

3. Electrochemical Reduction of Nitrate and Nitrite

The reduction of nitrate and nitrite in alkaline solution is not mass transfer controlled, but charge transfer controlled. Passing through the bed electrode, the concentration of electroactive species decreases (see Figure 37) according to the mass action law,

$$C_{outlet} = C_{inlet} - \frac{I}{nFau} \qquad (18)$$

where u is the flow rate of the solution through the bed. With the entire volume, V, of the solution to be electrolyzed, the concentration of the electroactive species is

$$-V\frac{dC}{dt} = au(C_{inlet} - C_{outlet}) = \frac{I}{nF} \qquad (19)$$

If the current is dependent on the concentration of the electroactive species, i.e.,

$$I = nFkCaL \qquad (20)$$

where k is a constant, C is the concentration, a is the cross-sectional area of the bed electrode, and L is the length of the bed electrode, the concentration decreases

exponentially.

$$C=C_o e^{-\frac{kaL}{V}t} \qquad (21)$$

The decrease in concentration is independent of the flow rate of the solution.

Since the volume of the supernatant liquor at the Savannah River Site is about 410000 $m^3$ and is stored in over 35 different tanks, it is not possible to treat all of the waste simultaneously. Thus, in this designing work, the waste is considered to be treated as a batch system with a volume of 2500$m^3$. The treatment facility would be composed of packed-bed electrodes with a pump to circulate the waste solution. The size of the packed bed electrode was determined by utilizing the experimental data obtained previously.

A Ni-particle packed bed electrodes was selected as the reactor for the conceptual treatment design. The required charge to reduce nitrate and nitirte in the Savannah River Site waste is calculated from

$$\int_0^t I dt = n_1 F m_1 + n_2 F m_2 \qquad (22)$$

where $n_1$ and $n_2$ are 8 and 6, respectively, assuming the final product is ammonia and $m_1$ and $m_2$ are the number of moles of nitrate and nitrite reduced, respectively. The concentrations of nitrate and nitrite are assumed to be 1.95 M and 0.66 M, respectively. Since the volume of one batch is 2500$m^3$, the charge required to reduce the nitrate and nitrite is

$$(1.95 \times 8 + 0.66 \times 6) \times 2500000 \times 96500 = 4.7 \times 10^{12} \text{ Coulombs}$$

If the operation period is assumed to be 6 months, then the total current is

$$4.7 \times 10^{12} \text{ Coulombs} \div (6 \times 30 \times 24 \times 60 \times 60) \text{ seconds} = 300000 \text{ A.}$$

The calculations do not take into account the results obtained for potentiostatic electrolysis.

Taking into account the experimental results, one can design the packed bed

electrode as follows. The length (or height) of the packed bed electrode was decided from the dependence of current on the bed length. The effective length was 4 cm (see Figure 20). Up to 4 cm, the current increased with the height of the Ni particle packed-bed electrode at -0.8 V vs NHE. Since the current was 3A at Ni particle packed bed electrode at -0.9 V with the height of 2 cm (see Figure 11), the current will be 5 A when the height is 4 cm. Considering the non-uniform distribution of current through the packed-bed electrode, the length (or height) of the packed bed electrode should not be increased beyond 4 cm.

The cross-sectional area can be enlarged as much as manufacturing allows. However, it is difficult generally to manufacture a cell with an individual electrode area greater than 1 $m^2$ [21] Thus, 1$m^2$, i.e., 10000 $cm^2$ is chosen as the cross-sectional area of the packed-bed electrode. Since the current is 5 A with the cross-sectional area of 12.6 $cm^2$, the current will be 4000 A with the cross-sectional area of 10000 $cm^2$.

When the current is dependent on the concentrations of nitrate and nitrite, as seen in equations (20) and (21), with I = 4000A, nFC = (8 x 96500 x 1.95 + 6 x 96500 x 0.66) = $1.9\times10^6$ Coulomb/L, L = 4 cm, a = 10000$cm^2$, the constant k in equation (20) is calculated to be $5.3\times10^{-5}$ $sec^{-1}$. From equation (21), with the numbers used previously, the concentrations of nitrate and nitrite are

$$C = C_o \exp\left(-\frac{5.3\times10^{-5}\times4\times10^4}{2500\times10^6}t\right) = C_o \exp(-8.5\times10^{-10}t) \qquad (23)$$

In 6 month electrolysis, the concentrations will be diminished just by 1.3%. Thus, a number of the bed electrodes are necessary. Introducing a parameter for the number of electrodes in a batch, equation (23) becomes

$$C = C_o \exp(-8.5\times10^{-10}Nt) \qquad (23)$$

To diminish the concentrations to 1% in 6 month (i.e., $C/C_o$ = 0.01 and t = 6 x 30 x 24 x 3600 = $1.6 \times 10^7$ sec), one needs 338 of the bed electrodes.

As another extreme case, when the current is not dependent on the concentrations of nitrate and nitrite but is a constant (galvanostatic, e.g., 4000 A per electrode), the number of a packed bed electrode to reduce the nitrate and nitrite in one batch ($2500 m^3$) is 300000 ÷ 4000 = 75.

Summary for the design of the reduction of nitrate and nitrite is as follows (see Figure 38);

1. Total volume of the waste to be treated : 410 thousand cubic meters
2. Volume of a vessel for electrolysis : $2500 m^3$
3. Number of packed-bed electrode per vessel : more than 75 less than 338
4. Cross-sectional area of the packed-bed electrode : $10000 cm^2$
5. Thickness or height of the packed-bed electrode : 4 cm
6. Average radius of the Ni particles in the packed-bed electrode : 0.0113cm
7. Applied potential : -0.9 V vs NHE
8. Current at a packed bed electrode will be : 4000A
9. Current in an electrolysis vessel will be : 300000A
10. Period for completion of electrolysis will be : 6 months

The successive processes for the electrochemical treatment are shown in Figure 39. Metal ions are removed by a single pass but nitrate and nitrite are reduced by a multi-pass in a batch.

## SUMMARY of RESULTS

At a planar Ni electrode, the electrochemical reduction of the solution containing 1.95 M $NaNO_3$, 0.66 M $NaNO_2$, and 1.33 M NaOH solution had three Tafel slopes in three different regions - 300 mV/decade at from -0.4 V to -0.6 V; 30 mV/decade at from -0.7 V to -0.75 V; and 180 mV/decade at from -0.75 V to -1.0 V. These Tafel slopes revealed consecutive reductions of nitrate to nitrite, nitrite to ammonia or

nitrogen, and competition with hydrogen evolution, respectively.

The electrochemcal reduction of 0.5 mM Hg(II) in the solution became a diffusion controlled reaction at a Ni electrode at potentials more cathodic than -0.1V vs NHE. The product of the reduction was mercury metal.

The electrochemcal reduction of 0.4 mM $Na_2[RuNO(NO_2)_4OH]\cdot 2H_2O$ in the solution became a diffusion controlled reaction at a Ni electrode at potentials more cathodic than -0.5 V vs NHE. The product of the reduction was ruthenium metal.

The electrochemical reduction of chromate in 1.33 M NaOH at a Ni electrode produced chromic hydroxide on the electrode surface at -0.5 V vs NHE. The chromic hydroxide passivated the electrode and reduced the rate of the reduction of nitrate. At Pb, chromate is reduced to $CrO_2^-$, which is soluble and does not passivate the electrode.

At packed-bed and fluidized-bed electrodes that consist of Ni particles (50-100mesh, average particle radius = 0.0113 cm) with bed size of 12.6 $cm^2$ (cross-sectional area) x 2cm (length), the Tafel slopes for the reduction of nitrate and nitrite in 1.33M NaOH solution was 340 mV/decade, which was about twice as much as the Tafel slope an a planar electrode.

The potentials for the diffusion-limited reduction of mercuric hydroxide and the ruthenium nytrosyl compound at packed-bed and fluidized-bed electrodes were similar to those at a planar electrode.

Parametric studies show: (1) that smaller particle size favored the reduction of nitrate and nitrite at a packed-bed electrode, (2) that increasing the flow rate in a fluidized-bed cell decreases the reduction rate, and (3) that about 4cm of the bed height has the maximum total reduction current for nitrate and nitrite reduction at a packed-bed electrode.

A packed bed electrode is better than a fluidized bed for nitrate and nitrite reduction because the fluidized bed electrode has lower effective conductivity of electrode phase due to particle-particle collisions.

As far as the efficiency of the reduction of nitrate compared to that of $H_2O$ is concerned, Ni is a better cathode than Pb, Ti, Fe, or Graphite. Considering the

efficiency of the nitrate to nitrogen not ammonia, Pb is favored as a bed electrode material.

As temperature increases, the rate of the reduction of nitrate increases, the yield of ammonia increases, and the yield of nitrogen decreases.

## CONCLUSION

The electrochemical reduction of nitrate and nitrite and the electrochemical removal of trace metal species like Hg, Ru, and Cr in a strong alkaline solution (1.33M NaOH) can be adapted as a process for the treatment of the liquid nuclear waste at the Savannah River Site.

The optimum potentials and electrode materials were selected for the removal of Hg (-0.1V at Ni), Ru (-0.5V at Ni), and Cr (-0.7V at Pb). For fast reduction of nitrate, Ni and high temperature are preferred. For a relatively higher yield of nitrogen, Pb and low temperature are recommended. A packed bed electrode is prefered to a fluidized bed electrode for the reduction of nitrate and nitrite.

A preconceptual design of a treatment facility has been made to treat 2500$m^3$ of waste in 6 months.

## ACKNOWLEDGEMENTS

This work was funded by the Office of Technology Development Office of Environmental Management through the Efficient Separations and Processing Integrated Program, Teresa B. Fryberger, Headquarters Program Manager, and Allison M. Blackman, Cognizant Technical Program Officer.

## REFERENCES


1. H.-L.Li, D.H.Robertson, J.Q.Chambers and D.Hobbs, *J.Electrochem.Soc.*, 35(1988) 1154
2. D.T.Hobbs and M.A.Ebra, in "Electrochemical Engineering Applications" ed., by White, R.E. et al., AIChE Symposium Series 254 Vol.83, 1987, pp.149-155
3. D.Pletcher, I.Whyte, F.L.Walsh and J.P.Millington, *J.Appl.Electrochem.*, 21 (1991) 659
4. G.Horanyi and E.M.Rizmayer, *J.Electroanal.Chem.*, 188 (1985) 265
5. W.J.Plieth in "Encyclopedia of Electrochemistry of the Elements" ed. by A.J.Bard, Marcel Dekker, vol. VIII, Chap 5, 1978
6. S. E. Lyke and S. H. Langer, *J. Electrochem. Soc.*, 138 (1991) 2327
7. C. Gabrielli, F. Huet, A. Sahar and G. Valentin, *J. Appl. Electrochem.*, 23 (1992) 801
8. J.Bockris and S.Khan, "Surface Electrochemistry", Plenum, New York, 1993, p.961; A. K. P. Chu, M. Fleischmann and G. J. Hill, *J. Appl. Electrochem.*, 4 (1974) 323
9. M. Fleischmann and J. W. Oldfield, *J. Electroanal. Chem.*, 29 (1971) 211, 231; G. Kreysa, *Electrochim. Acta*, 25 (1980) 813
10. J.M.Fletcher, I.L.Jenkins, F.M.Lever, F.S.Martin, A.R.Powel, and R.Todd, *J.Inorg.Nucl.Chem.*, 1 (1955) 378
11. I.M.Kolthoff, E.B.Sandell, E.J.Meehan and S.Bruckenstein, "Quantitative Chemical Analysis", 4th ed., Macmillan, London, 1969, p.1156
12. R.C.Weast, ed., "CRC Handbook of Chemistry and Physics", 60th ed., CRC press, 1979
13. D.Rai, B.M.Sass and D.A.Moore, *Inorg. Chem.*, 26 (1987) 345
14. S. Szpak, in "Techniques for Characterization of Electrodes and Electrochemical Processes" ed. by R. Varma and J. R. Selman, John Wiley and Sons, Inc., 1991, p.677.

15. J.Bockris and S.Khan, "Surface Electrochemistry", Plenum, New York, 1993, p.90
16. G.Kreysa and B.Hakansson, *J.Electroanal.Chem.* **201** (1986) 61
17. F.Goodridge and A.R.Wright, in "Comprehensive Treatise of Electrochemistry" ed. by E. Yeager et al., Vol.6, pp.393
18. H. L. Li, W. C. Anderson, J. Q. Chambers and D. T. Hobbs, *Inorg. Chem.*, **28** (1989) 863
19. H. L. Li, J. Q. Chambers and D. T. Hobbs, *J. Appl. Electrochem.*, **18** (1988) 454
20. S. Kuwabata, S. Uezumi, K. Tanaka, T. Tanaka, *Inorg. Chem.*, **25** (1986) 3018
21. D. Pletcher and F. C. Walsh, "Industrial Electrochemistry",Chapman and Hill, New York, 1989, p.141

Table 1 Chemical Composition of Nuclear Waste Salt Solution [2]

| Component | wt% |
|---|---|
| $H_2O$ | 68.8 |
| $NaNO_3$ | 15.6 |
| $NaNO_2$ | 3.9 |
| $NaOH$ | 4.2 |
| $NaAl(OH)_4$ | 3.6 |
| $Na_2SO_4$ | 1.9 |
| $Na_2CO_3$ | 1.7 |
| Others[a] | 0.3 |

[a] Others include NaCl, NaF, $Na_2CrO_4$, $Na_2MoO_4$, $Na_3PO_4$, $NaSiO_3$ and $NaB(C_6H_5)_4$.

Table 2 Molar Absorptivity ($M^{-1}cm^{-1}$)

| | nitrate ($NO_3^-$) | nitrite ($NO_2^-$) | chromate ($CrO_4^{2-}$) | ruthenium complex |
|---|---|---|---|---|
| 270nm | 2.2 | 7.5 | - | 855 |
| 300nm | 7 | 9 | 660 | 487.5 |
| 353nm | 0 | 23 | 3630 | 187.5 |
| 372nm | 0 | 13.8 | 5038 | - |

Table 3 Potentiostatic electrolysis of synthetic waste solution within packed-bed electrodes.

| | (a) | (b) | (c) | (d) | (e) | (f) | (g) | (h) | (i) | (j) |
|---|---|---|---|---|---|---|---|---|---|---|
| electrode material | Fe | Fe | Fe | Ni | Ni | Ni | Ni | Ni | Pb | Pb |
| particle size (radius, cm) | 0.016 | 0.016 | 0.016 | 0.00625 | 0.01125 | 0.017 | 0.036 | 0.05 | 0.065 | 0.065 |
| potential applied (V vs NHE) | -1 | -1.1 | -1.2 | -0.9 | -0.9 | -0.9 | -0.9 | -0.9 | -1.2 | -1.3 |
| volume of electrolyte (L) | 0.3 | 0.3 | 0.3 | 0.25 | 0.25 | 0.25 | 0.25 | 0.25 | 0.3 | 0.25 |
| electrolyzing time (hours) | 24 | 24 | 24 | 12 | 12 | 12 | 12 | 12 | 7 | 4.5 |
| average current (A) | 1.3 | 2.05 | 3.2 | 2.2 | 2.6 | 3.1 | 2.3 | 1.7 | 2.4 | 3 |
| initial conc. of nitrate (M) | 1.852 | 1.879 | 1.748 | 1.803 | 1.847 | 1.812 | 1.8 | 1.837 | 1.96 | 2.04 |
| final conc. of nitrate (M) | 1.496 | 1.174 | 0.862 | 1.186 | 1.184 | 1.135 | 1.341 | 1.474 | 1.19 | 1.32 |
| initial conc. of nitrite (M) | 0.639 | 0.621 | 0.605 | 0.638 | 0.635 | 0.622 | 0.623 | 0.598 | 0.72 | 0.73 |
| final conc. of nitrite (M) | 0.372 | 0.302 | 0.23 | 0.426 | 0.477 | 0.437 | 0.37 | 0.458 | 0.87 | 1.02 |
| ammonia produced (moles) | 0.114 | 0.175 | 0.245 | 0.114 | 0.111 | 0.118 | 0.11 | 0.073 | 0.041 | 0.036 |
| nitrogen produced (ml) | 130 | 270 | 512 | 25 | 30 | 51 | 29 | 41 | 215 | 174 |
| hydrogen produced (ml) | 4 | 6 | 18 | 19 | 1 | 3 | 52 | 171 | 108 | 77 |
| nitric oxide (ppm) | 400 | 320 | 120 | 440 | 2880 | 20160 | 480 | 160 | 4800 | 50 |
| nitrogen dioxide (ppm) | 44 | 8 | 4 | 100 | 360 | 2800 | 48 | 2 | 1500 | |
| yield for ammonia (%) | 61 | 57 | 65 | 55 | 54 | 55 | 62 | 58 | 18 | 20 |
| yield for nitrogen (%) | 6 | 7 | 11 | 1 | 1 | 2 | 1 | 3 | 8 | 8 |
| rate constant, $k_1$ (/sec) | 2.96E-05 | 6.24E-05 | 8.51E-05 | 9.55E-05 | 1.09E-04 | 1.18E-04 | 6.90E-05 | 5.85E-05 | 2.31E-04 | 3.43E-04 |
| rate constant, $k_2$ (/sec) | 1.67E-04 | 2.79E-04 | 3.74E-04 | 3.64E-04 | 3.47E-04 | 3.89E-04 | 3.28E-04 | 2.41E-04 | 3.34E-04 | 4.43E-04 |

Bed Size = 12.6 $cm_2$ x 2 cm high
Flow rate = 200cc/min

Table 4 Potentiostatic electrolysis of synthetic waste solution within packed-bed electrodes as a function of temperature

| | (a) | (b) | (c) | (d) | (e) |
|---|---|---|---|---|---|
| temperature (C) | 15 | 39 | 46 | 61 | 76 |
| average current (A) | 1 | 1 | 1.2 | 1.5 | 2.1 |
| initial conc. of nitrate (M) | 1.81 | 1.906 | 1.882 | 1.831 | 1.86 |
| final conc. of nitrate (M) | 1.585 | 1.579 | 1.529 | 1.438 | 1.3 |
| initial conc. of nitrite (M) | 0.65 | 0.644 | 0.668 | 0.645 | 0.655 |
| final conc. of nitrite (M) | 0.767 | 0.803 | 0.8 | 0.775 | 0.733 |
| ammonia produced (moles) | 0.00825 | 0.0154 | 0.018 | 0.027 | 0.0435 |
| nitrogen produced (ml) | 36 | 40 | 62 | 49 | 36.5 |
| hydrogen produced (ml) | 4.3 | 11.5 | 16.5 | 47.5 | 63.7 |
| yield for ammonia (%) | 15 | 19 | 20 | 27 | 31 |
| yield for nitrogen (%) | 5 | 4 | 6 | 4 | 2 |
| yield for nitrite(%) | 52 | 49 | 37 | 33 | 14 |
| rate constant, $k_1$ (/sec) | 6.74E-06 | 9.28E-06 | 9.93E-06 | 1.14E-05 | 1.61E-05 |
| rate constant, $k_2$ (/sec) | 9.31E-06 | 1.24E-05 | 1.35E-05 | 1.74E-05 | 2.81E-05 |

| | | |
|---|---|---|
| electrode material | : | Pb |
| particle size (radius, cm) | : | 0.065 |
| height of bed(cm) | : | 1 |
| area of bed(cm2) | : | 12.6 |
| direction of flow | : | down |
| flow rate(cc/min) | : | 200 |
| position of Luggin tip | : | bottom |
| potential applied (V vs NHE) | : | -1.2 |
| volume of electrolyte (L) | : | 0.25 |
| electrolyzing time (hours) | : | 6 |

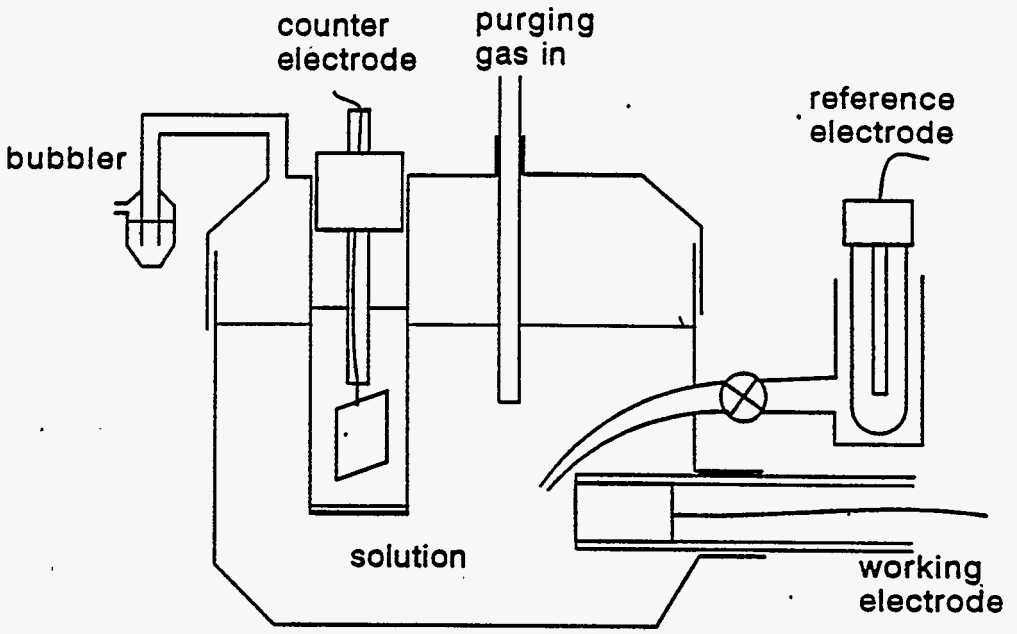


Fig. 1 Electrochemical Cell for a Planar Electrode

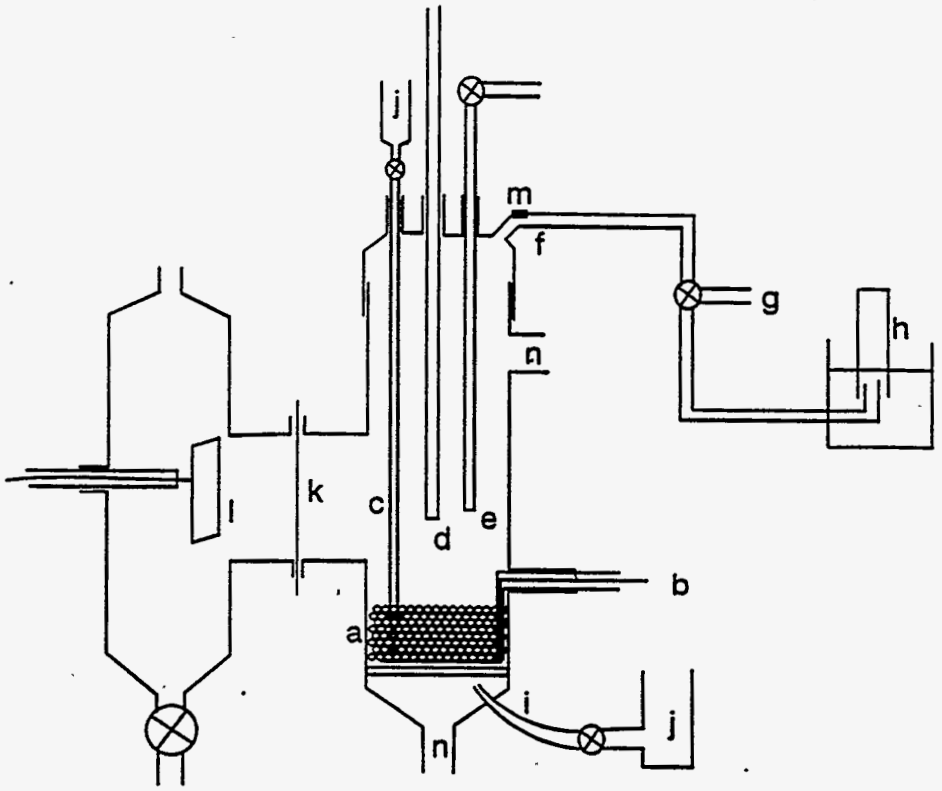


a : Bed of particles
b : Current Collector (Ni gauze)
c : Luggin Capillary
d : Thermometer
e : Purging Gas In
f : Gas Out
g : Bubbler
h : Gas Collector
i : Luggin Capillary
j : Reference Electrode
k : Nafion® Film
l : Counter Electrode
m : Septum for Gas Analysis
n : Solution Flow-In or Flow-Out

Fig. 2 Electrochemical Cell for 3-dimensional Electrodes

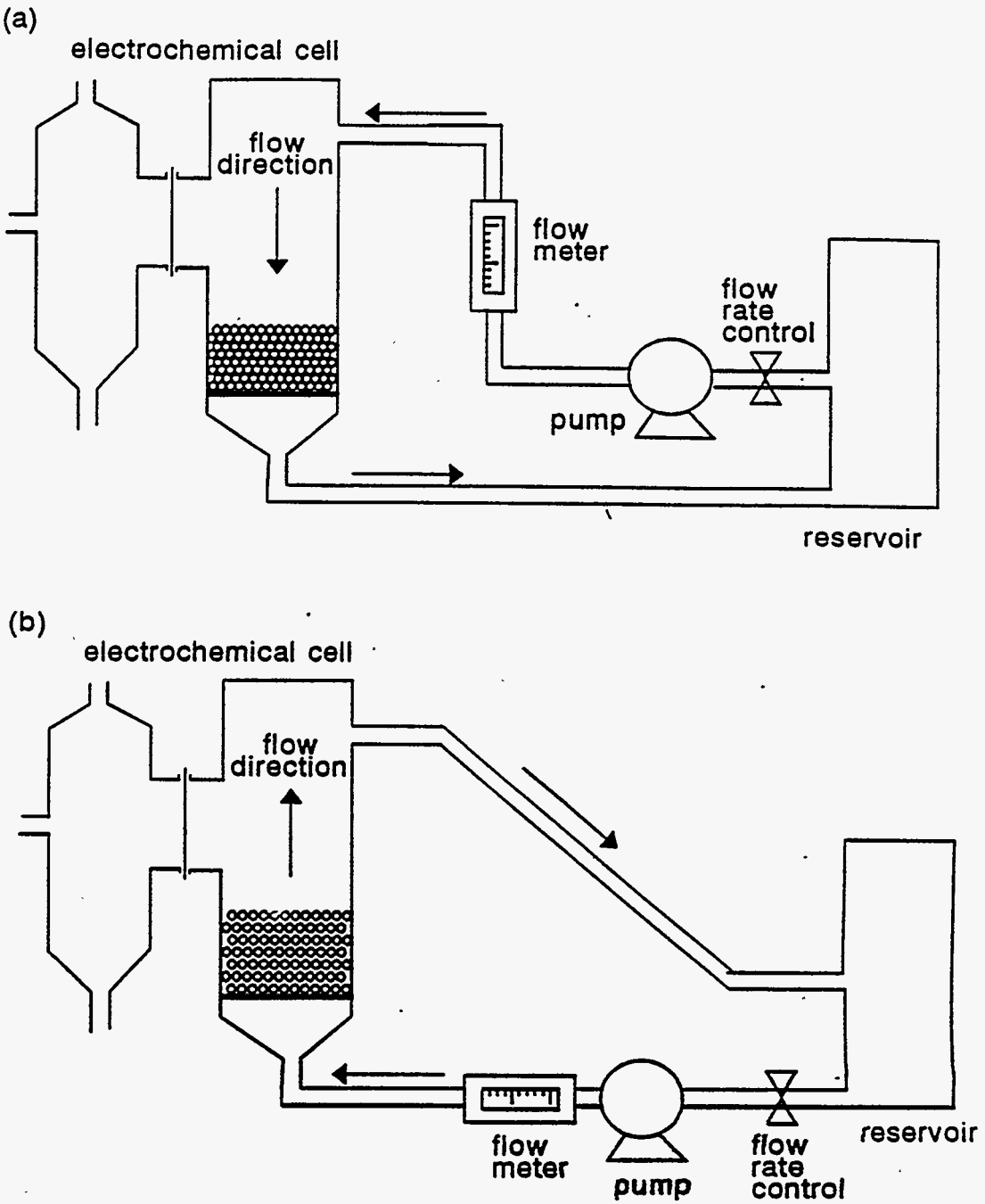


Fig. 3 Schematics for (a) a Packed Bed Electrode and (b) a Fluidized Bed Electrode

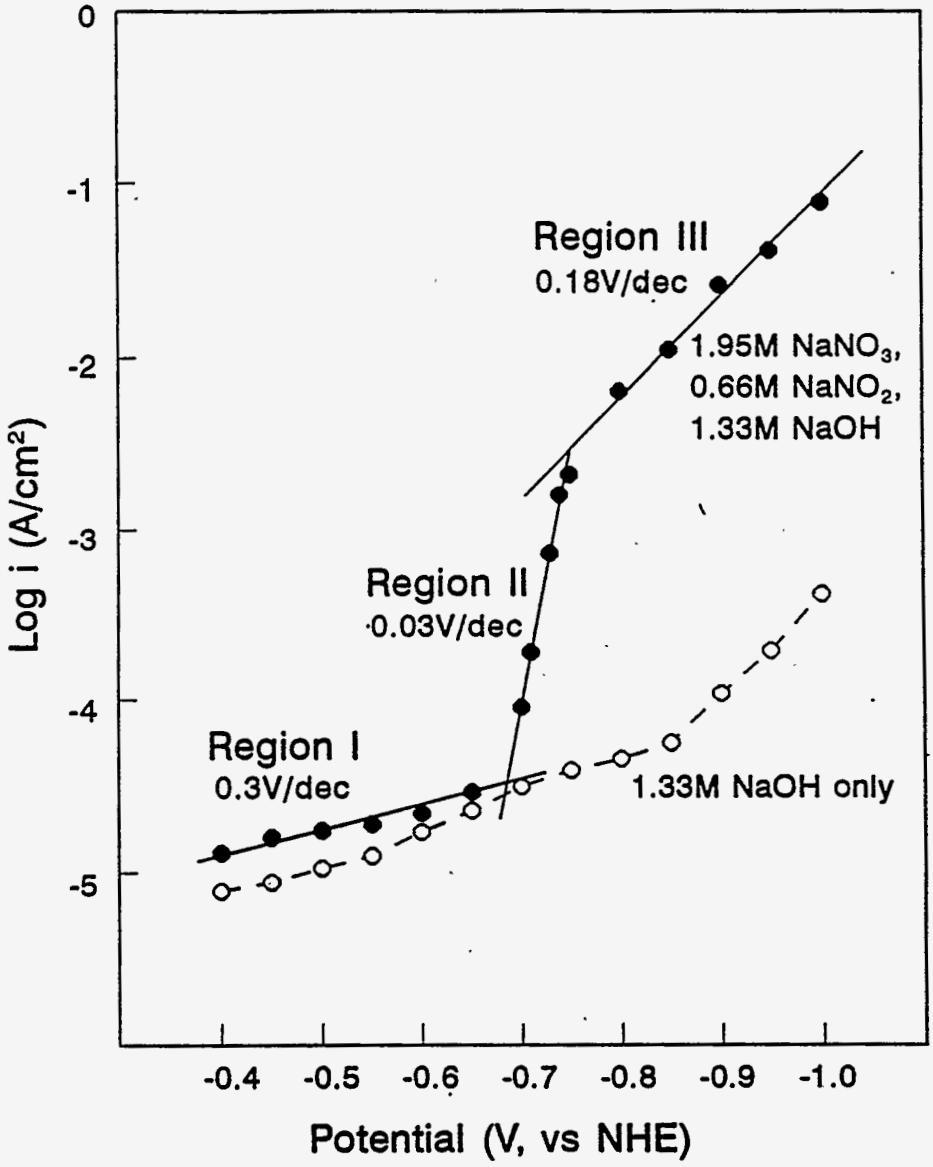


Fig. 4 Electrochemical Reduction of the Solution Containing 1.95M $NaNO_3$, 0.66M $NaNO_2$, and 1.33M NaOH at a Ni Electrode

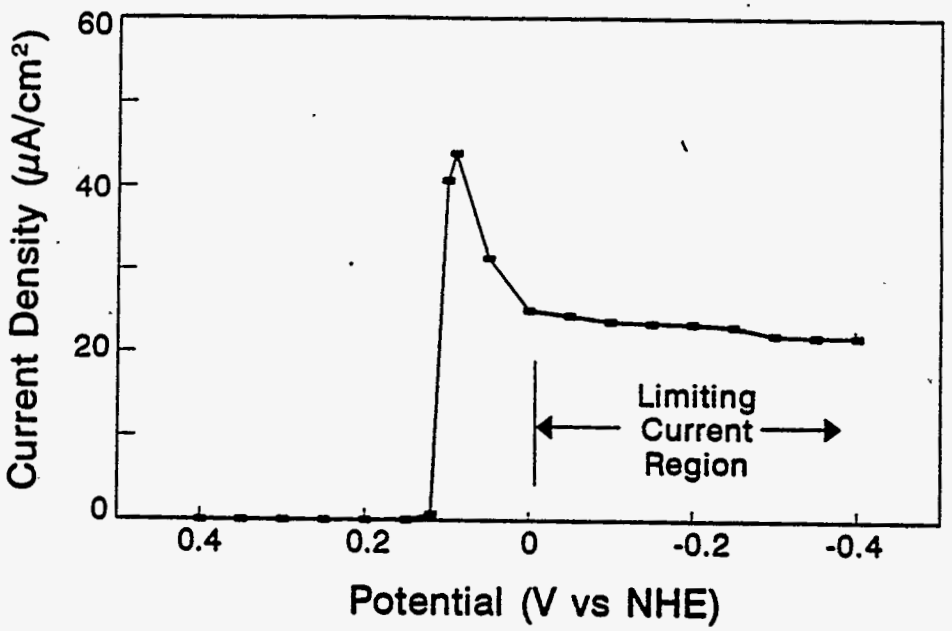


Fig. 5 I-V for the Reduction of Hg(II)

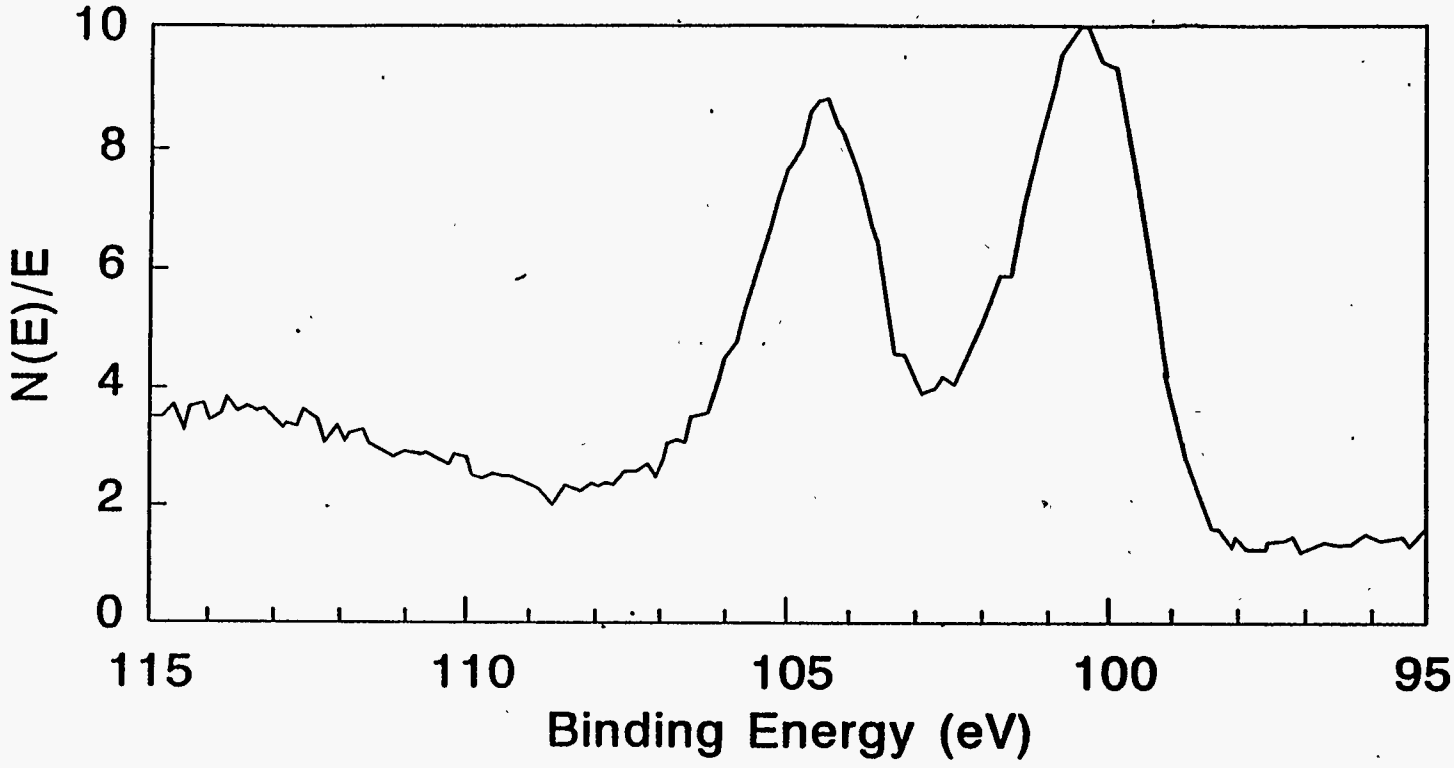


Fig. 6 XPS for the Deposit in a Solution Containing 0.5mM $Hg(NO_3)_2$, 1.95M $NaNO_3$, 0.66M $NaNO_2$, and 1.33M NaOH at -0.1V vs NHE

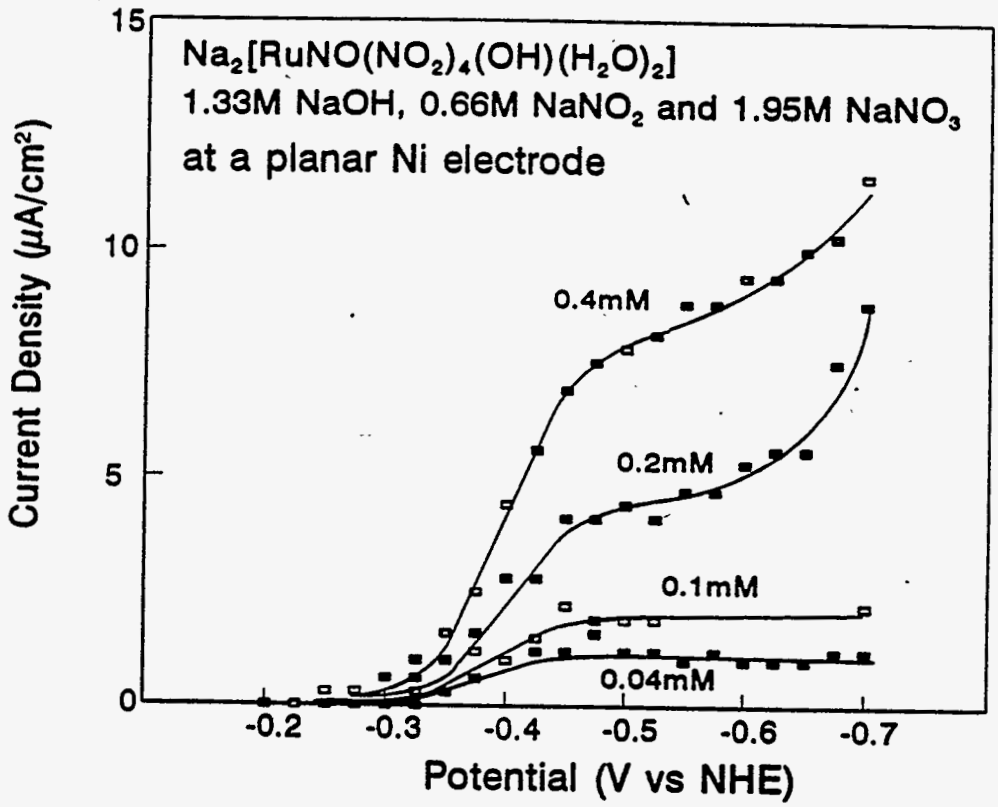


Fig. 7 The I-V curves for the reduction of the Ru complex

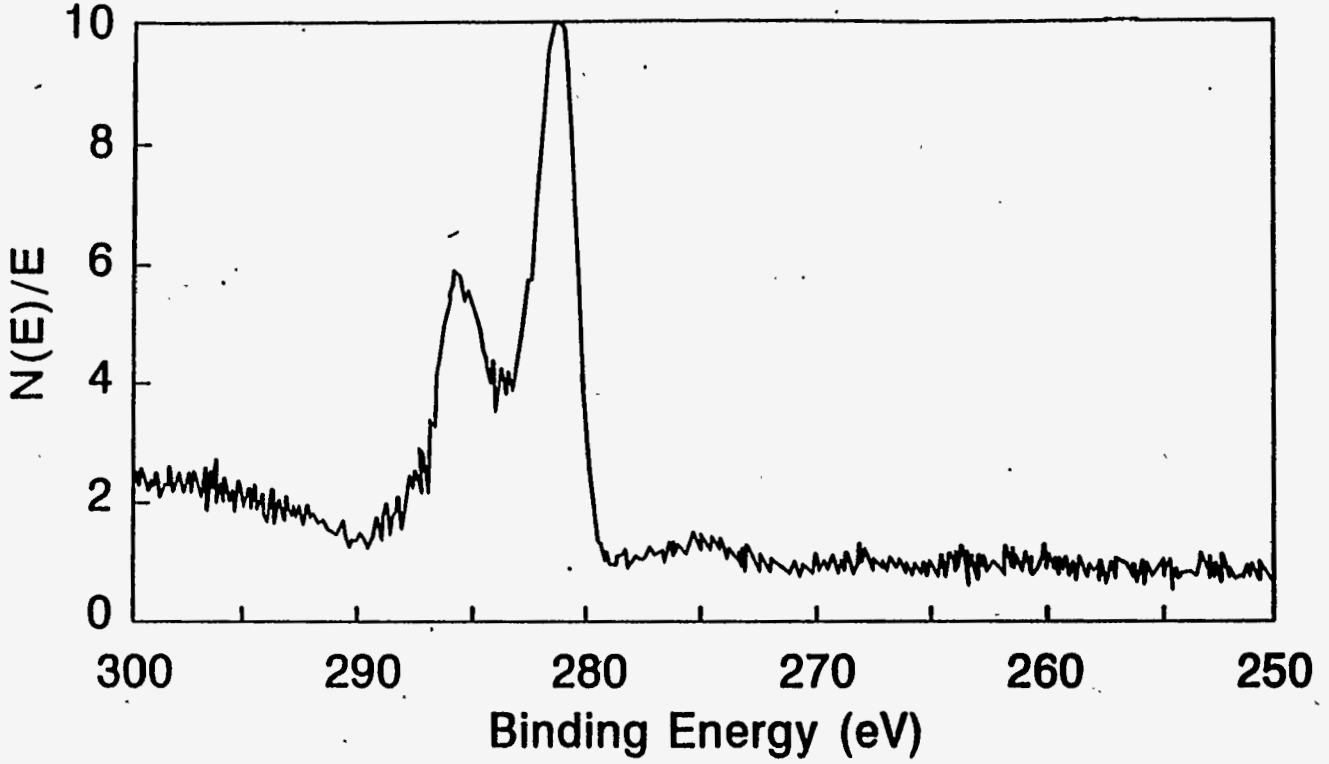


Fig. 8 XPS for Ruthenium Deposited in a Solution Containing 0.04mM Ru complex, 1.95M $NaNO_3$, 0.66M $NaNO_2$, and 1.33M NaOH at -0.5V vs NHE for 1 hour

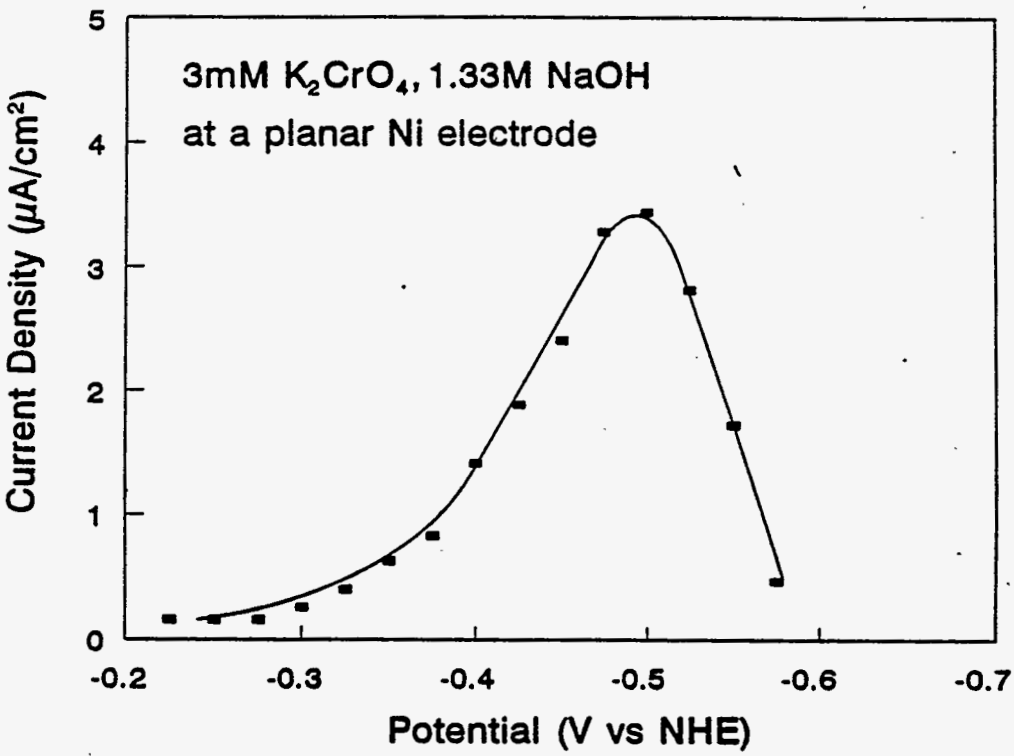


Fig. 9 The I-V curves for the electrochemical reduction of chromate

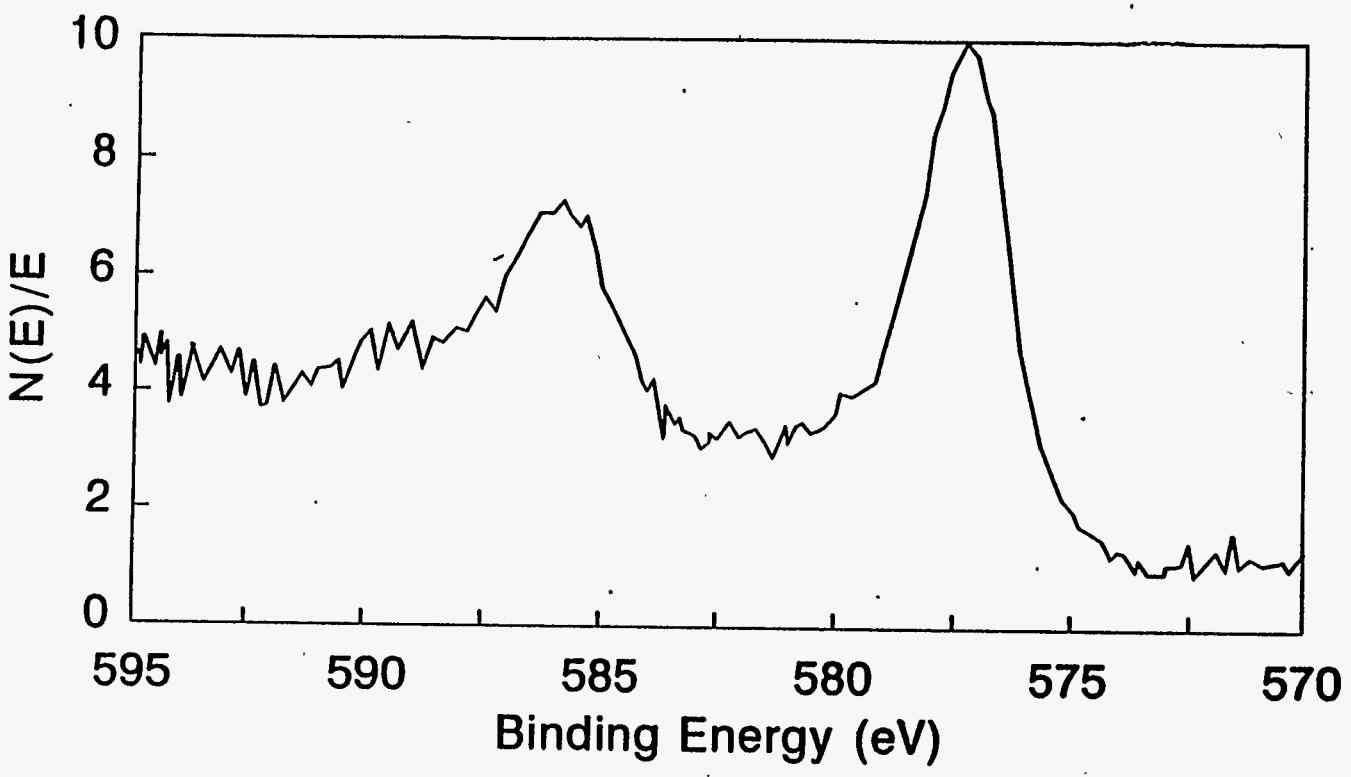


Fig. 10 XPS of the Product of Electrolysis of 0.3mM $K_2CrO_4$ in 1.33M NaOH at a Ni electrode at -0.5V vs NHE for 10 minutes

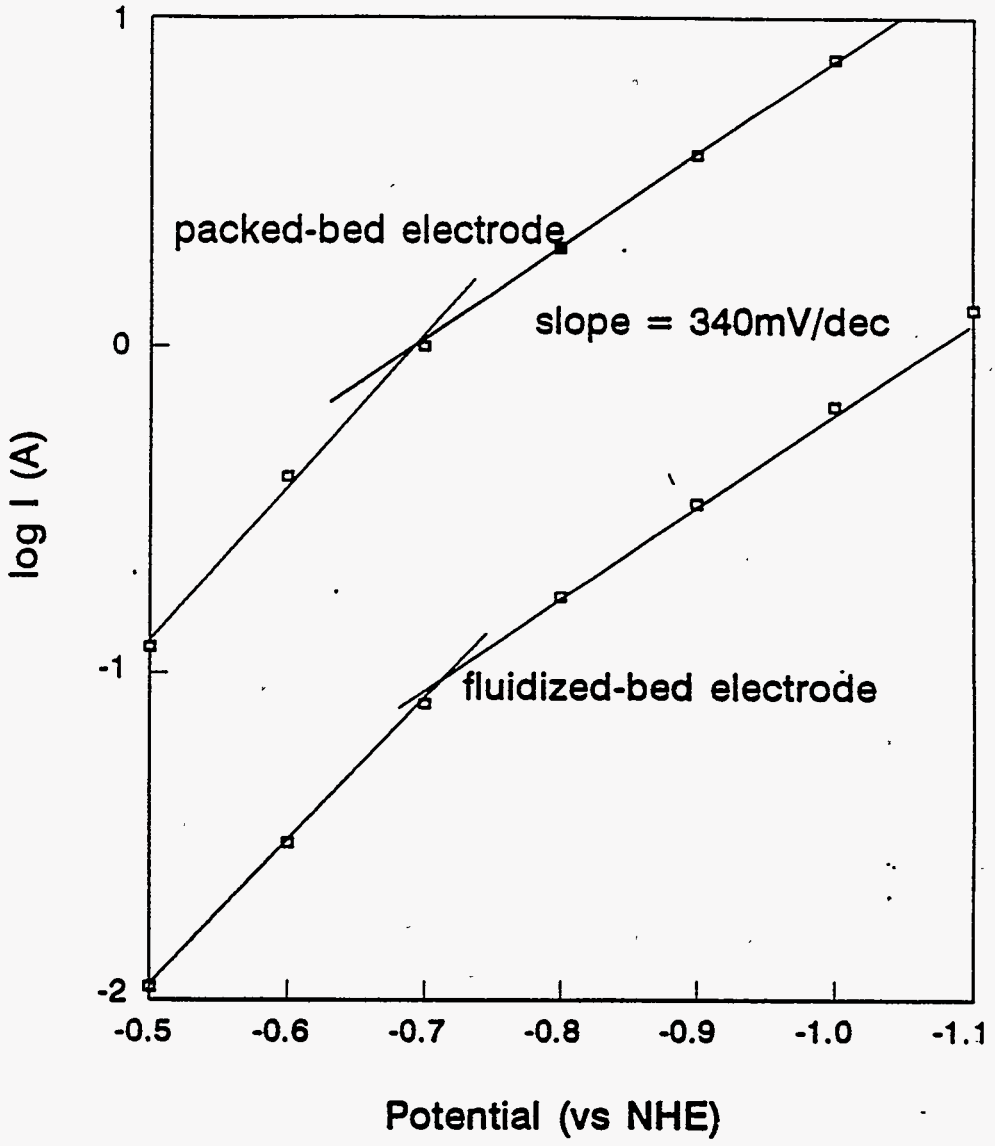


Fig. 11 Log I-V curves for the electrochemical reduction of the waste solution at three-dimensional electrodes

Ni particles (100-150 mesh)
12.6cm$^2$ x 2 cm

Ni particles (50-100 mesh)
Applied Potential = -0.7 V

Bed Size = 12.6 $cm^2$ x 2 cm
$[NaNO_3]$=0.1M, [NaOH]=1.33M

(a) Currents

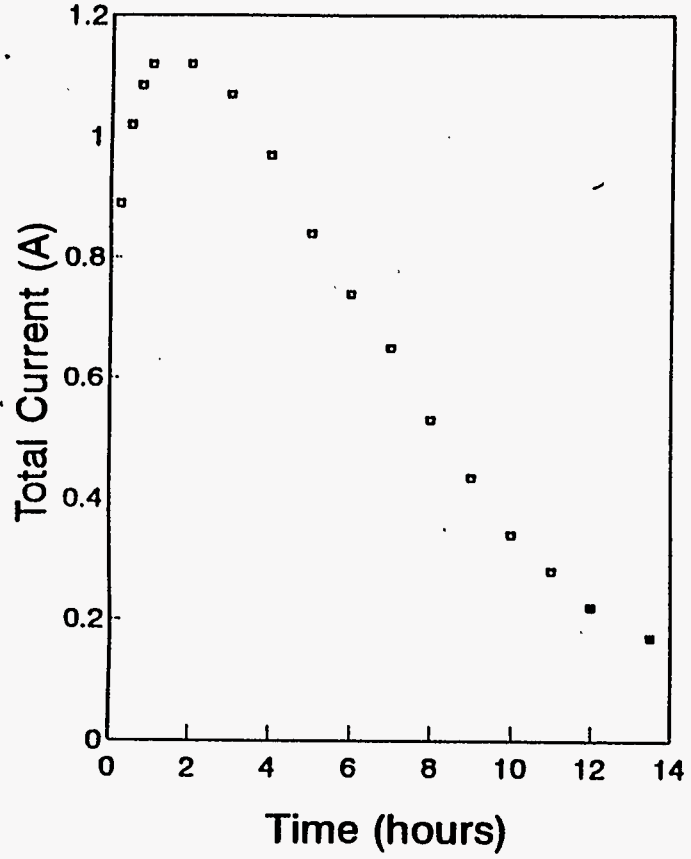


(b) Concentrations

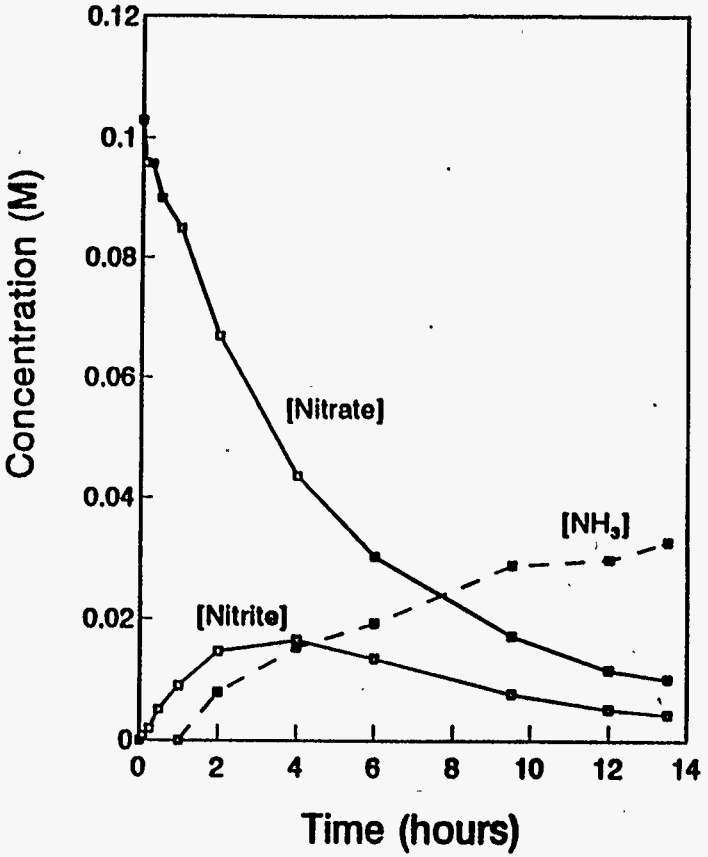


Fig. 12 Potentiostatic electrolysis at a Ni packed bed electrode

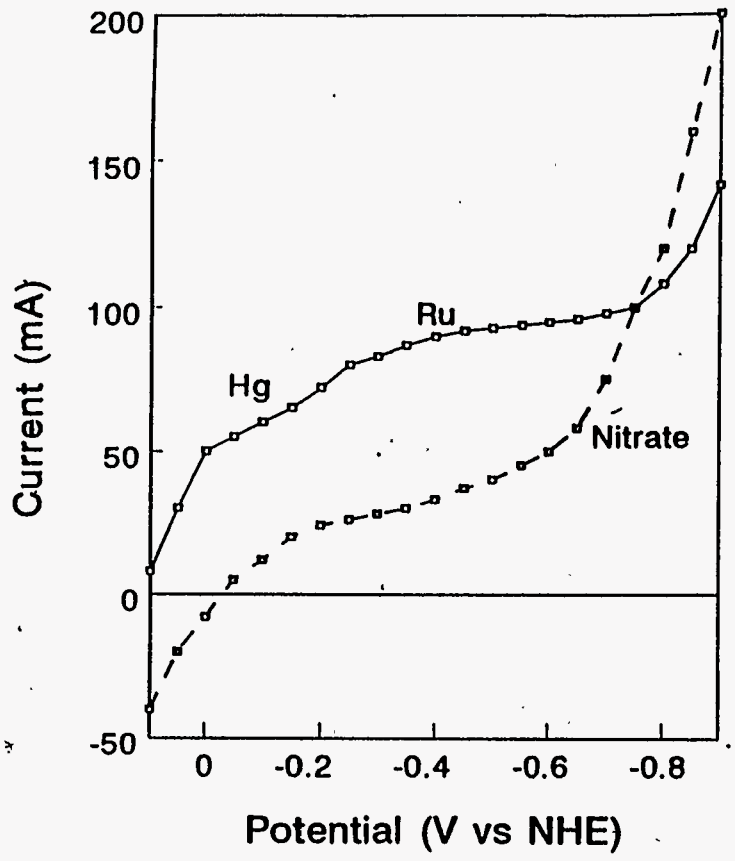


(a) at a packed-bed electrode

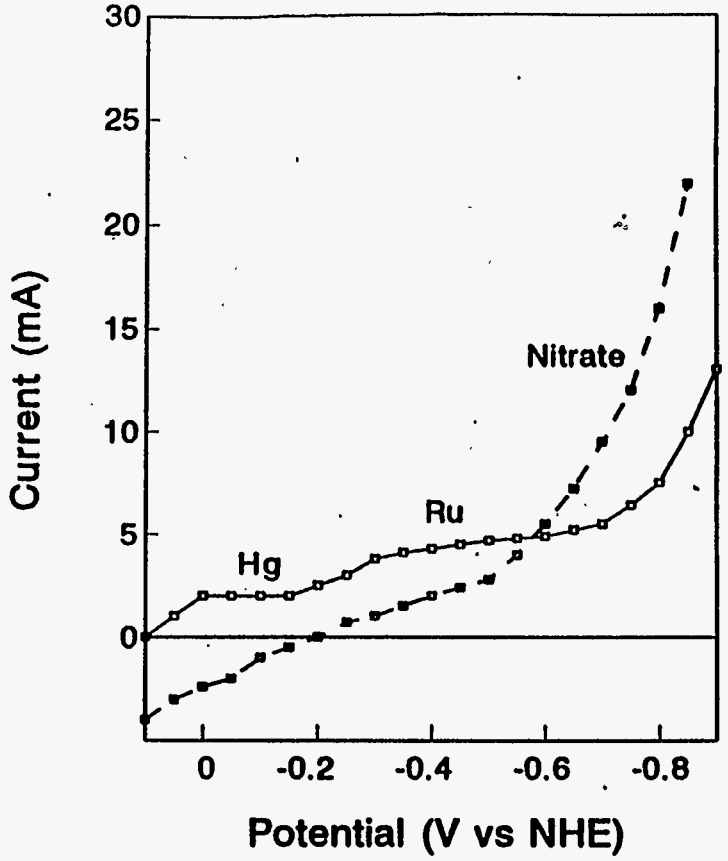


(b) at a fluidized-bed electrode

Fig. 13 I-V curves for the reduction of Hg(II) and Ru(III) at three-dimensional electrodes

Solution : 1.33M NaOH, 1.95M $NaNO_3$, and 0.66M $NaNO_2$
with (solid line) and without (broken line) 0.5mM $Hg(NO_3)_2$ and 1mM $RuCl_3$
Flow Rate : 240cc/min
Ni particles (100-150mesh) 12.6cm² x 2cm
Scan Rate : 2 mV/sec

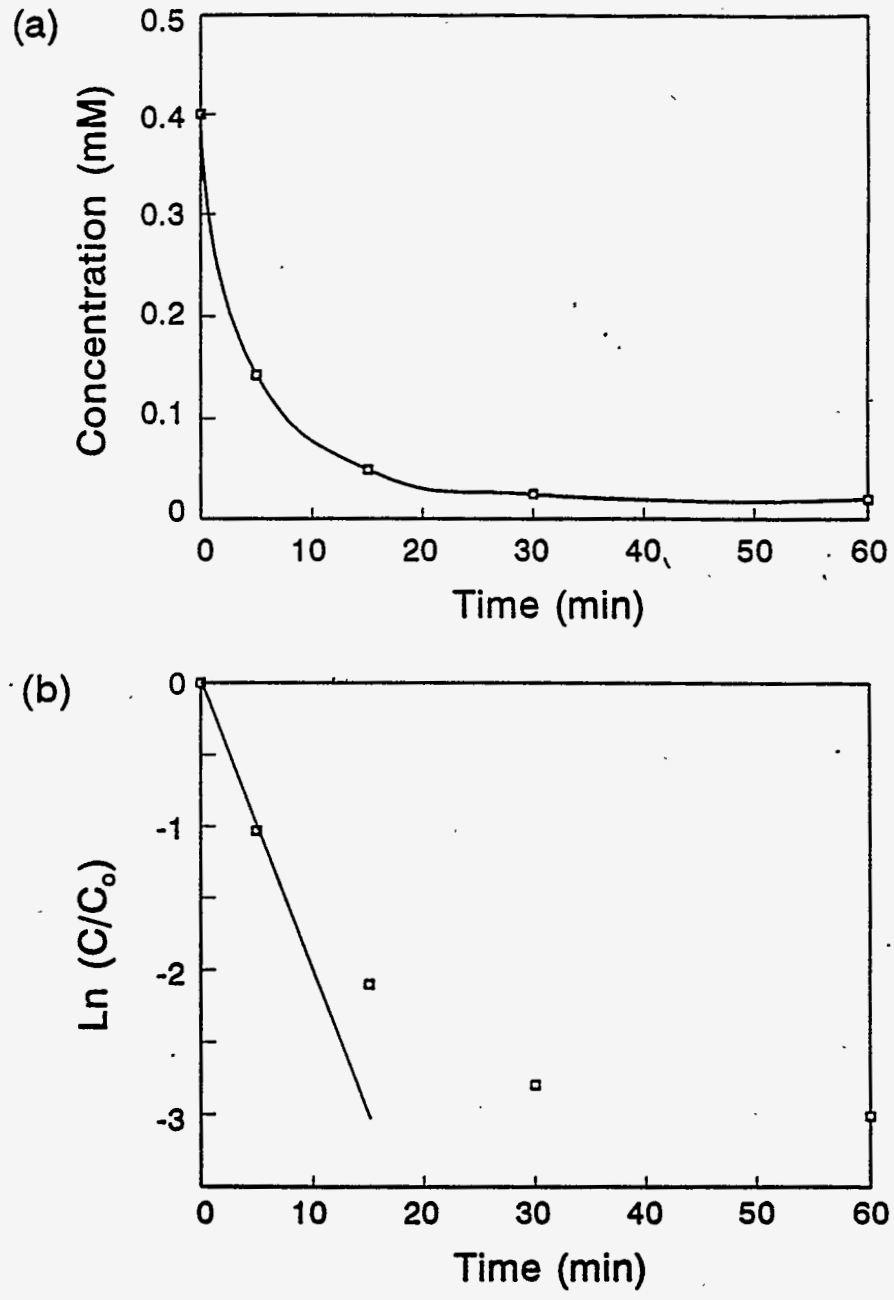


Fig. 14 Electrochemical Removal of Ru Complex in the electrolysis of 0.5L of a solution containing 0.4mM Ru complex, 0.1M $NaNO_3$, and 1.33M NaOH at -0.7V vs NHE at a Ni-particles-packed bed electrode
(a) Concentration vs Time
(b) ln ($C/C_o$) vs Time

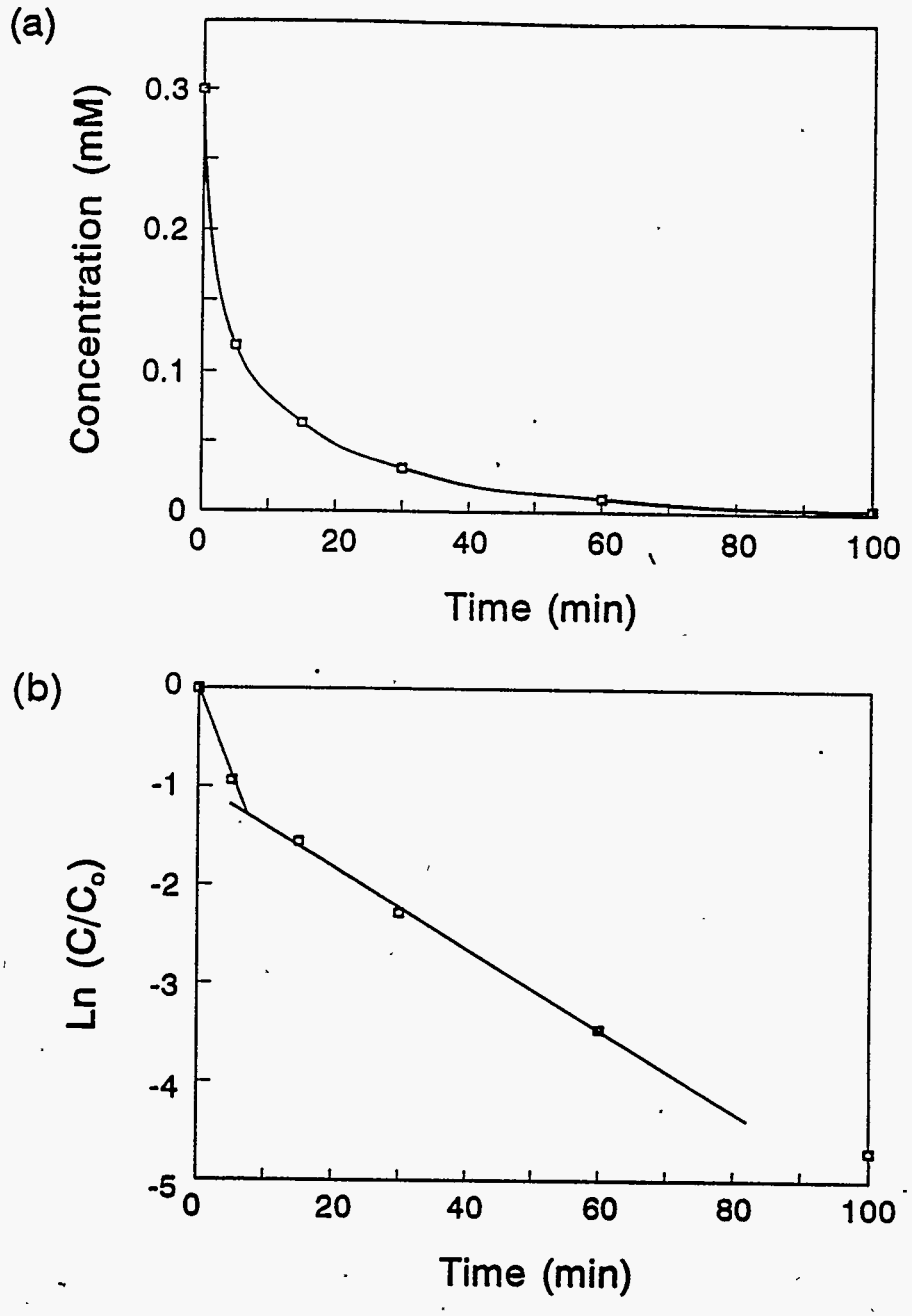


Fig. 15 Electrochemical Removal of Chromate in the electrolysis of 0.5L of a solution containing 0.3mM $K_2CrO_4$, 0.1M $NaNO_3$, and 1.33M NaOH at -0.7V vs NHE at a Ni-particles-packed bed electrode
(a) Concentration vs Time
(b) ln ($C/C_o$) vs Time

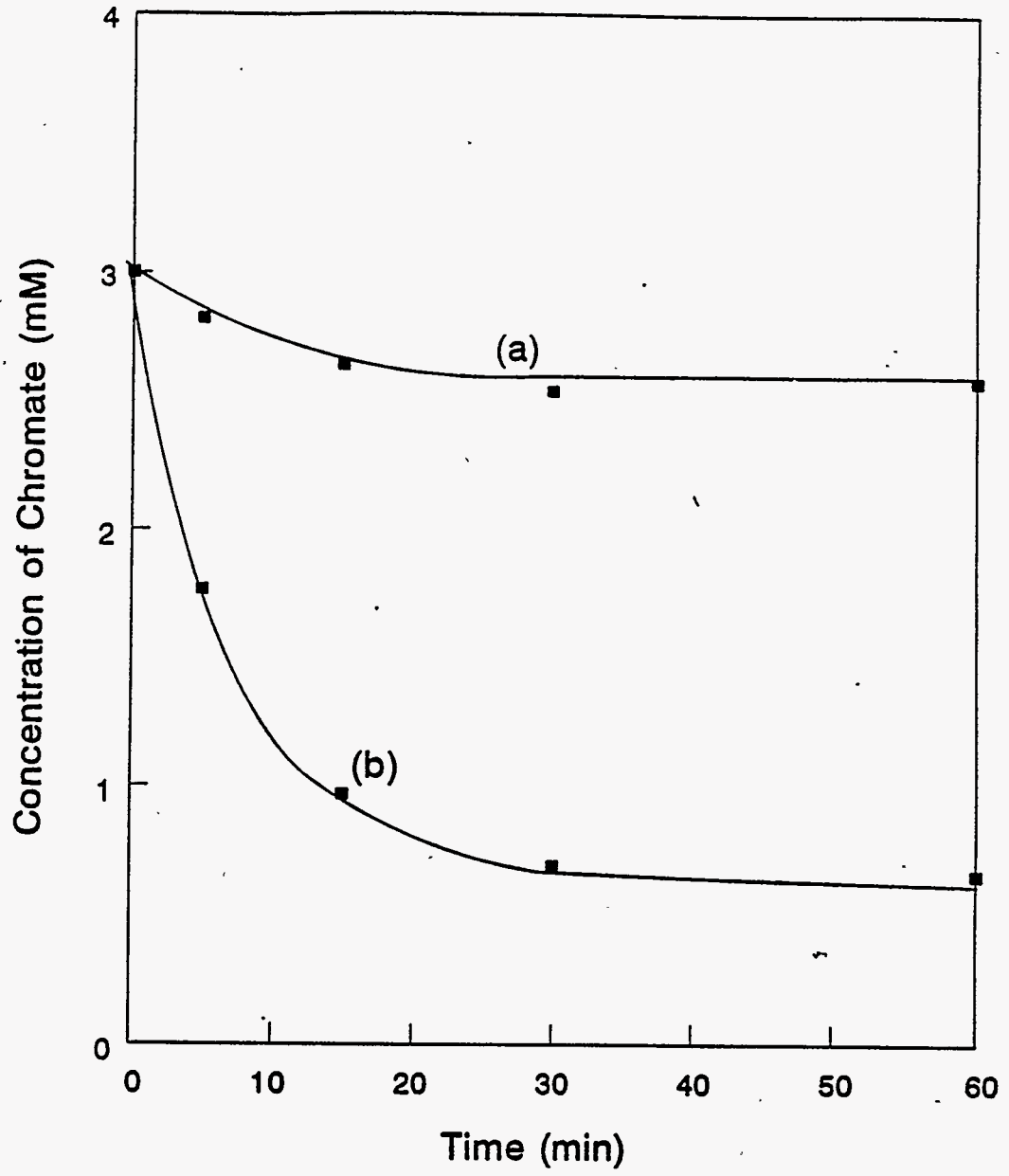


Fig. 16 Concentration of Chromate in the electrolysis of the solution containing 3mM $K_2CrO_4$, 2$\mu$M $Hg(NO_3)_2$, 40$\mu$M Ru complex, 1.95M $NaNO_3$, 0.66M $NaNO_2$, and 1.33M NaOH at -0.7V vs NHE at (a) a Ni packed bed electrode - <r> = 0.034cm and at (b) a Pb packed bed electrode - <r> = 0.065cm Flow Rate = 200cc/min; Volume of the solution = 300mL Cross-sectional area = 12.6cm$^2$; Bed length = 2cm

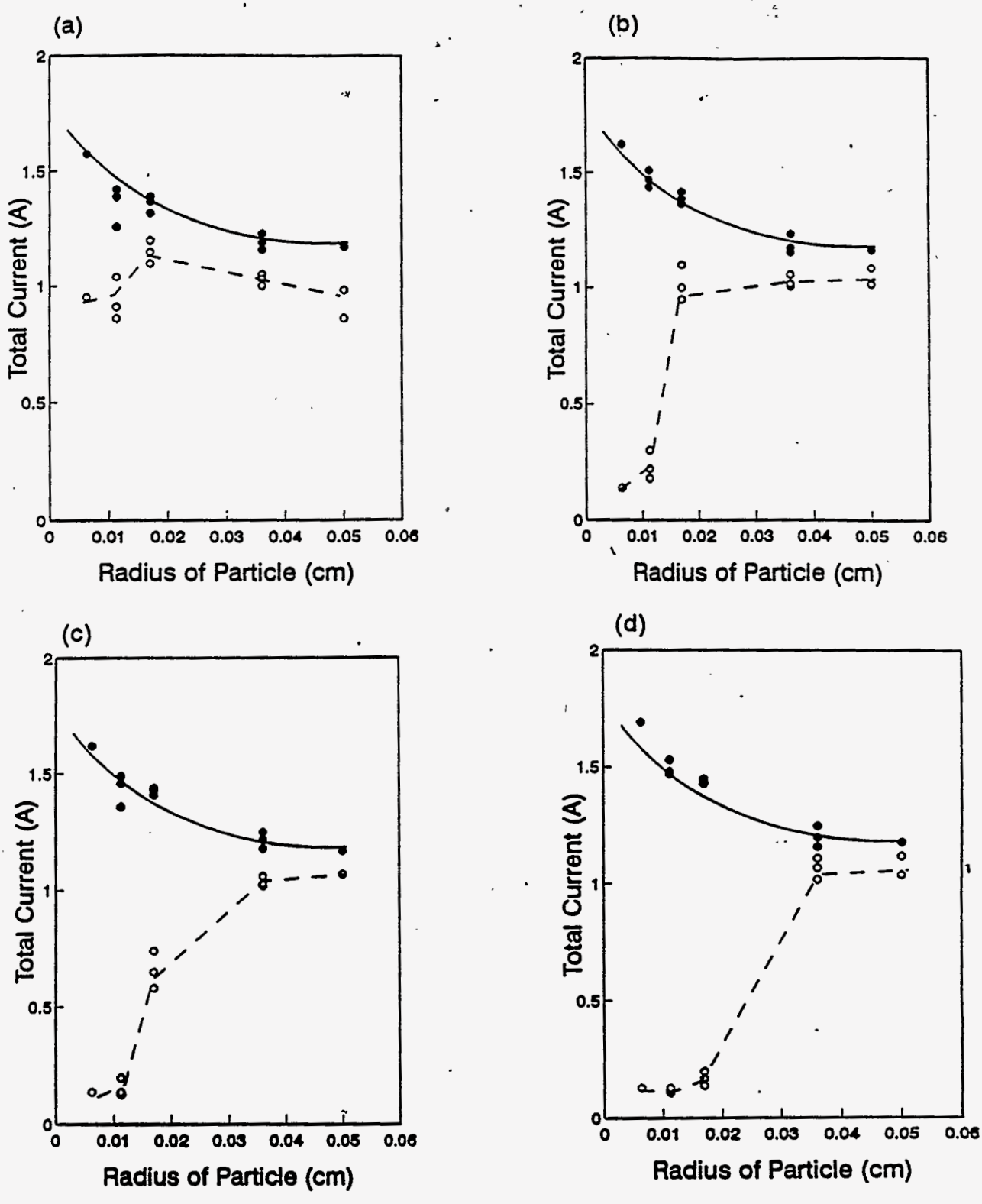


Fig.17 Dependence of Total Current for the Reduction of Nitrate and Nitrite at -0.8V at a packed-bed (solid line) and a fluidized-bed (broken line) on the size of the bed particle with the flow rate of (a)50, (b)100, (c)200, and (d)400 cc/min

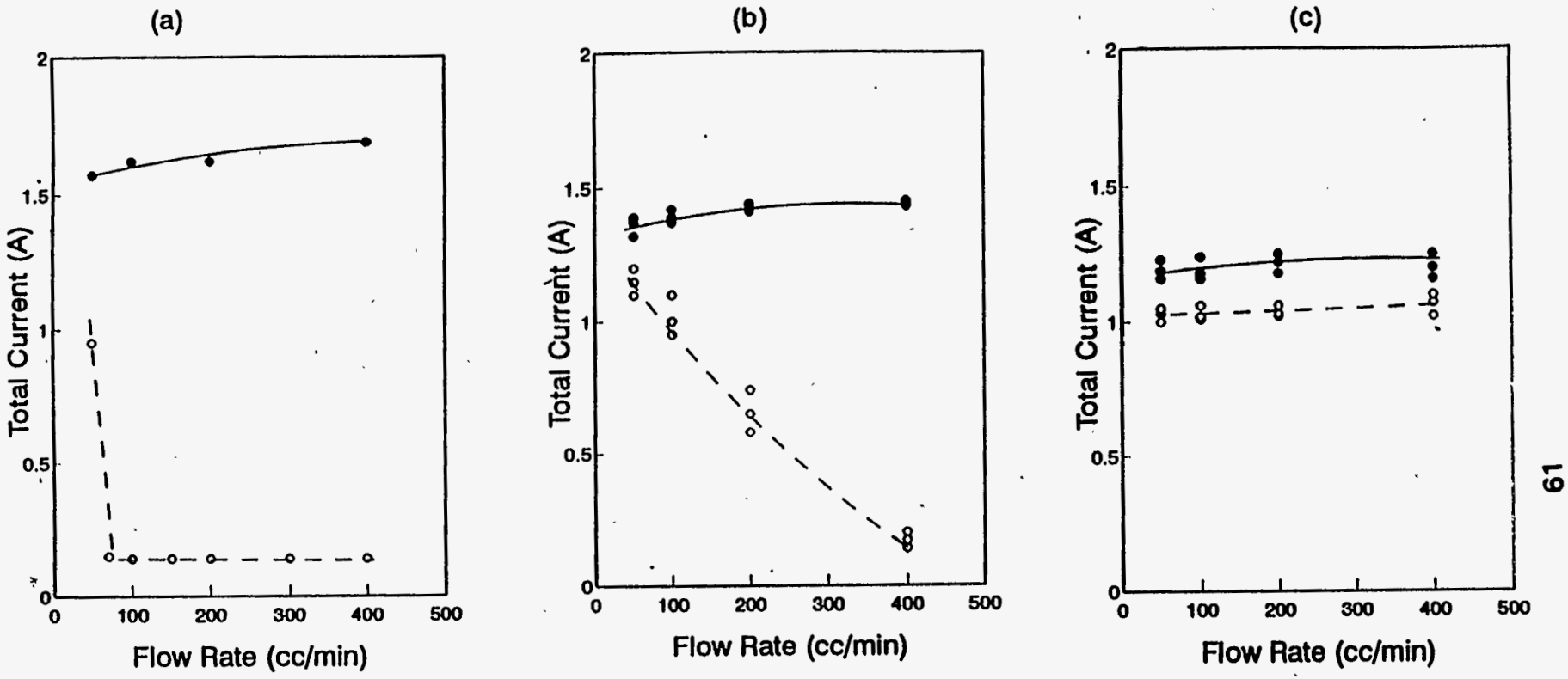


Fig. 18 Effect of the flow rate on the total currents at a packed-bed (solid line) and a fluidized-bed (broken line) electrode consisting of Ni particles of (a)0.00625, (b)0.017, and (c)0.036cm radius at -0.8V(NHS)

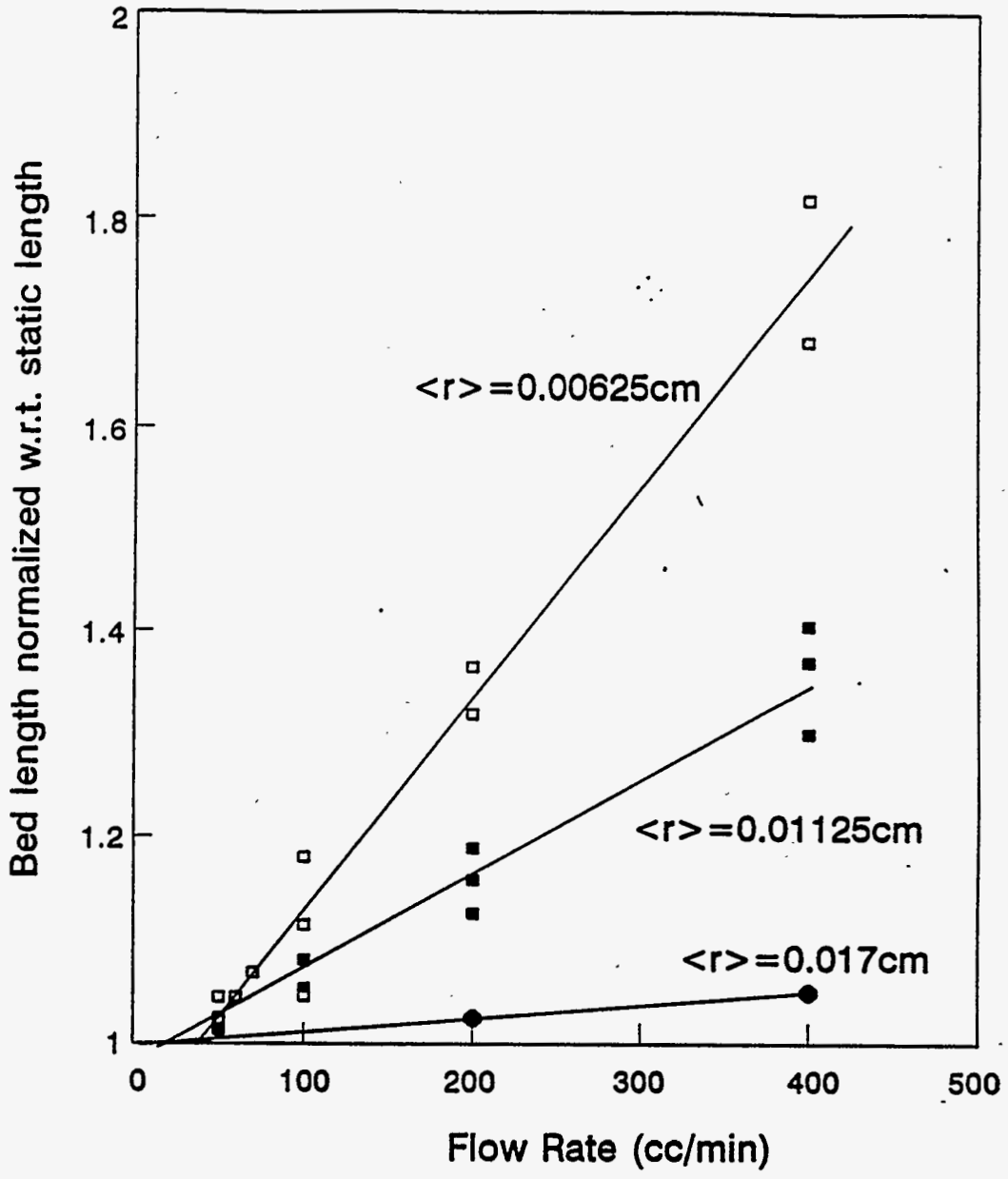


Fig. 19 Effect of FLow Rate on the Bed Length normalized with respect to the bed length at static state

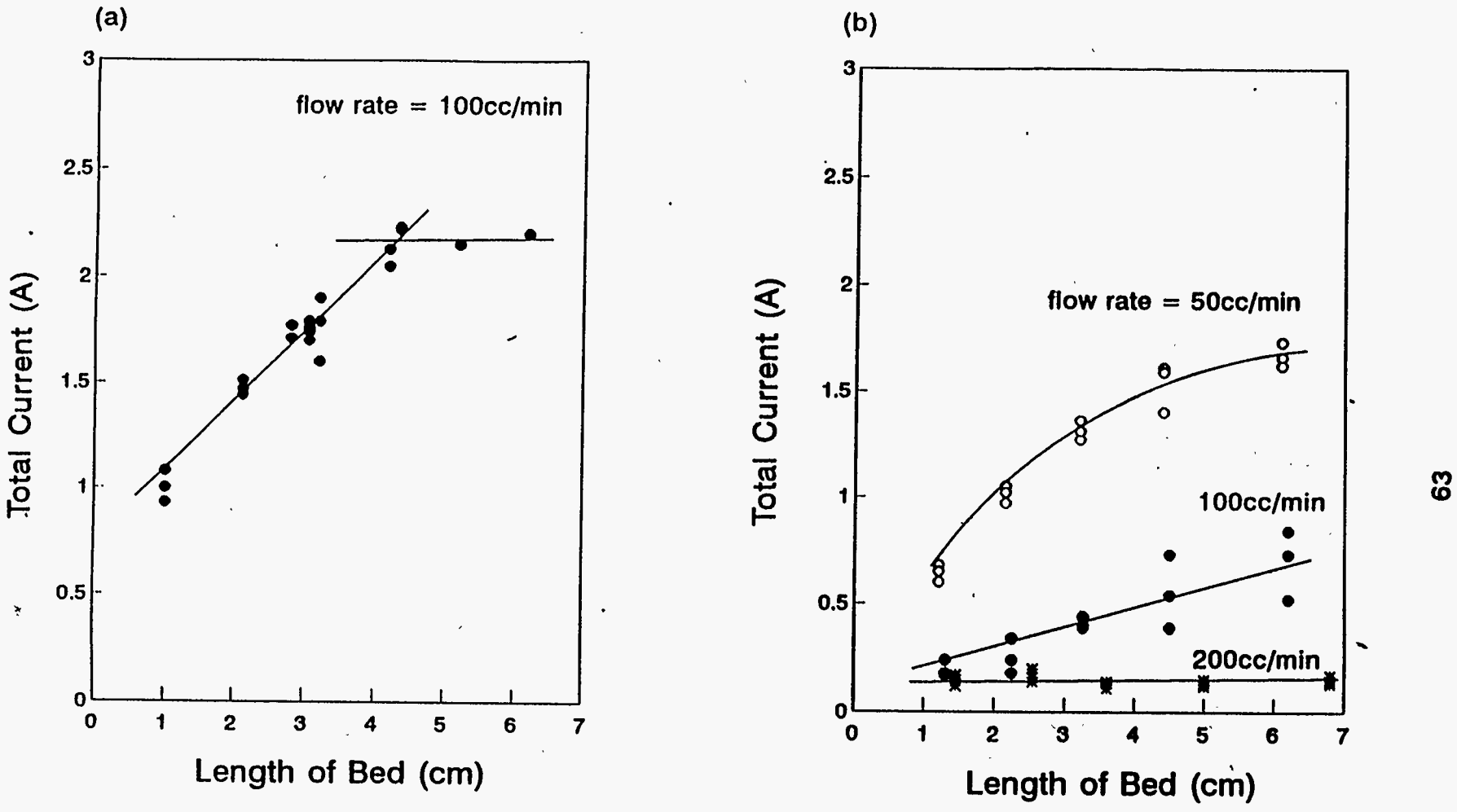


Fig. 20 Dependence of the Total Currents on the Length of bed at (a)a packed-bed and (b)a fluidized-bed electrode at -0.8V

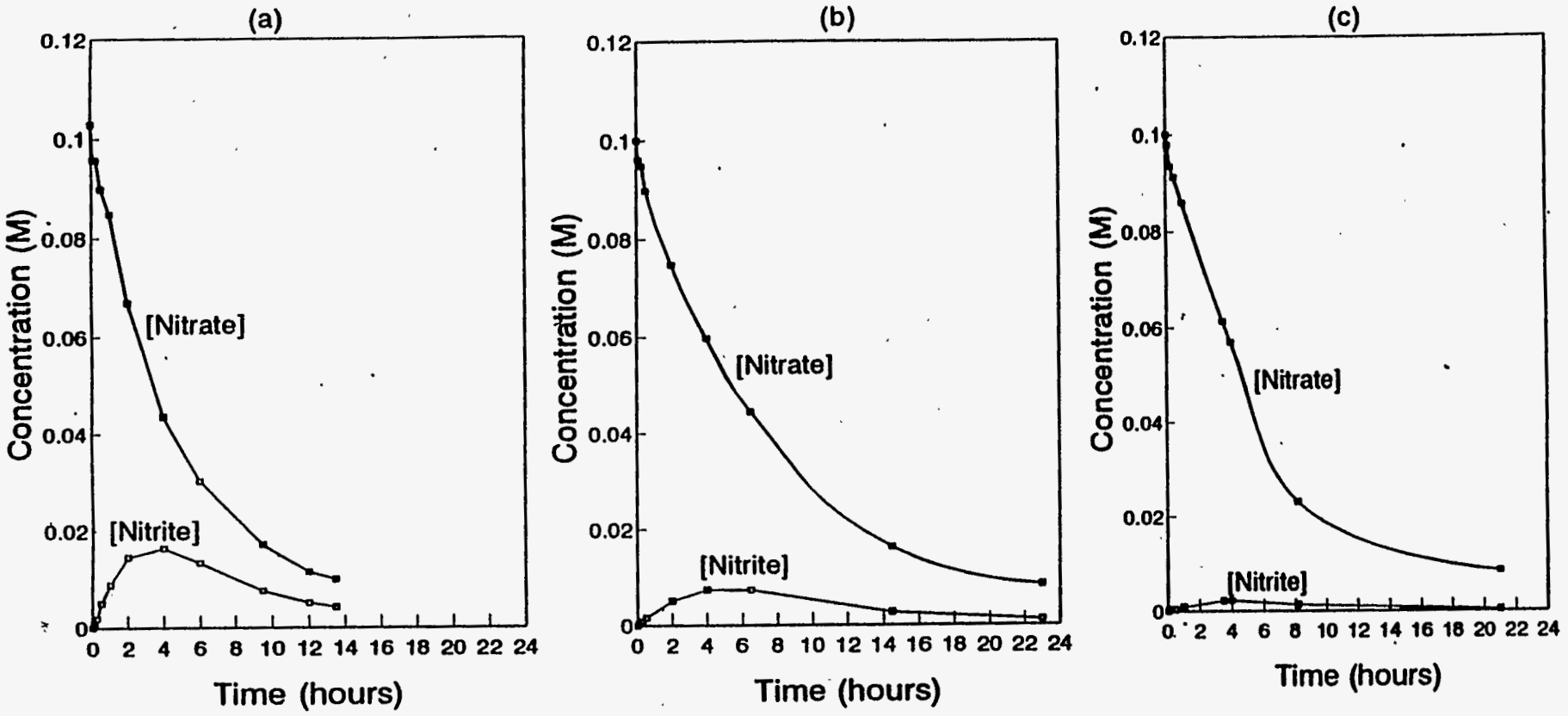


Fig. 21 Potentiostatic electrolysis of 0.1M $NaNO_3$ in 1.33M NaOH with (a)0, (b)0.04, and (c)0.4mM Ru complex at a Ni particle (50-100 mesh) packed-bed electrode(12.6$cm^2$ x 2cm) at -0.7V

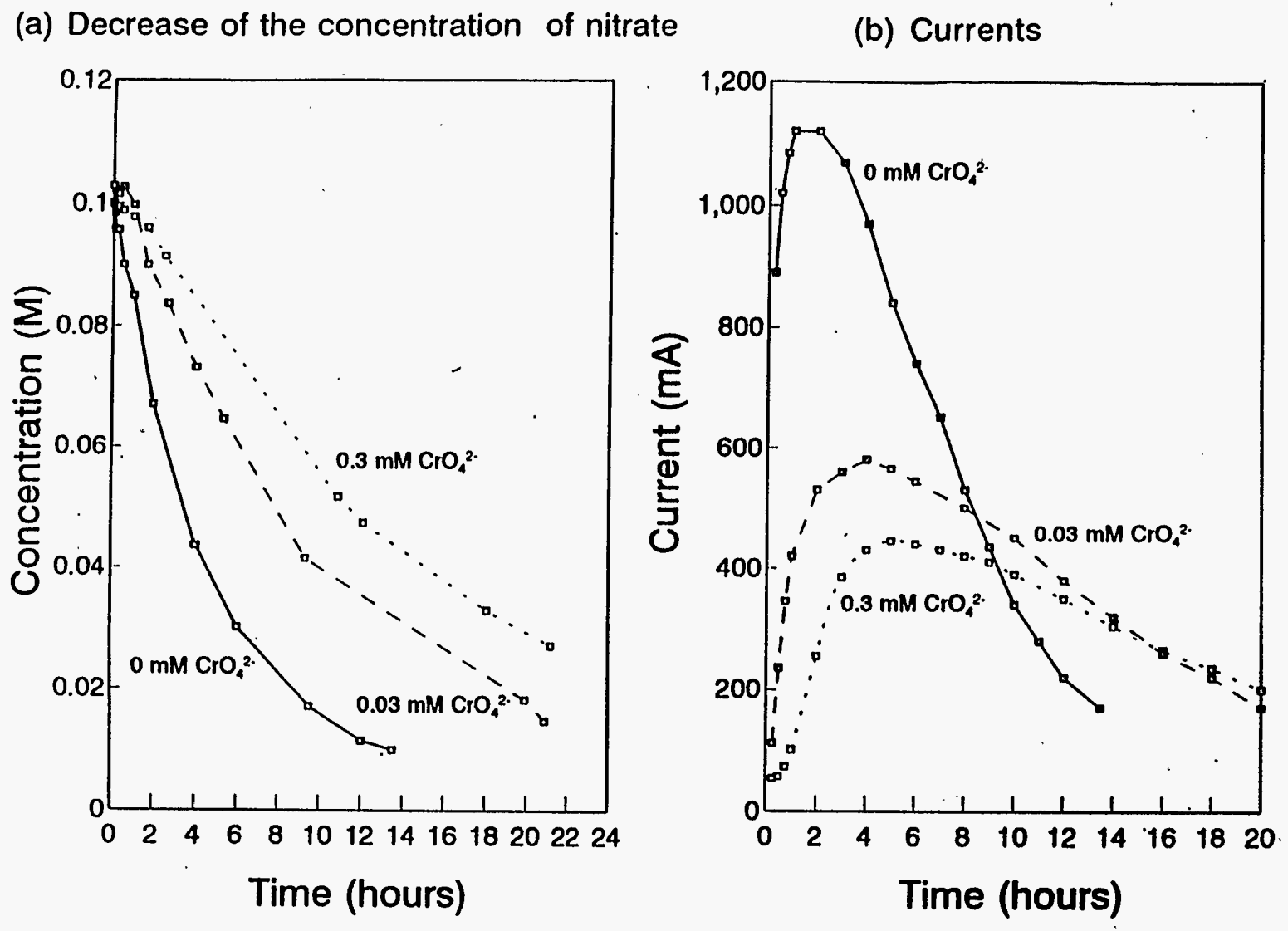


Fig. 22 Effect of the addition of chromate on the potentiostatic electrolysis of 0.1M $NaNO_3$ in 1.33M NaOH at a Ni particle (50-100 mesh) packed-bed electrode (12.6cm² x 2cm)

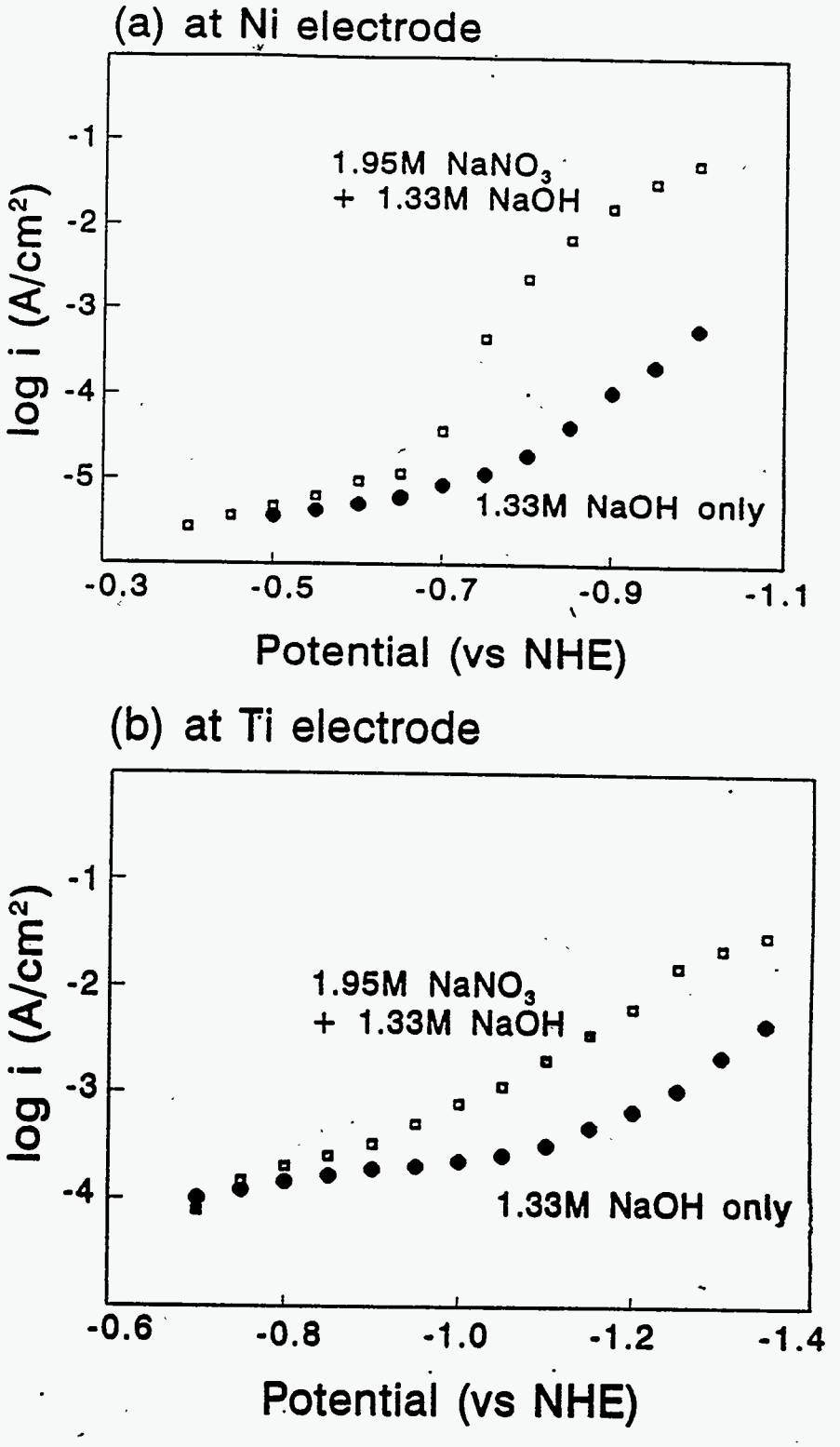


Fig. 23 Log i - V curves at (a) Ni, (b) Ti, (c) Pb, (d) Fe, (e) Graphite, and (f) Ebonex

(Continued)

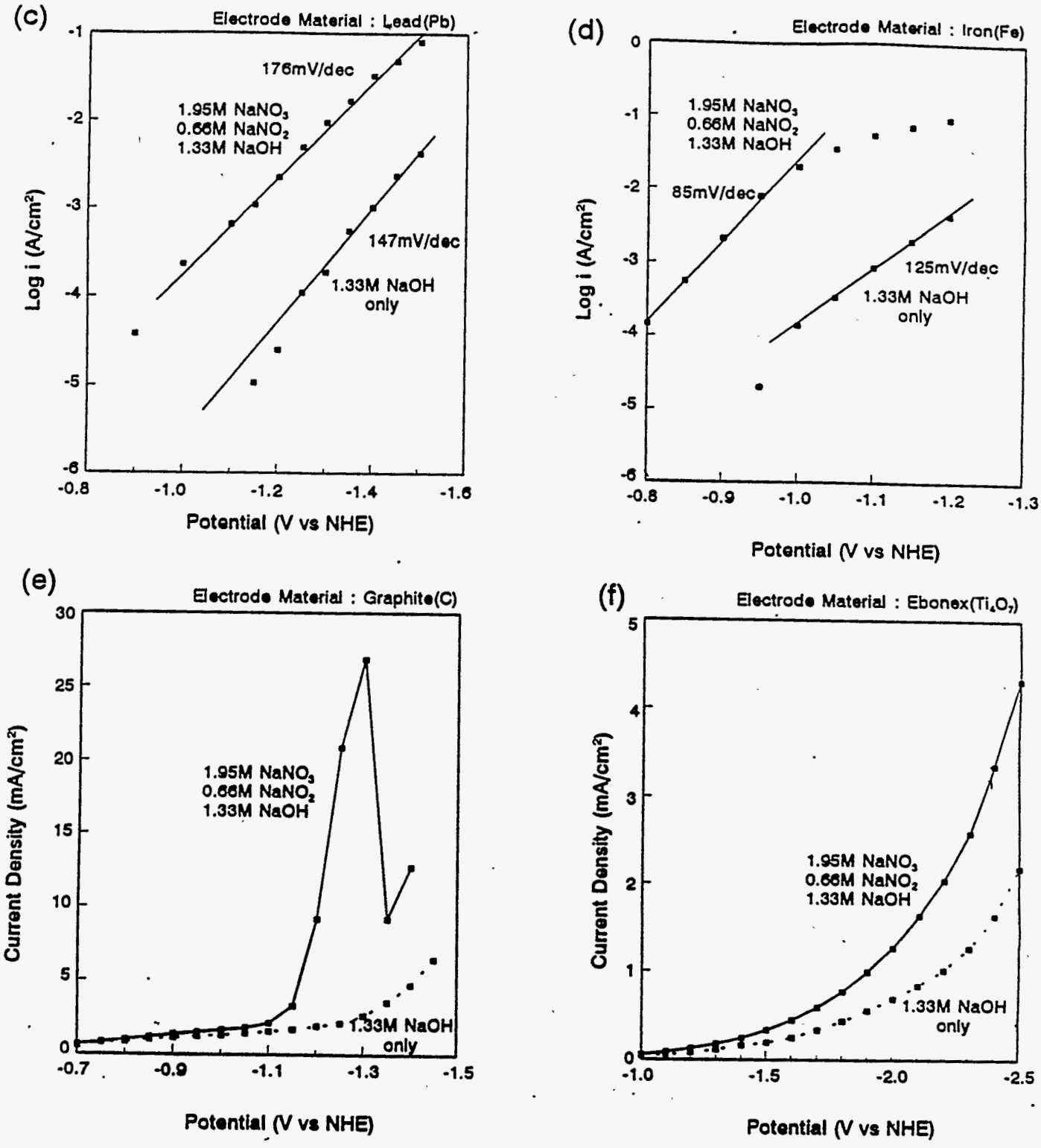


Fig. 23 (Continued)

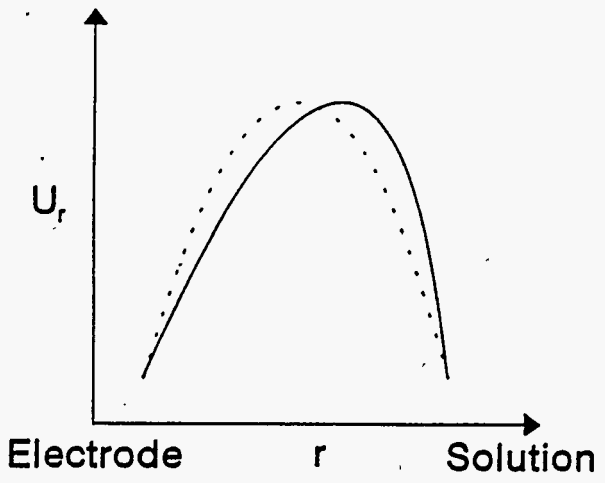


(a) Pb case, -0.6V from PZC

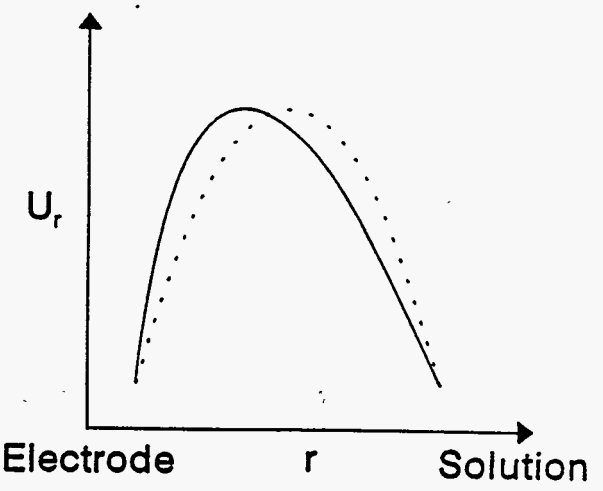


(b) Fe case, -0.25V from PZC

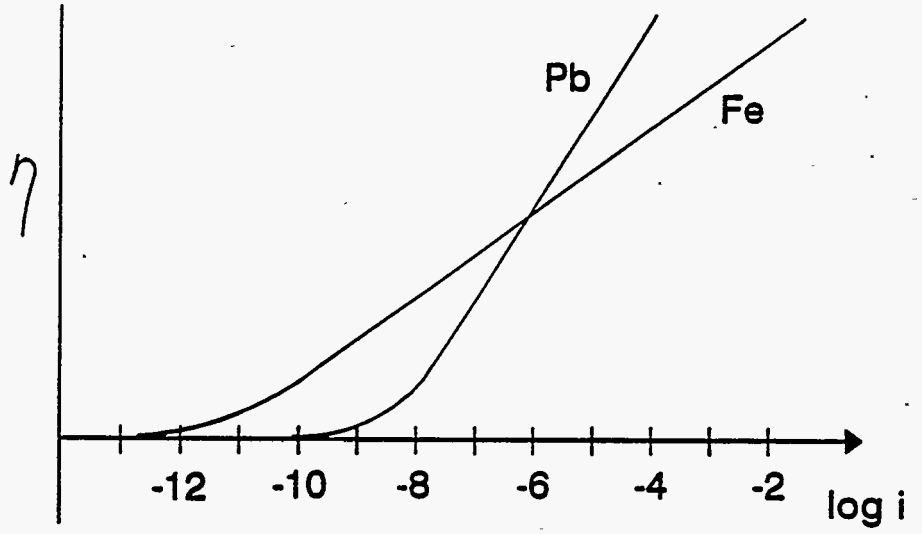


(c) $\eta$ - log i

Fig.24 Distortion of symmetric barrier at (a)Pb and (b)Fe electrode and Overpotential vs log i relation at both electrodes(c)

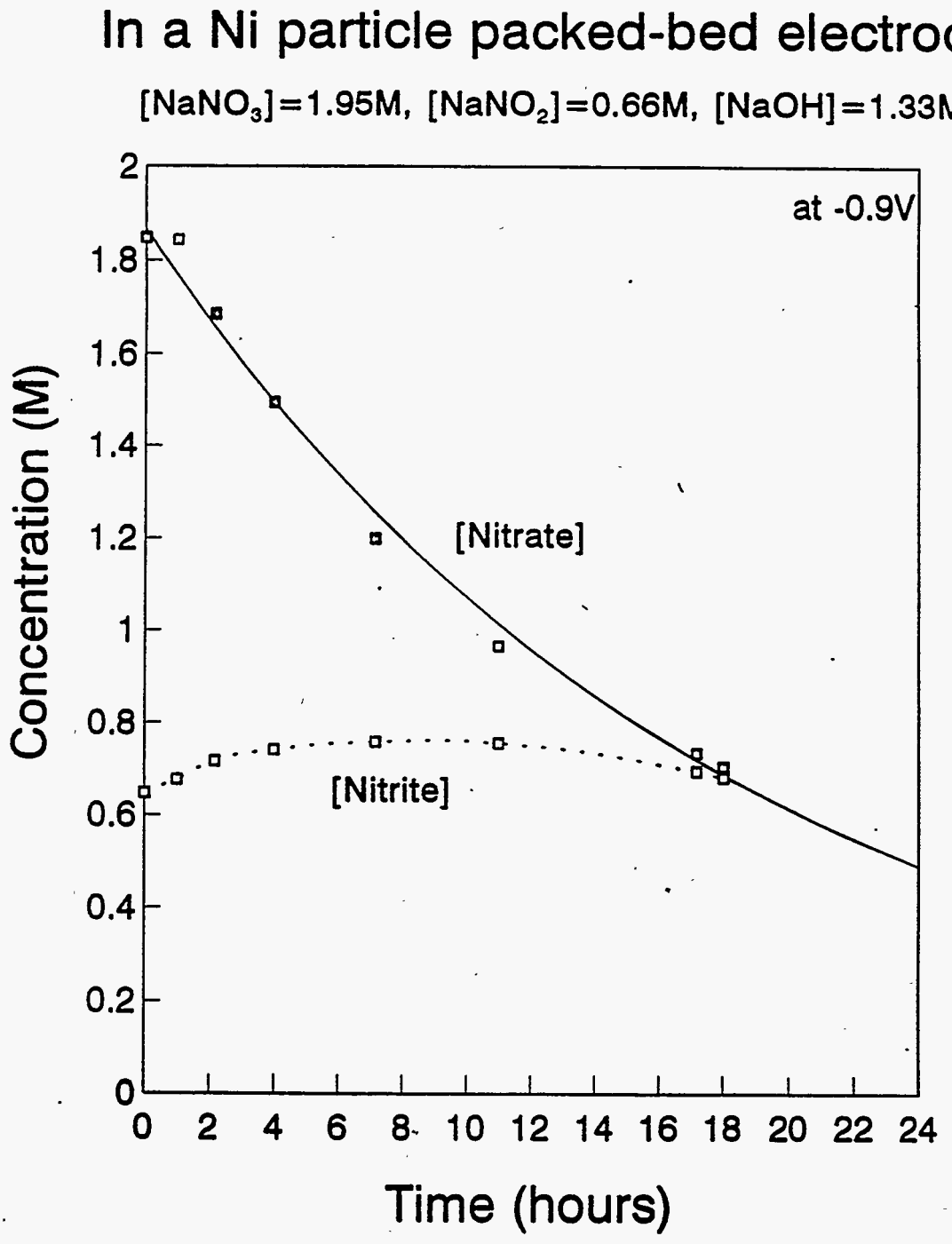


Fig. 25 Potentiostatic Electrolysis of the Solution
Bed Size : 12.6cm² x 2cm
Particle Size : 50-100 mesh
Flow Rate : 200cc/min
Volume of the solution : 300 cc

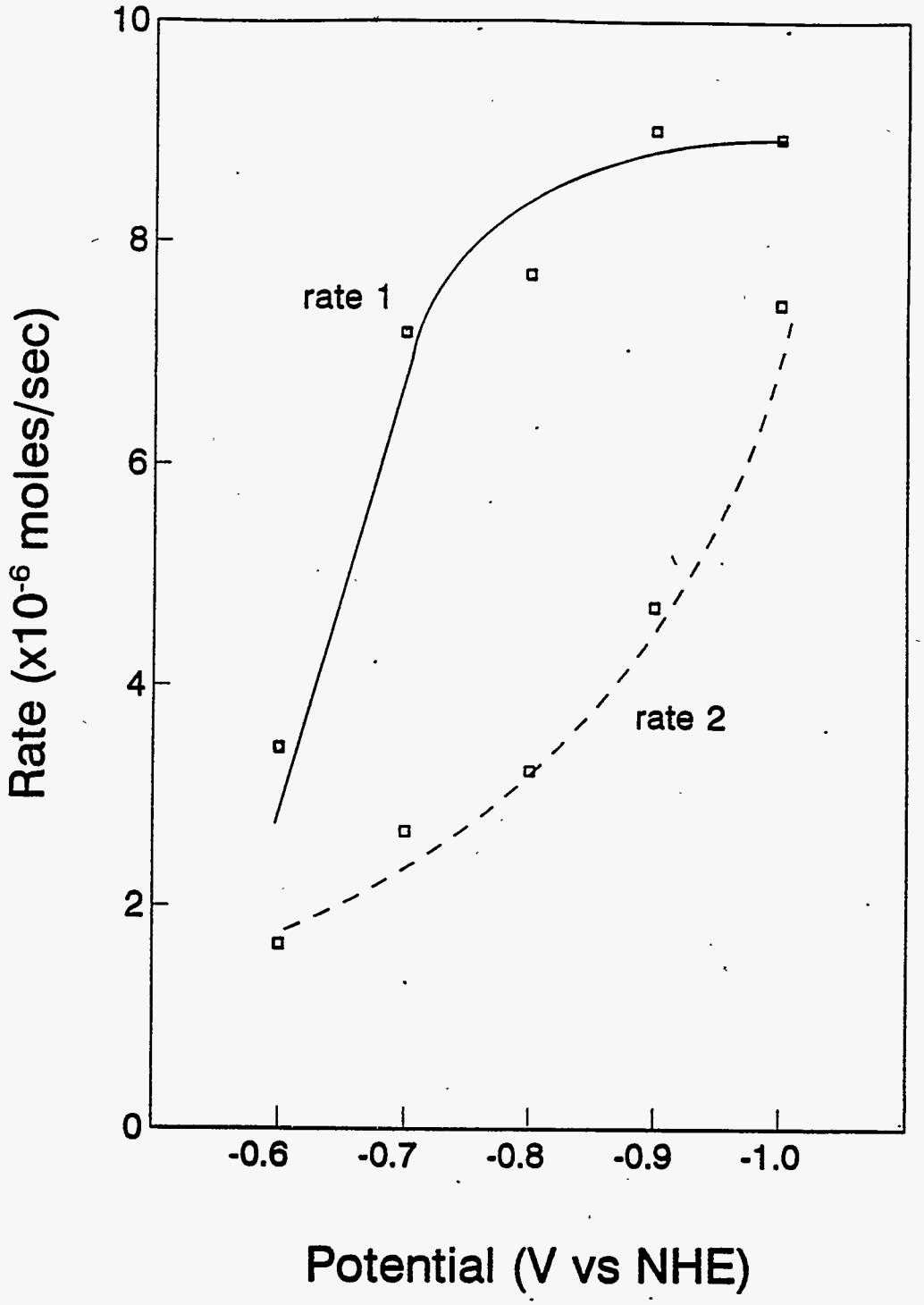


Fig. 26 The dependence of the rates for the reduction of nitrate to nitrite (rate 1) and the reduction of nitrite (rate 2) on the applied potential
Conditions are described in the Fig. 25.
Rate = rate constant x initial concentration.

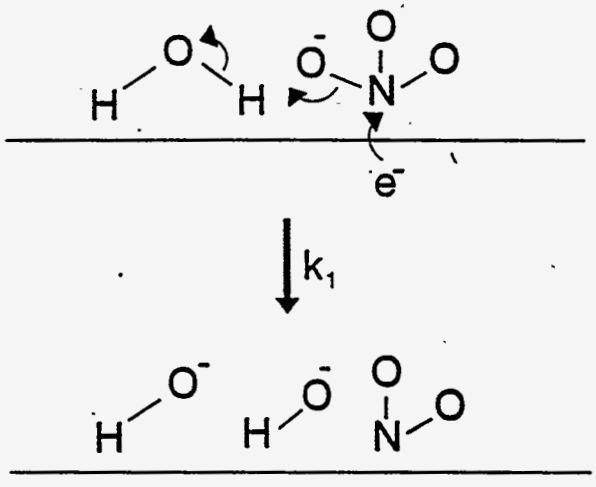


Fig. 27 A Model for the Reduction of Nitrate to Nitrite

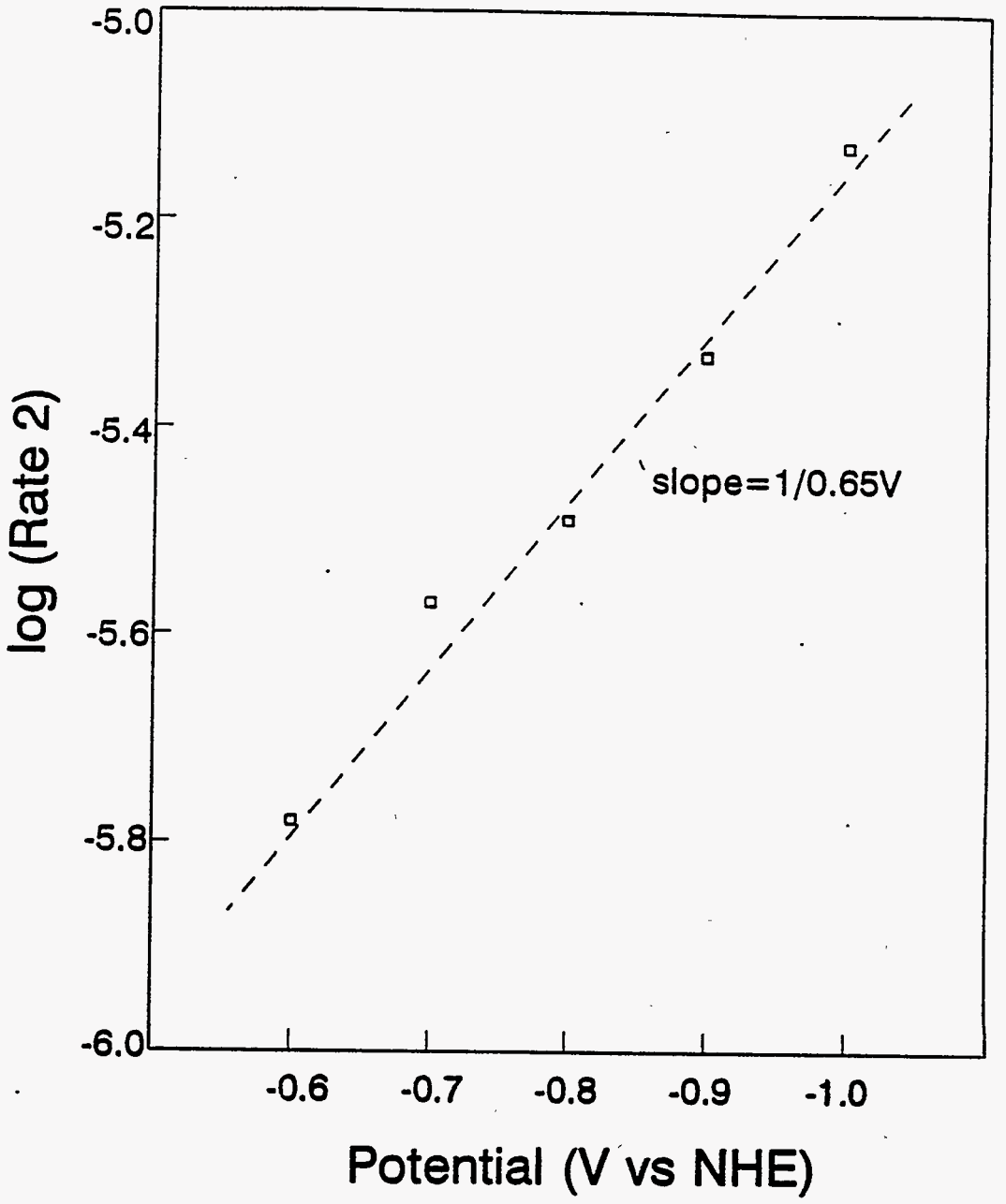


Fig. 28 Tafel slope for the reduction of nitrite

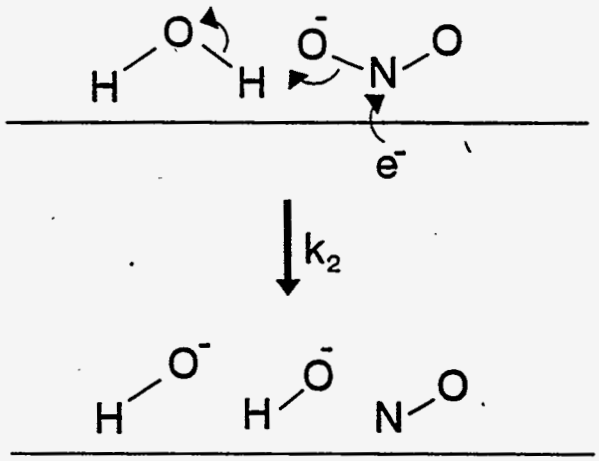


Fig. 29 A Model for the Reduction of Nitrite

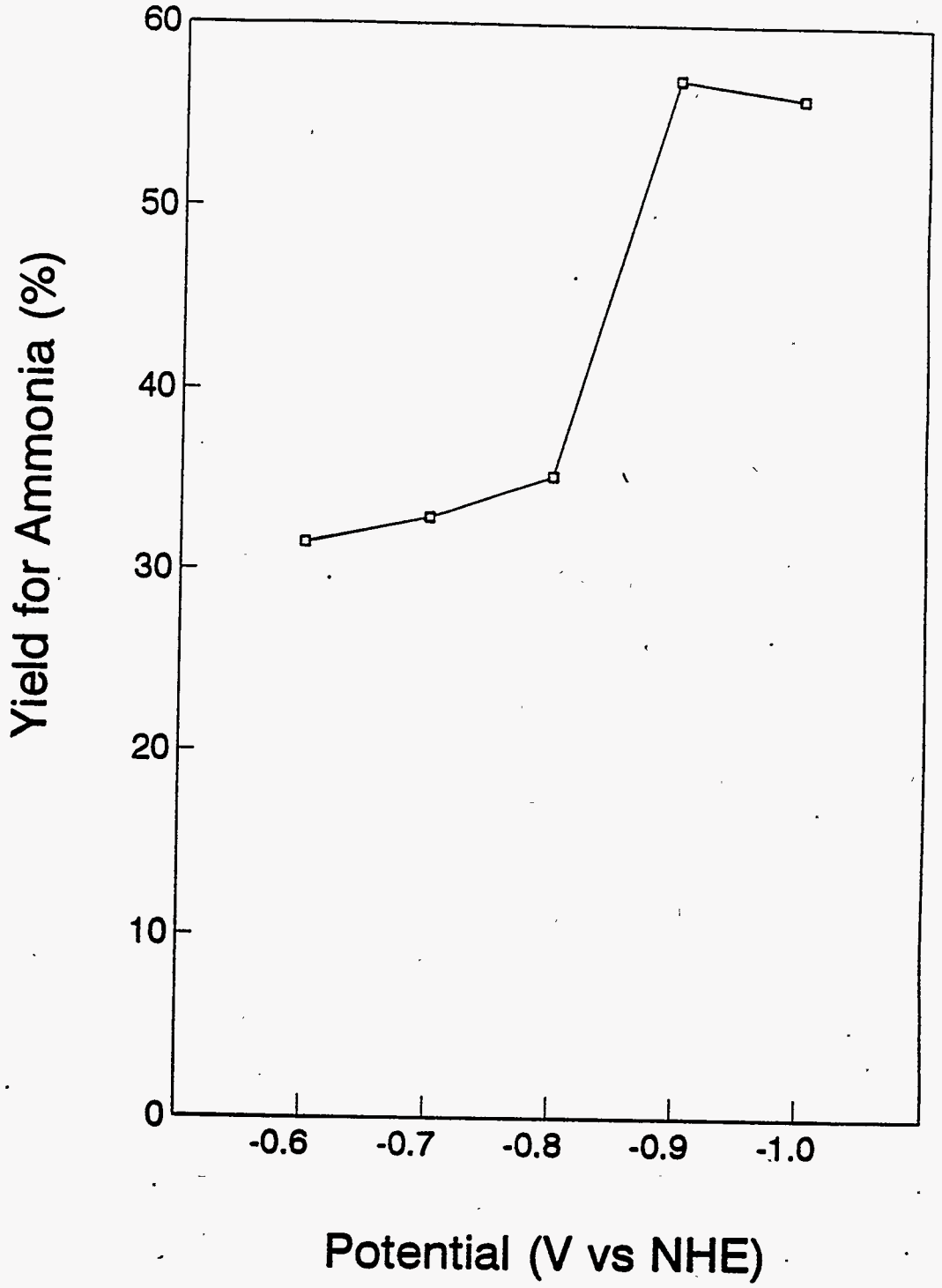


Fig. 30 The yield percent for ammonia in the electrolysis

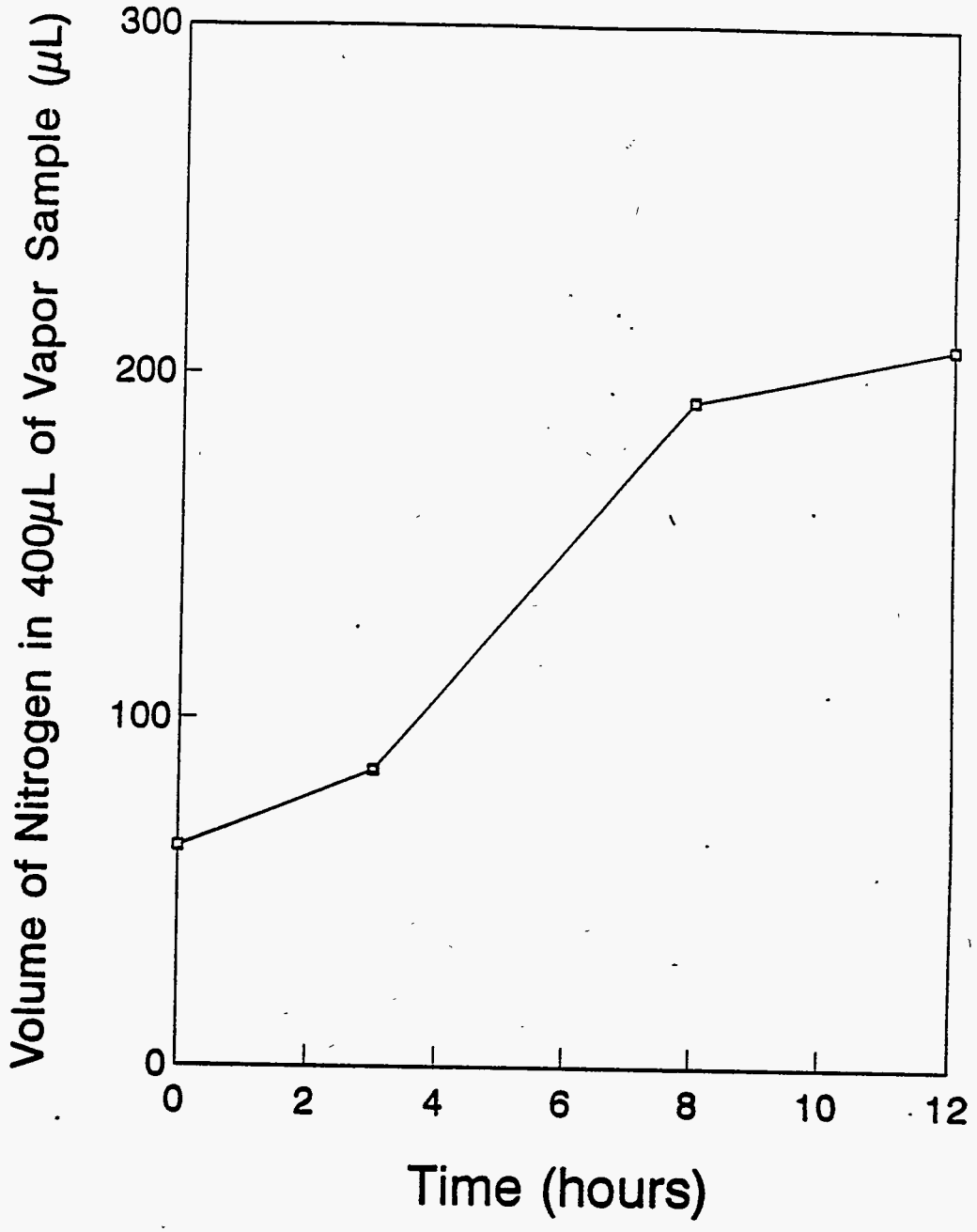


Fig. 31 Increase of nitrogen gas in the vapor produced by the electrolysis of the solution at -1.0V within a Ni packed-bed electrode

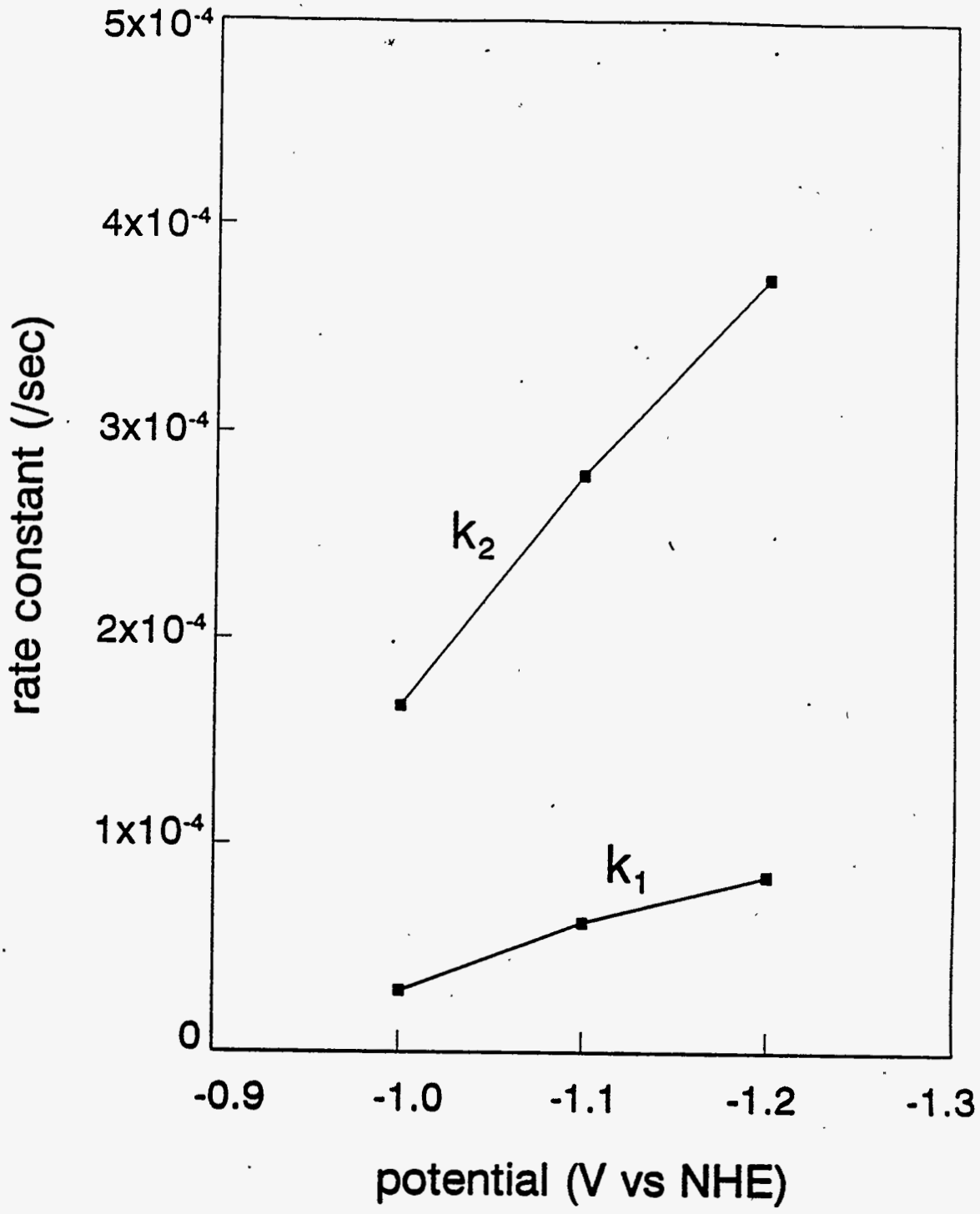


Fig. 32 Increase of the rate constants for the nitrate reduction($k_1$) and the nitrite reduction($k_2$) at Fe packed bed electrode

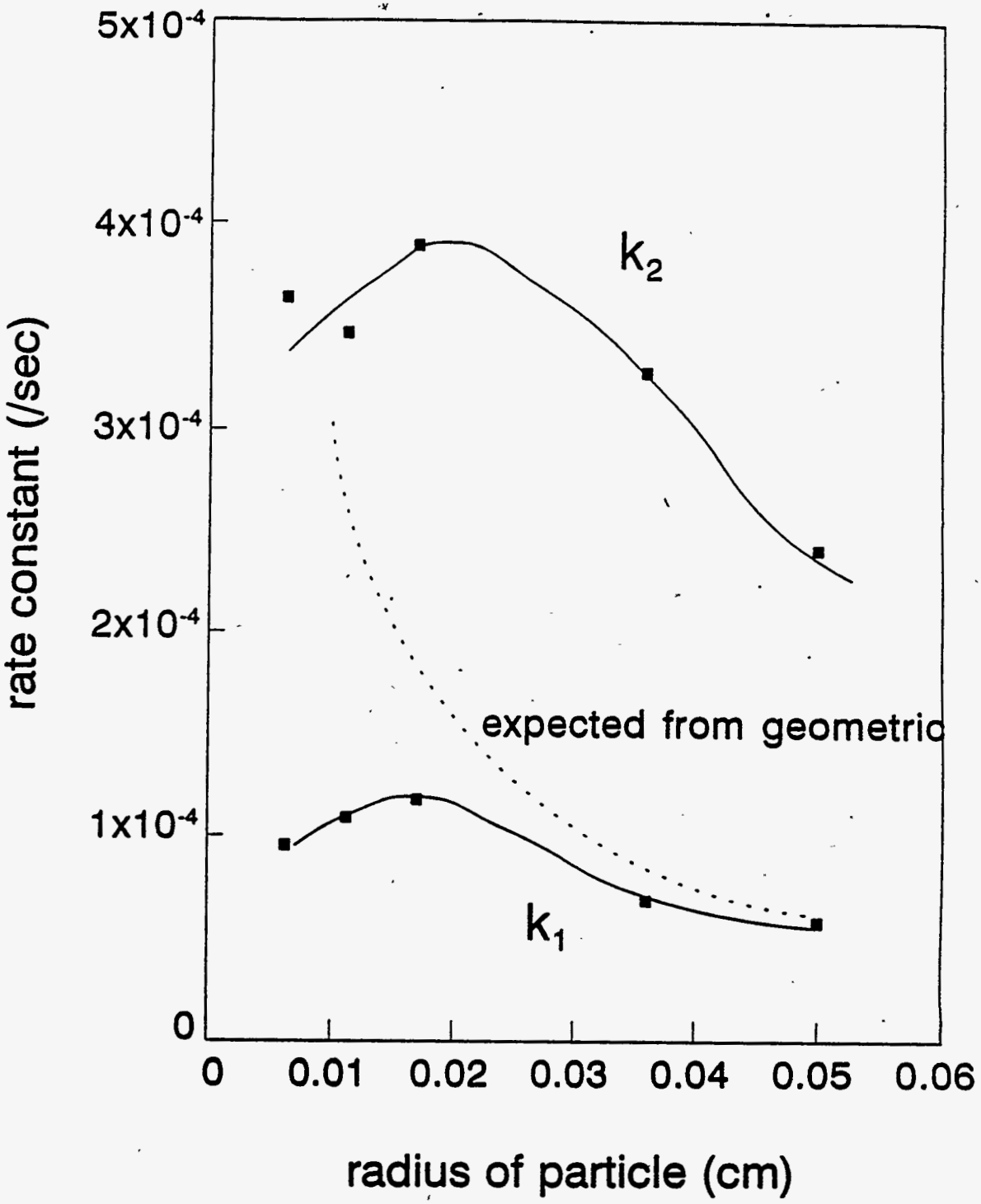


Fig. 33 The effect of particle size on the rate constants for the nitrate reduction($k_1$) and nitrite reduction($k_2$) at Ni particle packed-bed electrode

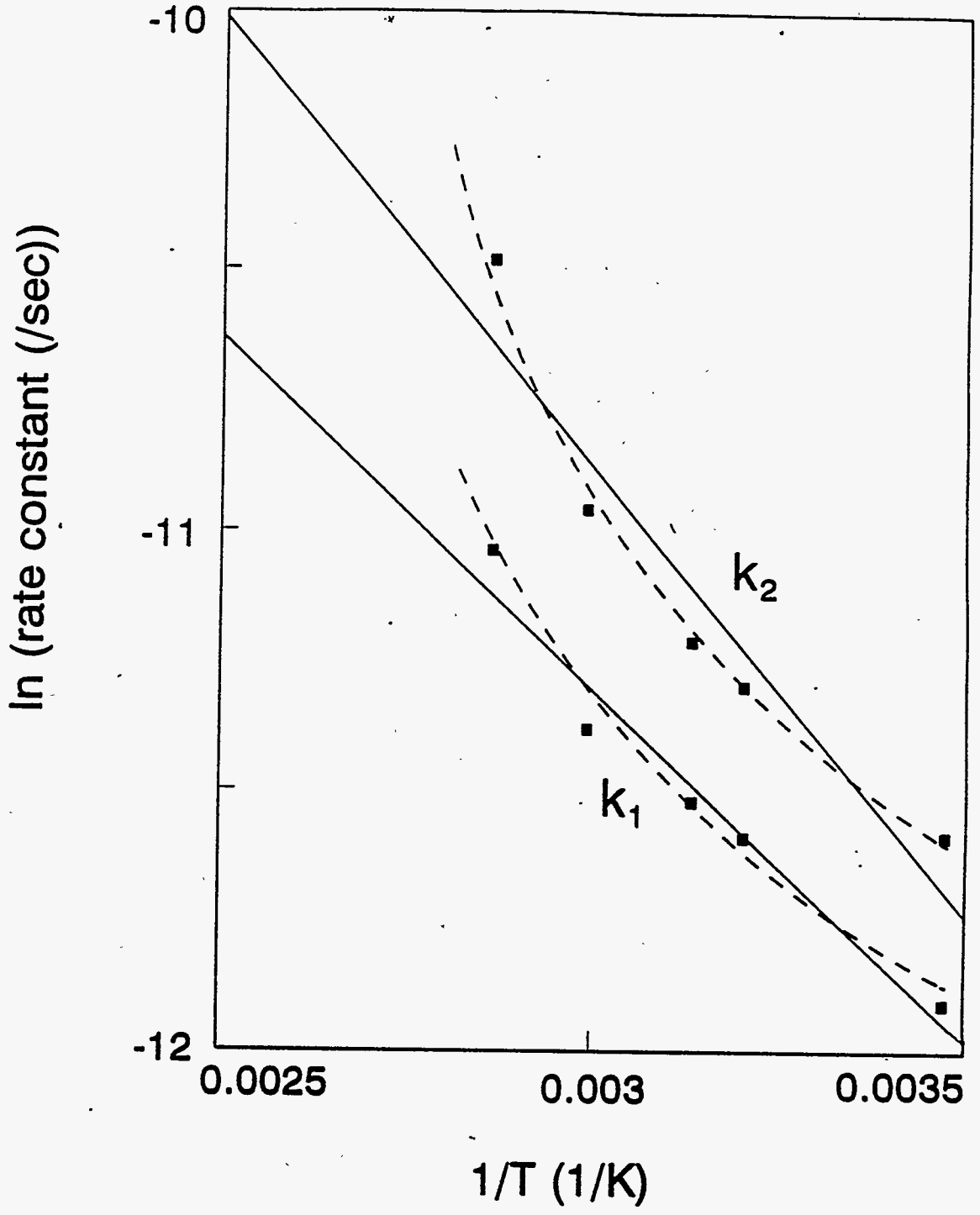


Fig. 34 Plot of ln k vs 1/T

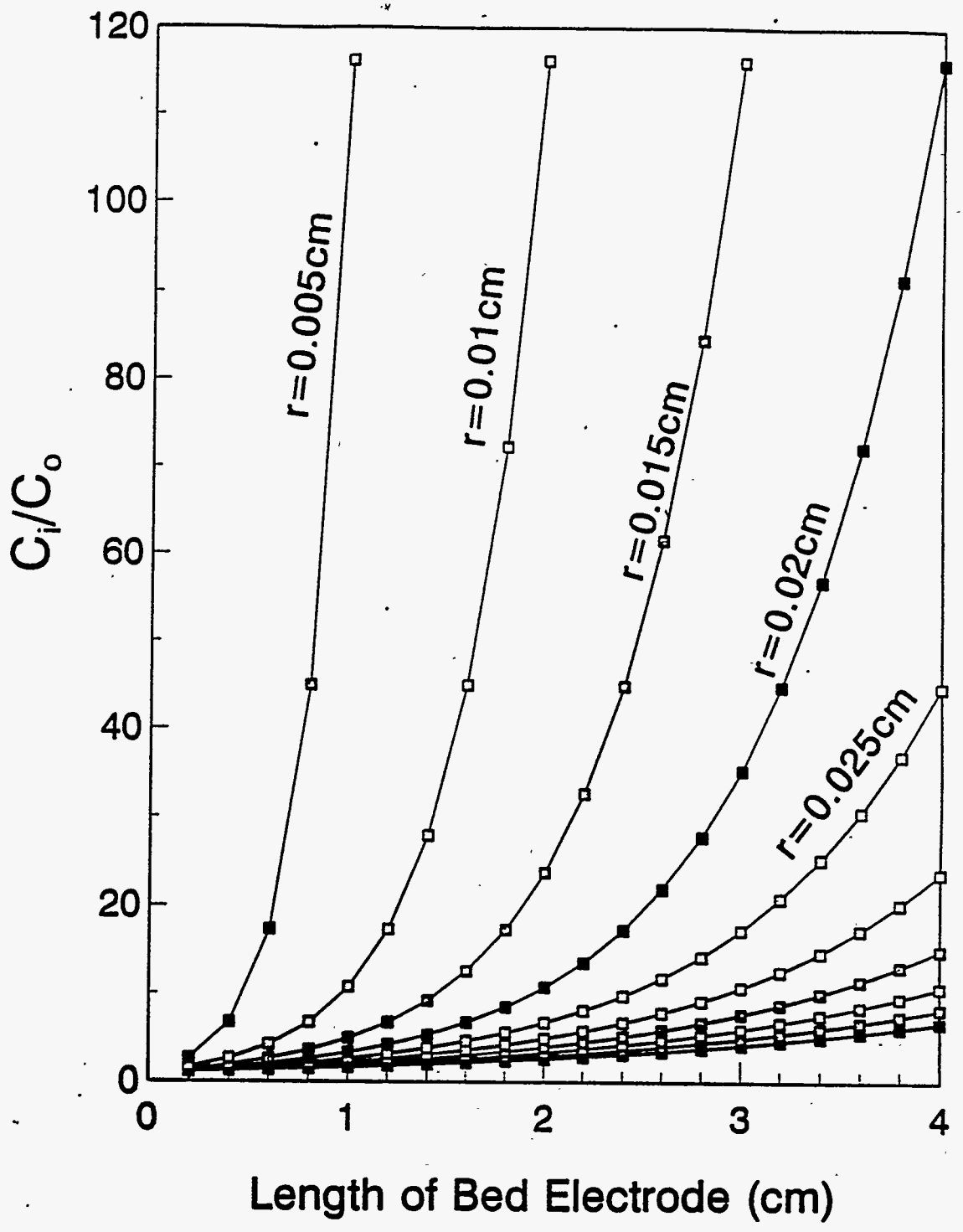


Fig. 35 $C_i/C_o$ as a function of bed length with a constant flow rate of 200cc/min

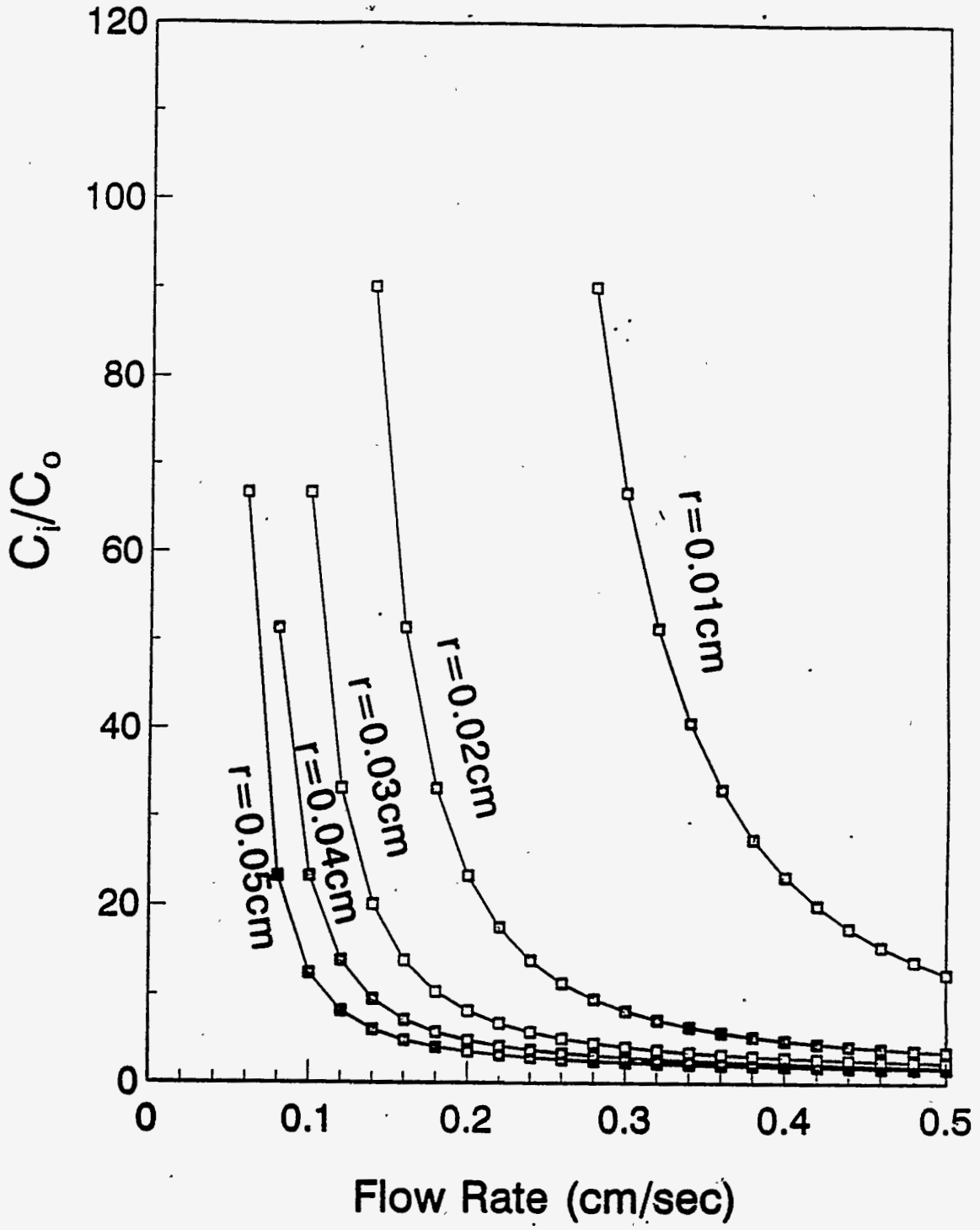


Fig. 36 $C_i/C_o$ as a function of flow rate with a constant bed length of 2cm

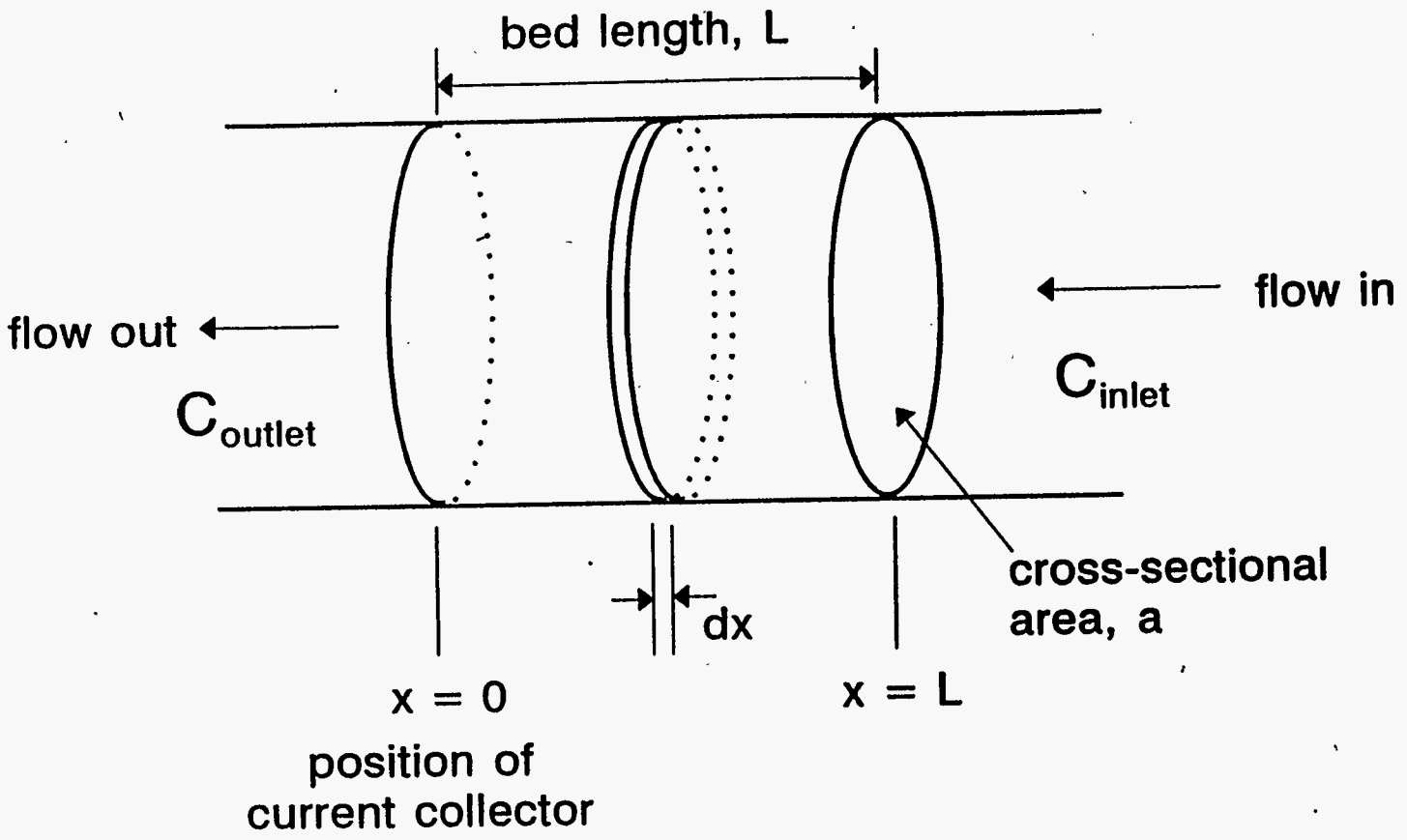


Fig. 37 Diagram of a packed bed electrode

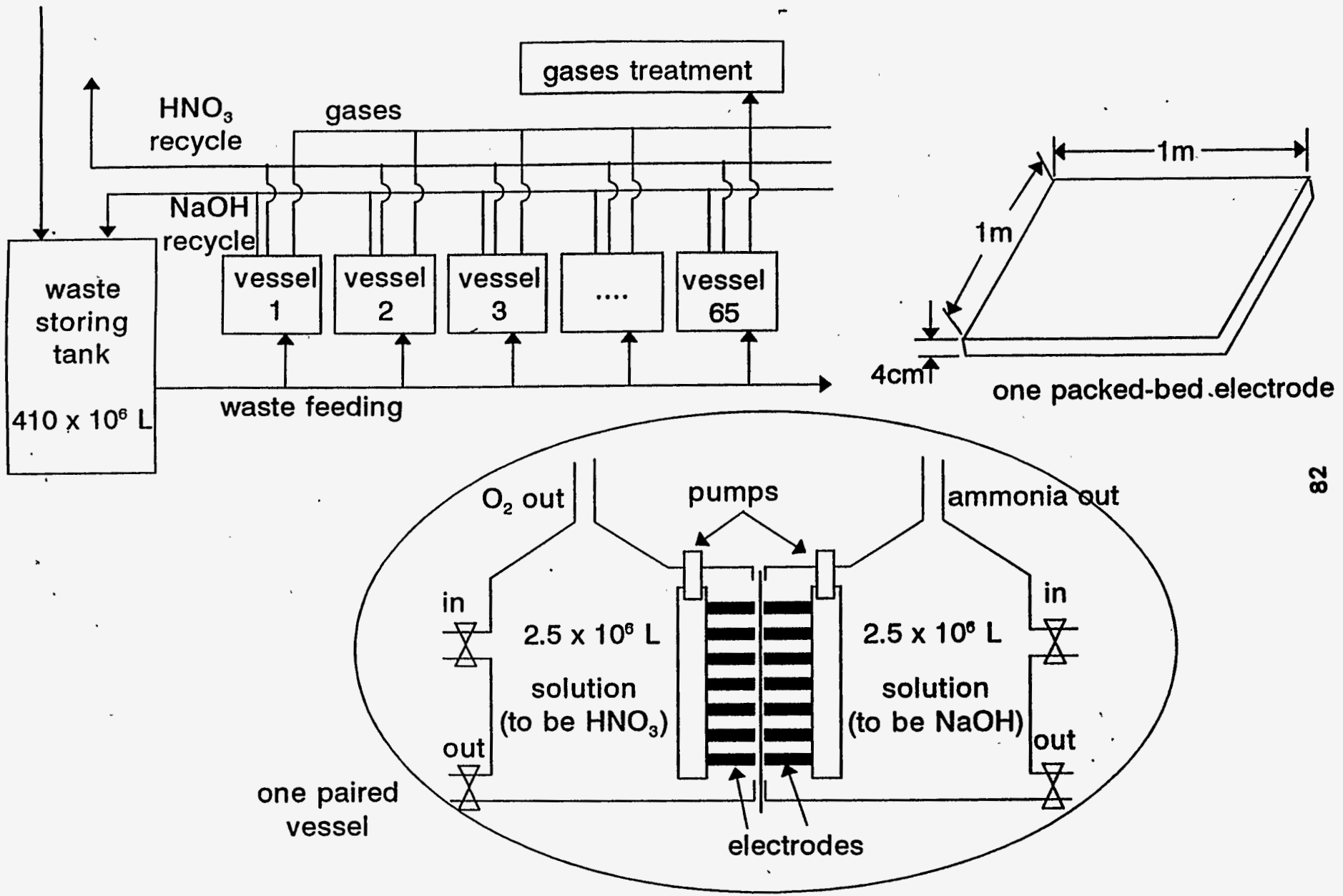


Fig. 38 Idealization of the electrochemical treatment of the liquid waste in the Savannah River Site

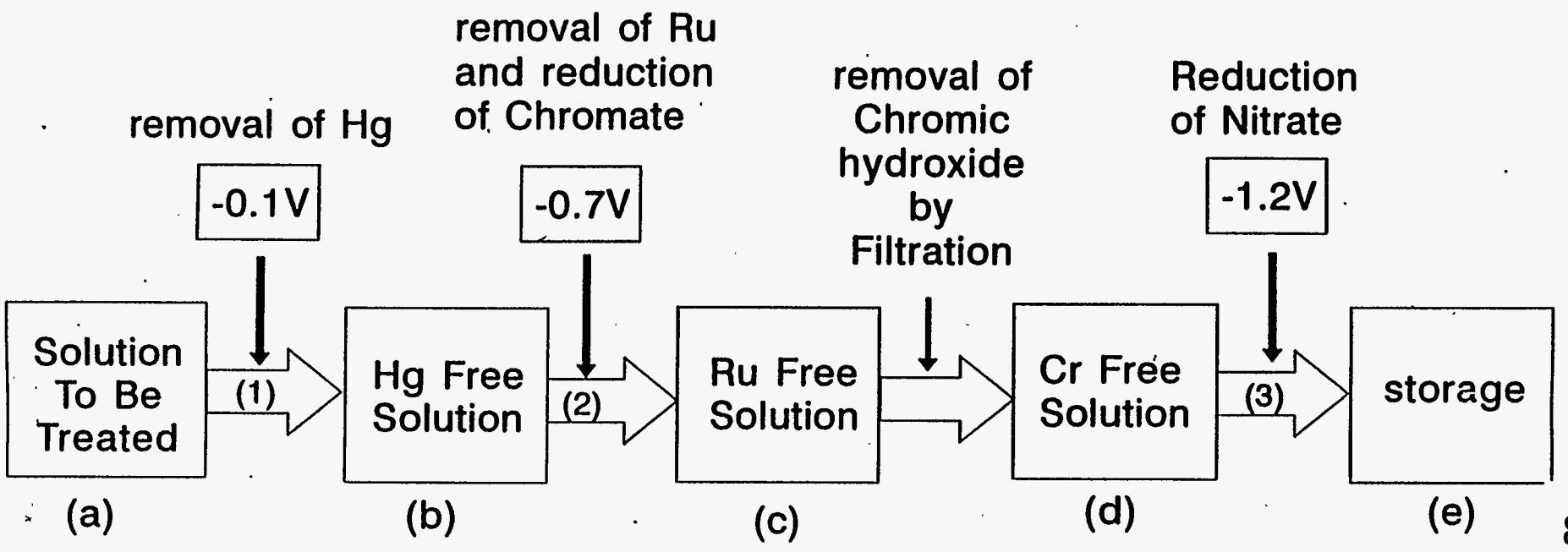


Fig. 39 Diagram for the electrochemical processes for the waste solution